

**EXPERIMENTALLY VALIDATED COMPATIBILITY STRUT AND TIE
MODELING OF REINFORCED CONCRETE BRIDGE PIERS**

A Thesis

by

REECE MELBY SCOTT

Submitted to the Office of Graduate Studies of
Texas A&M University
in partial fulfillment of the requirements for the degree of

MASTER OF SCIENCE

August 2010

Major Subject: Civil Engineering

Experimentally Validated Compatibility Strut and Tie

Modeling of Reinforced Concrete Bridge Piers

Copyright 2010 Reece Melby Scott

**EXPERIMENTALLY VALIDATED COMPATIBILITY STRUT AND TIE
MODELING OF REINFORCED CONCRETE BRIDGE PIERS**

A Thesis

by

REECE MELBY SCOTT

Submitted to the Office of Graduate Studies of
Texas A&M University
in partial fulfillment of the requirements for the degree of

MASTER OF SCIENCE

Approved by:

Co-Chairs of Committee,	John B. Mander
	Joseph M. Bracci
Committee Member,	Anastasia Muliana
Head of Department,	John Niedzwecki

August 2010

Major Subject: Civil Engineering

ABSTRACT

Experimentally Validated Compatibility Strut and Tie Modeling of

Reinforced Concrete Bridge Piers. (August 2010)

Reece M. Scott, B.E. (Hons), University of Canterbury

Co-Chairs of Advisory Committee: Dr John B. Mander

Dr Joseph Bracci

A compatibility-based strut-and-tie model C-STM is proposed for analyzing deep beams and disturbed regions with particular emphasis on reinforced concrete bridge piers. In addition to the normal strut-and-tie force equilibrium requirements the model accounts for non-linear behavior through displacement compatibility using inelastic constitutive laws of cracked reinforced concrete. The model is implemented into widely used commercial structural analysis software and validated against results from previously conducted large scale experiments. A near full-scale experiment on a reinforced concrete sub-assembly that represents cantilevered and straddle pier bents is conducted to investigate the shear-flexure performance of deep (disturbed) regions. Insights into the development of nonlinear behavior and the final collapse failure mechanism are then evaluated and accurately modeled using the C-STM. It is concluded that the proposed C-STM serves as an advanced method of analysis that can predict with suitable accuracy the force-deformation response of both D- and B- regions, deep beams, and beam-columns. This provides engineers with a supplementary analysis tool that can be used to assess the nonlinear behavior of bridge piers with stocky members and/or large disturbed regions.

ACKNOWLEDGEMENTS

The research presented in this thesis would not have been possible without the input from a number of people. Firstly, I would like to extend my gratitude to Dr. Mander, my thesis advisor, for giving me the opportunity to study at Texas A&M University and for his wealth of knowledge that was the driving force behind the computational modeling presented in this research. I would like to thank Dr. Bracci, the principal investigator of this research project (TxDOT project 5997), for his continued support, professional guidance, and financial support. I would also like to thank Dr. Muliana, from the Mechanical Engineering Department, for her support while serving on my committee.

I would like to acknowledge my research colleagues, Shih-Hsiang Liu and Mike Wilson, for their invaluable contribution in the experimental testing phase. None of the experimental results presented in this thesis would have been possible without their hard work and input, for which I am very grateful. It has been a privilege to work with them, and they have made the many hours spent working in the lab an enjoyable experience.

I would also like to acknowledge the Texas Department of Transportation for funding the experimental work presented in this thesis on behalf of the TxDOT project-5997. This was conducted in the High-Bay Structural and Materials Testing Laboratory of Texas A&M. I would like to thank Dr. Peter Keating and Mr. Matt Potter for their technical support with the experimental work.

A special thanks is due to all my family and friends who have supported me over the past two years and have made this an invaluable experience. Finally, my parents in New Zealand, thank you for your encouragement and loving support from afar.

TABLE OF CONTENTS

	Page
ABSTRACT	iii
ACKNOWLEDGEMENTS	iv
TABLE OF CONTENTS	vi
LIST OF FIGURES.....	viii
LIST OF TABLES	x
 CHAPTER	
I INTRODUCTION	1
1.1 Research Motivation.....	1
1.2 Research Objectives	2
1.3 Organization of Thesis	3
1.4 Historic Developments	3
II COMPUTATIONAL TRUSS MODELING OF SHEAR CRITICAL STRUCTURAL CONCRETE SYSTEMS	14
2.1 Chapter Scope and Background	14
2.2 Research Significance	15
2.3 Numerical Truss Modeling.....	16
2.4 Arch vs. Truss Action in C-STM	25
2.5 Stress and Strain Transformation for Flexural Equivalence.....	31
2.6 C-STM Truss Geometry and Axial Rigidity Assignments.....	40
2.7 Constitutive Material Relations of Truss Elements.....	44
2.8 Ultimate Strength and Softening of Constitutive Relations	50
2.9 Experimental Verification	56
2.10 Discussion.....	65
2.11 Chapter Closure	69

CHAPTER	Page	
III	EXPERIMENTAL AND ANALYTICAL INVESTIGATION OF REINFORCED CONCRETE BRIDGE BENTS.....	71
	3.1 Chapter Scope and Research Motivation	71
	3.2 Experimental Investigation.....	73
	3.3 Experimental Testing.....	76
	3.4 Test Results and Discussion	85
	3.5 Compatibility-based Strut and Tie Application.....	91
	3.6 Chapter Closure	105
IV	SUMMARY, CONCLUSIONS AND RECOMMENDATIONS	107
	4.1 Summary.....	107
	4.2 Conclusions	108
	4.3 Recommendations and Future Work	109
	REFERENCES.....	113
	APPENDIX A IMPLEMENTATION OF COMPUTATIONAL C-STM	119
	APPENDIX B DESIGN APPLICATION: C-STM FOR EXPERIMENTAL C-SPECIMENS	138
	APPENDIX C C-SPECIMEN EXPERIMENTAL RESULTS AND C-STM COMPARISONS	147
	APPENDIX D CODE FORCE-BASED PREDICTIONS.....	161
	APPENDIX E EXPERIMENTAL MATERIAL PROPERTIES	171
	VITA	177

LIST OF FIGURES

		Page
Figure 2.1	Truss model idealization adapted from Kim and Mander (1999) for a fixed-fixed beam.....	18
Figure 2.2	Results of convergence study for different numerical integration schemes for C-STM analysis.....	23
Figure 2.3	Composition of classic arch and truss action that leads to the overall compatibility strut and tie model.....	26
Figure 2.4	Graphical illustration proportionality scalar in relation to L/jd and reinforcement ratios.....	30
Figure 2.5	Equivalent stress block analysis for doubly reinforced sections.....	33
Figure 2.6	Stress block variables as defined by Reddiar (2009)	37
Figure 2.7	Equivalent stress block analysis for singly reinforced sections	39
Figure 2.8	Constitutive stress-strain relationships.....	45
Figure 2.9	Mohr's circle for defining the principal tensile strain.....	51
Figure 2.10	Illustration of concrete softening.....	54
Figure 2.11	RC-Bent cap model used to verify C-STM.....	57
Figure 2.12	Progression of nonlinear behavior for Specimen 2A	60
Figure 2.13	Compression softening failure of Specimen 2A	62
Figure 2.14	Experimental vs. analytical results for Specimen 5D (top row) and 8G (bottom row), where (LC) – Longitudinal Cracking; (TC) – Transverse Cracking; (LY) – Longitudinal Yield; (TY) – Transverse Yield.....	64
Figure 2.15	Flexure, shear, and STM strength comparison.....	67

	Page
Figure 3.1	Prototype bridge bents and the evolution of the experimental specimen....72
Figure 3.2	Reinforcement details.....75
Figure 3.3	Details of the experimental setup.....78
Figure 3.4	Specimen instrumentation80
Figure 3.5	PHASE I – Serviceability loading (200 kip)82
Figure 3.6	PHASE I – Yield (440 kip)83
Figure 3.7	PHASE II – Ultimate load at (474 kip)84
Figure 3.8	Experimental photos of failure mechanism.....88
Figure 3.9	Force vs. overall displacement in conjunction with code based predictions90
Figure 3.10	Applied C-STM of C-Specimen – Phase I modeling.....92
Figure 3.11	Global force-deformation behavior94
Figure 3.12	Beam only (drift) response95
Figure 3.13	Nonlinear response and early concrete cracking effects97
Figure 3.14	Nonlinear concrete and steel response98
Figure 3.15	Failure analysis of compression softening effects.....101
Figure 3.16	Interaction of arch and truss action103
Figure 4.1	Illustrative force-deformation response of deteriorated concrete.....103

LIST OF TABLES

	Page
Table 2.1 Convergence study of higher order truss models for a cantilever beam.....	22
Table 2.2 Elastic truss member axial rigidities	42
Table 2.3 Concrete strengths and arch breadth scalar.....	58
Table 3.1 Mechanical properties of concrete.....	76
Table 4.1 Illustrative deteriorated concrete strengths	112

CHAPTER I

INTRODUCTION

1.1 Research Motivation

It is well known that the behavior of deep beams or disturbed (D-) regions in structural systems can no longer be described according to conventional Bernoulli beam theory alone. The high irregularity of internal stress and strain distributions, accompanied by the interaction of flexure and shear make it exceedingly difficult to evaluate the response of such structural elements. As a result, the shear analysis of structural concrete deep beams and beam-columns has been a contentious issue to both researchers and structural engineers for decades.

In order to address this problem, this thesis primarily focuses on developing a computational analysis method based on rational mechanics that can be used to demystify the current anomalies associated with analyzing the internal stress and strain fields of D-regions in reinforced concrete bridge piers. Building upon the existing body of knowledge, a compatibility based strut-and-tie model (C-STM) is presented that can be used to accurately model the force-deformation response and interrogate the internal response of highly cracked reinforced concrete members. Satisfying equilibrium, compatibility, and nonlinear constitutive laws of cracked reinforced concrete, the proposed C-STM serves as a minimalist computational model that will provide a

This thesis follows the style of *Journal of Structural Engineering*.

framework for the performance assessment of reinforced concrete bridge piers with deep or stocky members whose behavior is governed by D-regions.

This research also lays a pathway for further research to be conducted in order to evaluate: *i*) the effects of cyclic loading in D-regions; and *ii*) the structural integrity of reinforced concrete structures when subjected to premature concrete deterioration. This is presented in Chapter IV.

1.2 Research Objectives

To provide an adequate means of assessing the structural performance of reinforced concrete bridge piers, the major objectives of this research are outlined below:

- 1) To develop a computational means of analyzing reinforced concrete bridge piers using compatibility truss modeling techniques that is derived from rational mechanics. Existing theories are either heavily computationally involved and are difficult to implement, or are simplified to the point of providing over conservative estimations of the structures behavior. Hence the proposed model must be sufficiently accurate to capture the full nonlinear response, as well as elegantly simplified in order to be to be implemented by practicing engineers.
- 2) To then validate the proposed model through a direct and in-depth comparison between experimental and computational results based on previous and current research.

1.3 Organization of Thesis

This thesis is divided into four chapters that progressively describe the development, validation, and application of the proposed compatibility based strut-and-tie-model (C-STM).

The remainder of this chapter reviews the historical developments to date of shear analysis for deep beams and D-regions. This existing body of knowledge is used as a basis for developing the proposed C-STM.

Chapter II presents the theory and development of the proposed C-STM, which is then validated against previously conducted large-scale bent cap experiments.

Chapter III presents an experimental study on large scale bridge specimens. The experimental design, setup and results are presented and then analyzed using code-based methods and the proposed C-STM analysis for comparison.

Finally, Chapter IV provides a general summary, overall conclusions and recommendations of how the C-STM can be applied for future applications.

1.4 Historic Developments

A comprehensive review on the historical developments of truss modeling approaches was presented by the ASCE-ACI Committee 445 (1998). Based on this pre-existing body of knowledge, this section focuses on three truss modeling approaches that were considered to be applicable to the research presented in this thesis. This includes plastic truss modeling; shear panel modeling; and compatibility truss modeling (N.B. neither

finite element modeling (FEM) nor shear friction theory was considered in this study as they do not specifically pertain to truss modeling). Each modeling type is presented in chronological order. Subsequent to this is an overview of different methods that have been proposed for defining the geometry of truss models.

Plastic Truss Modeling

For concrete structures, the difficulty in dealing with flexure-shear interaction has long been recognized. More than 100 years ago, Ritter (1899) and Morsch (1909) independently dealt with the problem by converting a reinforced concrete beam into an equivalent reinforced concrete truss. This design problem is arguably the commencement of early plastic truss (or strut-and-tie) methods.

The Strut-and-Tie Model (STM) was later presented as a consistent modeling solution for the design of D-regions by Marti (1985). Schlaich et al. (1987) defined the behavior of beam (B-regions) and disturbed (D-) regions and recommended a strut-and-tie modeling approach based on the uncracked elastic force path as a consistent modeling solution. This led to the development of STM theory and was extensively promoted by MacGregor (1992) in his widely-used textbook. STM is also well suited for designing anchorage regions in prestress concrete structures as presented by Collins and Mitchell (1991).

Marti (1999) shows how STM, compression field, and limit analysis can be used to supplement each other in order to provide a consistent and rational means of evaluating the shear strength of structural concrete members. He concludes by stating

that the treatment of shear problems should correspond to the context to which they are applied, where different methods should be used depending on the task at hand.

Sritharan and Ingham (2003) developed a force transfer method (FTM) for the design and assessment of bridge joints subjected to in-plane seismic actions. This was based on similar principles to STM, but specifically used in the seismic performance of bridge joints subjected to shear and bending, as well as accounting for post-tensioning.

Alcocer and Uribe (2008) investigated the monolithic and cyclic behavior of four simply supported deep beams in order to validate the adequacy of using STM approaches for seismic design. They concluded that the response of each specimen exceeded the STM expectations in terms of strength, stiffness, and deformation capacity, and hence STM is appropriate for seismic design provided that the reversed cyclic shear and inelastic deformation demands do not exceed a specified criterion. This conclusion is flawed because only strength based predictions were made in comparison to experimental results, thus demonstrating that STM is insufficient for assessing the deformation demands of a structure. Instead, this research shows that inherent conservatism in STM design procedures was the reason for the acceptable cyclic response. This conservative approach should not be blindly used to design structural elements subjected to seismic conditions as deep beams are typically shear critical, hence brittle failure mechanisms may result if not carefully identified and accommodated for accordingly through capacity design principles.

Collins et al. (2008) uses an extensive database of previously conducted experimental shear tests to discuss the safety of shear provisions used in North America.

He concluded that current ACI shear provisions were unconservative for members with large effective depths or higher reinforcement ratios. An example of a thick transfer slab is used to illustrate that when using ACI 318-08 design procedures, a ductile flexural failure is predicted. Whereas in reality a brittle shear failure is more likely to occur using their recommendations. This further signifies the dangers associated with using STM design procedures purely as a means of design without truly understanding interacting and interdependent failure mechanisms (flexure, bond, anchorage etc) associated with shear behavior.

Kuo et al. (2010) presents a rational approach for defining the force transfer mechanism and shear strength of reinforced concrete beams. Their proposed analytical model considers the force transfer in beam (B-) and disturbed (D-) regions, thus different shear failure modes were defined for each region. Although their analytical model is based on a detailed flow chart that considers the member geometry, making it more cumbersome than current design methods, it was shown to be a more accurate approach for the shear analysis of structural elements.

In summary, since the development of the reinforced concrete truss analogy by Ritter (1899) and Morsch (1909), plastic truss modeling has predominantly been developed using strut-and-tie models. Typically used as a design tool, STM is purely a force-based approach that implicitly assumes a lower bound solution by establishing a plastic truss consisting of concrete compression struts and steel tension ties, satisfying both equilibrium and ultimate material strength requirements. Consequently the eventual mode of failure and overall deformability is often illusive to the designer as deformation

compatibility requirements are not part of the design or analysis process. Therefore, as shown by Collins et al. (2008), the incorrect application of STM could lead to the formation of an undesirable brittle shear failure mechanism.

Shear Panel Modeling

Mitchell and Collins (1974) first introduced the Compression Field Theory as a means to solve the unknown variables associated with the variable-angle truss model for an idealized reinforced concrete element. By applying equilibrium, compatibility, and constitutive stress-strain relationships of reinforced concrete materials, the angle of inclination of concrete struts θ and thus the concrete stresses can be determined (Collins 1978; Collins and Mitchell 1980).

Vecchio and Collins (1986) rectified the omission of the concrete tensile strength contribution with the proposed Modified Compression Field Theory (MCFT), where following parameters were proposed: (i) a constitutive material model for concrete in compression that accounted for compression softening effects; and (ii) a constitutive material model for cracked concrete in tension that accounted for tension stiffening effects.

In parallel to this, Mau and Hsu (1987) developed the Softened Truss Model assuming a uniform state of stress in a web shear element and idealizing the concrete compressive stresses as a series of parallel compressive struts. This model is also based on axioms of equilibrium and compatibility, and can be used to analyze a member

subjected to any combination of bending, axial load, shear and torsion (Hsu 1994; Hsu 1996).

The models above mentioned have been experimentally validated and have been demonstrated to accurately model reinforced concrete *panel elements* subjected to different applied states of stress. However, the practical application of these models remains irksome due to the mathematical implementation required. Moreover, the well-know arch and truss actions for shear resistance in beams cannot be easily uncoupled when the analysis essentially takes place on small panel elements.

Compatibility Truss Modeling

An extensive study was conducted by Dilger (1966) on the formulation of cracked elastic shear stiffness of reinforced concrete beams using constant angle continuum truss models. Using strain energy concepts of the analogous truss, the inclination of the compression struts can be determined and the shear distortions calculated using Williot's principles.

Paulay (1971a) investigated the interaction between flexure and shear demands, mechanisms of shear resistance, deformation characteristics, and elastic stiffness of thin webbed deep coupling beams. He was the first to model the contribution of truss action using a variable angle truss model where the elastic components of rotation were characterized as: Truss action, Arch action, Flexural rotations, and Beam elongation; where *Truss action* refers to the transfer of shear force to the transverse reinforcement through diagonal concrete struts that resembles a truss; *Arch action* pertains to the shear

force resisted by a single diagonal concrete strut; *Flexural rotations* is the flexural rotation of a plane section owing to the longitudinal reinforcement strains; and *Beam elongation* is the total elongation of the flexural reinforcement.

Kim and Mander (1999; 2000a; 2000b; 2005; 2007) extensively studied compatibility-based compound truss models to analyze the flexure-shear interaction of disturbed regions and thereby derive an analytic solution for the cracked elastic shear stiffness of concrete elements. They considered both constant and variable angle compound truss models, where the former is applicable to B-regions and the later represents the distribution of cracks in a D-region. Cyclic Inelastic Strut-Tie (CIST) modeling was introduced as a means of modeling the shear-flexure behavior of reinforced concrete beams using general-purpose inelastic computer software (Kim and Mander 1999; 2000a). This required the use of numerical integration schemes to effectively and efficiently select element models and the associated dimensioning of truss members.

Hwang et al. (2000) presented a softened strut-and-tie model for analyzing the shear strength of deep beams. Their truss model is composed of a diagonal, horizontal, and vertical shear resisting mechanism, where the diagonal mechanism consists of one diagonal concrete strut, and the horizontal and vertical mechanisms consist of one tie and two struts that engage the transverse steel. Although this method effectively considers compatibility, constitutive material relations, and softening effects of cracked reinforced concrete, it is unable to provide the global deformational behavior. Hence the model is still limited to predicting the overall force-displacement response.

To et al. (2001) developed a nonlinear strut-and-tie computational model to assess the behavior of reinforced concrete beams and rectangular hoops when subjected to monotonic loading. This was later developed to model the behavior of circular column (To et al. 2002). Their proposed modeling approach was experimentally verified against large-scale columns and portal frame experiments. Although the model effectively predicted the experimental force-deformation behavior, a trial-and-error procedure was required for defining the contribution of the concrete members in compression and tension, where some factors were based on comparisons between experimental and analytical results.

To et al. (2003) further refined their nonlinear strut-and-tie computational model to account for cyclic behavior of reinforced concrete structures using an idealized uniaxial fiber model. This was extended to modeling the hysteretic behavior of large scale interior beam-column joints as well as the dynamic response of a multistory concrete frame building system (To et al. 2009). This approach was demonstrated to be a very effective and efficient way of modeling the hysteretic response of structures. However, some of the definitions used for area and stiffness assignments were either arbitrarily reduced or based on comparisons between experimental and analytical results, making it difficult to be replicated by practicing engineers.

Zhu et al. (2003) proposed a compatibility-aided strut-and-tie model for predicting the diagonal crack widths at re-entrant corners of structures such as the dapped ends of bridge girders and ledges of inverted T bent caps. Using a stiffness based approach, two sub-trusses were used to obtain the combined response of inverted T

bent caps with flexural and diagonal rebars. This method illustrated how two truss mechanisms could be combined using displacement compatibility to predict the overall response. This model was used to predict the behavior of seven full-scale specimens each showing good agreement with experimental results.

Salem and Maekawa (2006) presented a computer-aided nonlinear strut and tie model to predict the response of one-quarter-scale simply supported bottom-loaded deep beams. They compared using linear and nonlinear finite element modeling techniques to establish the nonlinear STM geometry. They found that a linear-based nonlinear STM was 37% conservative in predicting the ultimate load, while the nonlinear-based nonlinear STM was only 8% conservative. Thus, they concluded that a nonlinear-based approach for defining the STM geometry provides a more economical design solution, as it allows for the internal redistribution of stresses due to material nonlinearity. The dilemma of this approach is that two separate models are required to get the final analysis: one FEM model to define the truss geometry; and then the nonlinear STM to analyze the response. This approach is not appealing to practicing engineers; furthermore, their proposed model did not show good post-yield agreement with all the experimental results.

Geometry of Truss Model

The primary difficulty associated with truss modeling approaches is the limitation of selecting a single truss model that captures the full force-deformation over a range of both elastic and inelastic response. Due to the highly complex nature of D-regions and

the inelastic redistribution of internal forces at ultimate failure, the issue of defining a truss geometry that is appropriate for analysis of shear critical members has been disputed among researchers.

Drucker (1961) first introduced the concept of stress fields as a limit analysis for structural concrete members. Later developed by Thürlimann et al. (1983), stress fields were used to establish effective concrete nodal and strut stresses based on the theory of plasticity, truss geometry, and the type of stress field within the structure. An application of this method was proposed by Schlaich et al. (1987), where elasticity considerations were used to provide a simple and consistent strut-and-tie model. Hwang et al. (2000) define the lever arm between the tension and compression chord truss members using elastic bending theory. They justify this by stating that it simulates a situation where deep beams fail in shear with reserve flexural capacity still remaining.

In contrast to this, other researchers [eg., MacGregor (1992), Yun (2000), Sritharan and Ingham (2003), Salem and Maekawa (2006)] contend that the use of elastic stress analysis is inappropriate when assessing the ultimate limit state of a structure due to highly nonlinear development of strains associated with D-regions. To et al. (2009) proposed using a *first yield limit state* analysis corresponding with B-regions, and an *ultimate limit state* analysis in D-regions. However the exact method of identifying the truss geometry is not specifically presented.

Current design codes are also vague on the definition of the compression chord (or CCC node) location. This is typically achieved by satisfying effective nodal stresses

in the concrete. As a result, classical STM practice typically neglects the contribution of compression steel, resulting in unduly large node sizes and conservative plastic truss solutions.

Summary

This section has demonstrated that previously proposed shear panel and compatibility-based truss models (or strut-and-tie models) can be used as very powerful analysis tools for accurately predicting the shear behavior of deep beam and D-regions in comparison to the plastic truss. However the majority of these models are either: computationally involved and difficult for practicing engineers to replicate; require nonlinear structural analysis software not commonly available to engineering firms; or are not versatile and thus cannot be applied to a variety of structures.

In light of this, the primary objective of this research is to develop a compatibility-based strut and tie model that is sufficiently accurate to capture the full nonlinear response of reinforced concrete structures, as well as elegantly simplified in order to be implemented by practicing engineers. This research is an extension of the research conducted by Kim and Mander (1999; 2005; 2007) and is adapted specifically for the behavior of bridge piers with stocky members and/or large disturbed regions.

CHAPTER II

COMPUTATIONAL TRUSS MODELING OF SHEAR CRITICAL STRUCTURAL CONCRETE SYSTEMS

This chapter presents a *Compatibility Strut-and-Tie Model (C-STM)* that is intended for analyzing the nonlinear force-deformational behavior of disturbed regions and structural concrete deep beams and beam-columns. The model is implemented in commercially available structural nonlinear analysis software in order to predict the structures nonlinear response. An in-depth comparison between experimental and computational results is made to validate the model and illustrate how it can be used to predict the hierarchy of failure mechanisms of the structure. Supplementary to this chapter is a user manual for implementing the C-STM into structural analysis software, this can be found in Appendix A.

2.1 Chapter Scope and Background

Due to the complex nature of shear behavior in reinforced concrete deep beams and D-regions, conventional U.S. design standards have historically been based on empirically derived expressions. The concept of strut-and-tie modeling (STM) was introduced as a method of strength design in the AASHTO LRFD Bridge Design Specification in 1994, and ACI 318 in 2002 for bridges and buildings, respectively. However, as STM only satisfies force equilibrium and is intentionally formulated as a lower bound (plastic) solution, the critical mode (flexure, shear, bond, anchorage) or location of failure (i.e. element or node failure) is often illusive to the designer. Thus the ultimate failure mechanism might be an undesirable brittle collapse due to imposed overload scenarios.

Current nonlinear models of shear analysis in structural concrete deep beams, previously discussed, are generally complicated to use and have limited applicability or appeal to practicing engineers. Clearly, it is desirable to have a model that is derived from rational mechanics, validated with experimental evidence, and easy to implement as a supplementary tool for capacity analysis purposes.

This chapter presents a *Compatibility Strut-and-Tie Model* (C-STM) that is implemented in commercially available structural analysis software, SAP2000 (1995), to predict the nonlinear response of reinforced concrete deep beams and D-regions. The model is used to analyze the behavior of previous experimental studies in order to validate the model and illustrate how it can be used to predict the hierarchy of failure mechanisms of the structure. This research supplements previous work by Kim and Mander (1999; 2005; 2007), and is adapted specifically for the behavior of cantilevered bridge bents.

2.2 Research Significance

Current U.S. practice for the design of deep beams and D-regions applies strut-and-tie principles to evaluate the shear strength of a structure. As a result, current codes (AASHTO LRFD, 2008; and ACI 318-08, 2008) use an iterative lower bound (plastic) truss method that satisfies force equilibrium and stress checks of the elements and nodal regions. Consequently the eventual mode of failure and overall deformability is often illusive to the designer as deformation compatibility requirements are not part of the design or analysis process. This research presents a computational method of analyzing

the flexure-shear interaction of deep beams and disturbed regions with particular emphasis on cantilevered reinforced concrete bridge bent caps. In addition to the normal strut-and-tie force equilibrium requirements, the proposed C-STM accounts for nonlinear behavior through displacement compatibility using inelastic constitutive material relations for cracked reinforced concrete. The intention of this research is to provide a minimalist computational model that can accurately assess the structural force-deformation response of a structure, identifying the progression of nonlinear behavior that results in an ultimate collapse mechanism. The C-STM is not intended to supplant present force-based strut-and-tie design methods, but rather supplement existing design approaches as an advanced performance-based analysis method for checking and identifying failure modes and overall deformability.

2.3 Numerical Truss Modeling

As described by Paulay (1971a), the total shear of a deep reinforced concrete beam is resisted by truss and arch action. This section specifically focuses on *truss modeling* pertaining to the force transferred to the transverse reinforcement through diagonal concrete struts that resembles a truss.

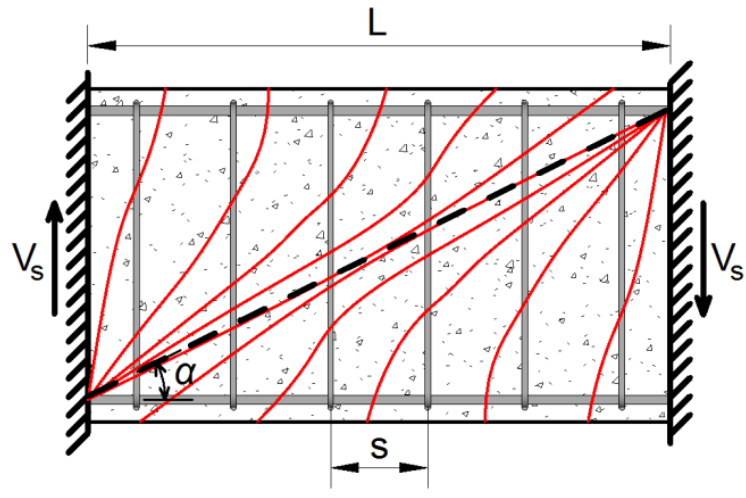
Discrete Truss Modeling

Figure 2.1 (a) illustrates the variable angle crack pattern that typically forms in disturbed regions of reinforced concrete deep beams. After the development of first cracking, compression struts acting through the concrete form diagonal concrete struts that are tied together by the reinforcing steel thus forming a truss model. Starting with a differential truss, Kim and Mander (1999; 2007) integrated this to form a so-called “continuum truss” where cracking is implicitly smeared. By separating the elastic and flexural deformation contributions of their truss model, they were able to show that the shear stiffness of a cracked fixed-fixed beam can be assessed as follows:

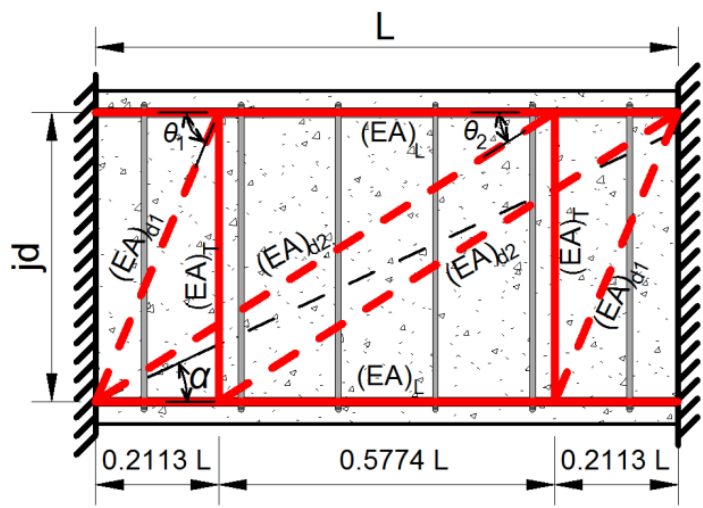
$$K_{s,approx}^{continuum} = \frac{n\rho_v \cot^2 \alpha}{1 + 4n\rho_v (1 + 0.39 \cot^2 \alpha)^2} E_c A_v \quad (2.1)$$

in which n = the modular ratio of steel to concrete (where $n = E_s/E_c$, E_s and E_c are Young’s Modulus for steel and concrete, respectively); $\rho_v = A_{sh}/sb_w$ is the volumetric ratio of shear steel to concrete area over one hoop spacing (where A_{sh} = area of one set of stirrups; s = stirrup spacing; and b_w = section width); $\cot \alpha = L/jd$ = section aspect ratio (where jd = internal lever arm, and L = member length); $A_v = b_w d$ is the shear area of concrete; and d = effective section depth.

To enable the analysis of specific structures, alternative numerical integration schemes were also considered by Kim and Mander (1999) and explored further herein. For a fixed-fixed beam, the simplest of these numerical integration schemes uses two-point Gaussian quadrature leading to a so-called two-point Gauss Truss shown in Figure



(a) Discrete representation



(b) Two-point Gauss truss

Figure 2.1: Truss model idealization adapted from Kim and Mander (1999) for a fixed-fixed beam

2.1 (b); where the solid lines represent tension ties, and the dashed lines represent diagonal concrete struts in compression. Through experimental and analytical validation, this two-point Gauss Truss was found to be a suitably accurate numerical integration scheme for capturing both shear and flexure deformations of disturbed regions with fixed-fixed end conditions. Higher order numerical schemes were also considered by Kim and Mander (1999), however the two-point Gauss Truss model has the appeal of being statically determinate (due to anti-symmetry).

The ultimate shear resistance was decomposed into the well-known three-component sectional shear model and proportioned according to strength:

$$V_u = V_s + V_c + V_p \quad (2.2)$$

in which V_s = shear contribution of the transverse reinforcement; V_c = shear contribution of tensile stress in the concrete; and V_p = shear carried by the axial compression, where

$$V_s = A_{sh} f_{yh} \frac{jd}{s} \cot \theta \quad (2.3)$$

$$V_c = \beta \sqrt{f'_c} b_w d \cot \theta \quad (2.4)$$

$$V_p = P \tan \alpha \quad (2.5)$$

in which f_{yh} = yield strength of transverse reinforcement; θ = crack angle measured to the longitudinal axis of the element; β = strength factor depending on the tensile capacity of the concrete; d = effective section depth; and P = applied axial load.

Paulay (1971a; 1971b) related a portion of the vertical shear force resisting mechanism in shear coupling beams to a concrete corner-to-corner ‘arch action’ mechanism. The V_p contribution in Eq. (2.5) refers to the enhanced shear strength with an applied axial load via a combination of this corner-to-corner arch action and the postulated compression field of a diagonal strut from an applied axial load. As a result, the model proposed by Kim and Mander (1999) is more specific for modeling axially loaded beam and column members, and may not sufficiently capture arch action for deep beam members without axial load. This research aims to rectify this absence of arch action in deep beam members and D-regions without an applied axial load, and derives an alternative approach to define the interaction of arch to truss action.

Truss Modeling Integration Schemes for Cantilevered Beams

By taking only one-half of an anti-symmetric fixed-fixed beam that is represented by the two-point Gauss Truss, a statically determinant cantilever remains which can be represented by a so-called *Single-Point Gauss Truss*. However, due to its simplicity, the question of numerical accuracy remains.

A convergence study of higher order numerical integration schemes was conducted in order to verify the accuracy of the proposed single-point Gauss truss. Based on recommendations of Kim and Mander (1999, 2007), the axial rigidities assigned to each truss member at the i^{th} integration point are given by:

$$(EA)_{Ti} = \omega_i E_s A_{sh} \frac{L}{s} \quad (2.6)$$

$$(EA)_{di} = \frac{0.5\omega_i}{\sqrt{x_i + \tan^2 \alpha}} E_c A_v \quad (2.7)$$

$$(EA)_L = A_L E_s \quad (2.8)$$

in which $(EA)_{Ti}$ = axial rigidity of the vertical transverse ties; $(EA)_{di}$ = axial rigidity of the diagonal concrete struts; $(EA)_L$ = axial rigidity the longitudinal tension ties; x_i = normalized coordinate of the i^{th} integration point, ω_i = numerical weight factor for transverse reinforcement; and A_L = is the sectional area of steel assigned to the longitudinal tension tie.

Table 2.1 presents the four different numerical integration schemes that were considered: single, two, and three-point Gauss quadrature, and Boole's rule, where an illustration of each integration scheme is provided in Figure 2.2. The right column of Table 2.1 presents the relative elastic shear stiffness (K) of each truss normalized with respect to the two-point Gauss Truss. Although some variability between schemes exists, it can be concluded that any reasonable integration scheme may be used to provide a satisfactory representation of shear stiffness. However, a more in-depth study should be considered to compare the flexure-shear interaction between truss models.

Table 2.1: Convergence study of higher order truss models for a cantilever beam

Numerical Scheme	i	x_i	ω_i	$\frac{K_{Truss}}{K_{2-point}}$
Single-Point Gauss	1	0.42265	1	1.0429
	2	0.57735	1	
Two-Point Gauss	1	0.21132	0.5	1.0000*
	2	0.78868	0.5	
Three-Point Gauss	1	0.11270	5/18	1.0007
	2	0.50000	8/18	
	3	0.88730	5/18	
Boole's Rule	1	0.00	7/90	0.9371
	2	0.25	32/90	
	3	0.50	12/90	
	4	0.75	32/90	
	5	1.00	7/90	

* Continuum model, Eq. (2.1), calculated a relative stiffness of 1.0431

A 3ft. by 2ft. illustrative cantilevered deep beam is considered for analysis with longitudinal and transverse reinforcing ratios of 0.010 and 0.003 respectively. Figure 2.2 shows the force-deformation responses of each truss model normalized with respect to the two-point Gauss Truss solution considering the following nonlinear failure mechanisms: (a) flexure steel yielding; (b) transverse steel yielding; and (c) concrete crushing. Each truss is modeled using commercial structural analysis software (SAP2000 1995), and considers nonlinear stress-strain relationships for steel and concrete as a bi-linear response with a 3% strain hardening stiffness, and an elasto-plastic response with a maximum compression stress of $0.85 f_c'$ respectively.

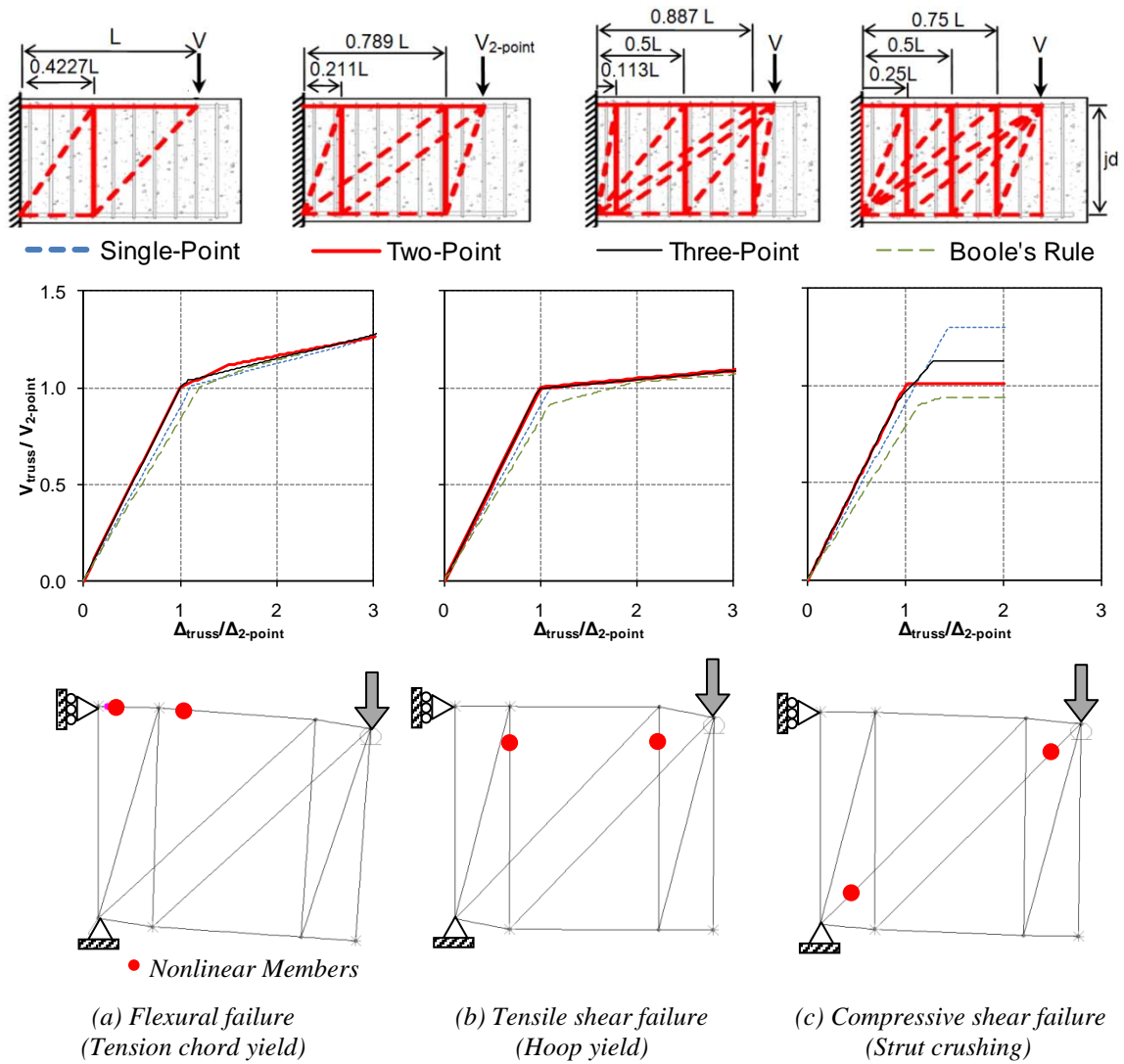


Figure 2.2: Results of convergence study for different numerical integration schemes for C-STM analysis

When nonlinear behavior is governed by longitudinal tensile steel yielding (Figure 2.2 (a)), the post-yield response is ductile. Despite similar yield strengths, the single-point Gauss Truss model resulted in a slightly more flexible elastic stiffness than the higher order Gauss quadrature truss models. The Boole's truss was the most flexible of the truss models and provided a slightly lower initial yield strength, but had a similar post yield response.

When nonlinear behavior is governed by transverse steel yielding (Figure 2.2 (b)), similar stiffness results were obtained. However the post yield stiffness was less than that with longitudinal steel yielding. This shows that yielding of the transverse reinforcement can increase shear deformations which can result in the formation of other shear critical mechanisms such as sliding shear or concrete softening, discussed in subsequent sections.

When nonlinear behavior is governed by strut crushing (Figure 2.2 (c)), the ultimate strength had a variation up to 30% with the single-point truss giving the largest difference. An elasto-plastic response of concrete was used for illustrative purposes only and does not accurately model concrete crushing, hence the response of each was stopped at a ductility of two.

In summary, the single-point Gauss Truss proved to be a sufficiently accurate model for considering the nonlinear flexure-shear interaction relative to the higher order truss models. However, if strut crushing is expected, a convergence study is recommended to ensure the single-point Gauss Truss does not over-estimate the failure mechanism.

2.4 Arch vs. Truss Action in C-STM

It is well known that concrete shear resistance can be conceived of as two complementary resistance mechanisms: arch and truss action (Park and Paulay 1975; Paulay 1971a). To model each of these shear resisting mechanisms, the load path for an applied point load can be decomposed into: (a) arch action through the center of the section, and (b) truss action engaging the transverse steel along with a tube of concrete around the member perimeter, as illustrated in Figure 2.3.

Arch action (presented in Figure 2.3 (a)), consists of a compressive stress field forming the main diagonal concrete strut (idealized as a dashed line in Figure 2.3 (a)) that passes through the center of the section. Following the approach of Holden et al. (2003) the strut is assumed to have a parabolic stress distribution with a width W_A that is proportional to the depth and length of the beam and is defined in subsequent sections. This approach is similar to that proposed for coupling beams by Paulay (1971a). The free end of the strut is connected to the tension tie (longitudinal reinforcement, idealized as a solid line).

Truss action (presented in Figure 2.3 (b)), specifically pertains to the shear mechanism engaging the transverse reinforcement as defined by Paulay (1971a). Diagonal compression struts are ‘smeared’ along the line of the stirrup legs (idealized as dashed lines) and are tied back into the member by transverse reinforcement ties (idealized as solid lines). Truss action can be represented through any valid truss model. However, in light of the foregoing convergence study, a single-point Gauss truss will be adopted for the remainder of this chapter.

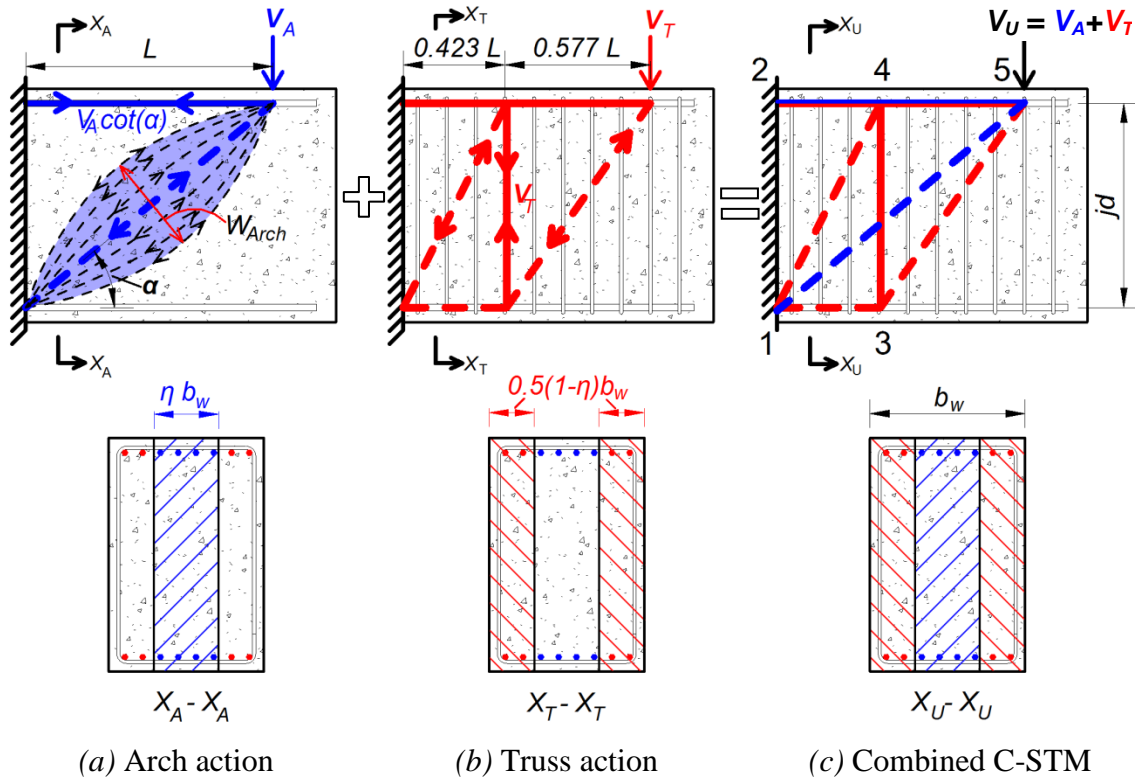


Figure 2.3: Composition of classic arch and truss action that leads to the overall compatibility strut and tie model

The combined C-STM (presented in Figure 2.3 (c)), is the amalgamated response of arch and truss action, where displacement compatibility is inherently accounted for such that the two mechanisms work in parallel to one another. A method of apportioning the relative contributions of arch and truss action is described below.

Different methods of allocating the shear resisting mechanisms have previously been proposed based on the following parameters: (i) strength (Kim and Mander 1999; Paulay 1971a); (ii) stiffness (Zhu et al. 2004); (iii) geometry (Hwang et al. 2000); or (iv) the shear span-to-internal lever arm ratio (in accordance with the FIP-Commission 3. (1996) recommendations). An investigation into the merits of each of these strategies was conducted, and the following conclusion was drawn: the relative proportions of arch and truss action was minimal with respect to the elastic force deformation response, however significant differences in the nonlinear response of the flexure and shear failure mechanisms were observed. Similar observations were concluded by Paulay (1971a), who found that the total elastic rotations owing to truss and arch actions for a given beam were about the same, irrespective of the relative proportions.

Hence it is considered necessary to apportion the arch and truss mechanisms according to the longitudinal and transverse reinforcement ratios, in order to accurately model the flexure and shear responses, respectively. An arch breadth scalar η was used to apportion the section breadth (shown in the cross-sections of Figure 2.3), and is defined by the following ratio:

$$\eta = \frac{V_{Arch}}{V_{Arch} + V_{Truss}} = \frac{\rho_L}{\rho_L + \rho_T j \cot^2 \alpha} \quad (2.9)$$

in which V_{Arch} = shear resisted by arch action over the entire section and is proportional to the longitudinal reinforcement given below; and V_{Truss} = shear resisted by truss action over the entire section and is proportional to the transverse reinforced given below:

$$V_{Arch} = f_y A_L \tan \alpha = \rho_L f_y b_w d \tan \alpha \quad (2.10a)$$

$$V_{Truss} = f_y A_{sh} L / s = \rho_T f_y b_w j d \cot \alpha \quad (2.10b)$$

where $\rho_L = A_L / b_w d$ is the volumetric ratio of longitudinal steel to concrete; A_L = is the area of longitudinal reinforcement contributing to the tension tie; $\rho_T = A_{sh} / b_w s$ is the volumetric ratio of transverse steel to concrete over one hoop spacing; and j = the internal lever arm coefficient which in lieu of a more precise analysis may be taken as $j = 0.9$. It should be noted that Eq. (2.9) is based on the assumption that f_y is constant for longitudinal and transverse steel.

The total shear resistance of the combined C-STM, as shown in Figure 2.3 (c), can now be defined as:

$$V_u = V_A + V_T \quad (2.11)$$

where V_u = the total applied shear force; V_A = is the contribution of arch action; and V_T = is the contribution of truss action.

In order to maintain deformation compatibility and equilibrium between the arch and truss mechanisms, it is assumed that the section breadth b_w is proportioned according to the component strength as follows

$$\frac{V_a}{V_u} = \frac{\eta b_w}{b_w} ; \quad \frac{V_t}{V_u} = \frac{(1-\eta)b_w}{b_w} \quad (2.12)$$

where ηb_w = the arch breadth, and $(1-\eta)b_w$ = the truss breadth as shown in the cross sections of Figure 2.3 (c).

Figure 2.4 illustrates the results of the arch breadth scalar η (Eq. (2.9)) when plotted against L/jd with varying ratios of transverse to longitudinal reinforcement. As one might intuitively expect, this relationship shows that arch action is more prominent in beams with smaller L/jd and ρ_T/ρ_L ratios, while truss action has more of an effect in beams with larger L/jd and ρ_T/ρ_L ratios. Others have made similar conclusions (Hsu 1996).

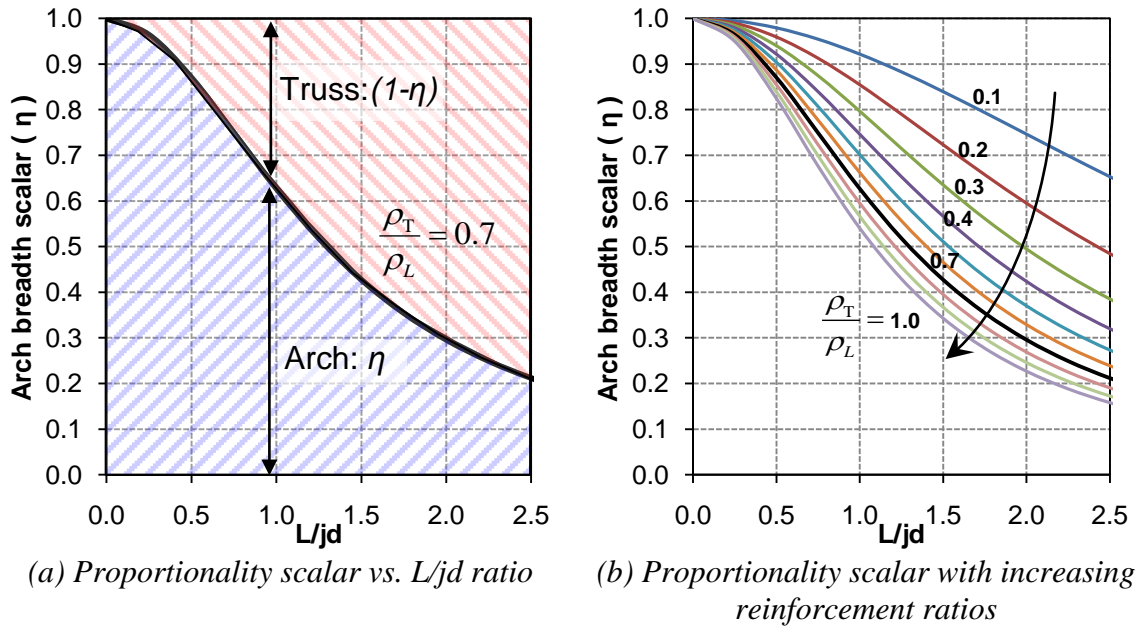


Figure 2.4: Graphical illustration proportionality scalar in relation to L/jd and reinforcement ratios

2.5 Stress and Strain Transformation for Flexural Equivalence

A primary difficulty associated with accurate truss modeling approaches is the limitation of selecting a single truss model that captures the full force-deformation over a range of both elastic and inelastic response. In reality, the concrete neutral axis depth varies with increasing moment demand, thus shifting the centroid of the concrete resultant force.

However, when using numerical truss modeling techniques, the compression and tension flexural chord members (member 1-3, and 2-4-5, respectively in Figure 2.3 (c)), have a fixed internal lever arm jd throughout the analysis. Hence it is not possible to replicate the increasing lever arm associated with the concrete force resultant. Therefore, for the C-STM, an internal lever arm depth must first be assumed, and then the stress-strain constitutive material relationships need to be transformed accordingly in order to provide an equivalent force that provides a comparable sectional moment.

The significance of this transformation is to ensure that concrete compression force obtained by the C-STM chord member is in accordance with standard stress-block analysis and incorporated over the entire range of loading. Given the limitations of truss modeling, the method described in the following provides a rational solution to modeling the combined response of steel and concrete in the compression chord members.

In comparison, previously proposed models either: ignore the presence of compression steel [MacGregor (1992) and other classical strut and tie modeling approaches]; or assumes a uniform strain in the concrete compression zone by modeling the concrete compression chord axial rigidity as $EA = E_c(cb)$, thus over predicting the chord members stiffness [To et al. (2001, 2009)].

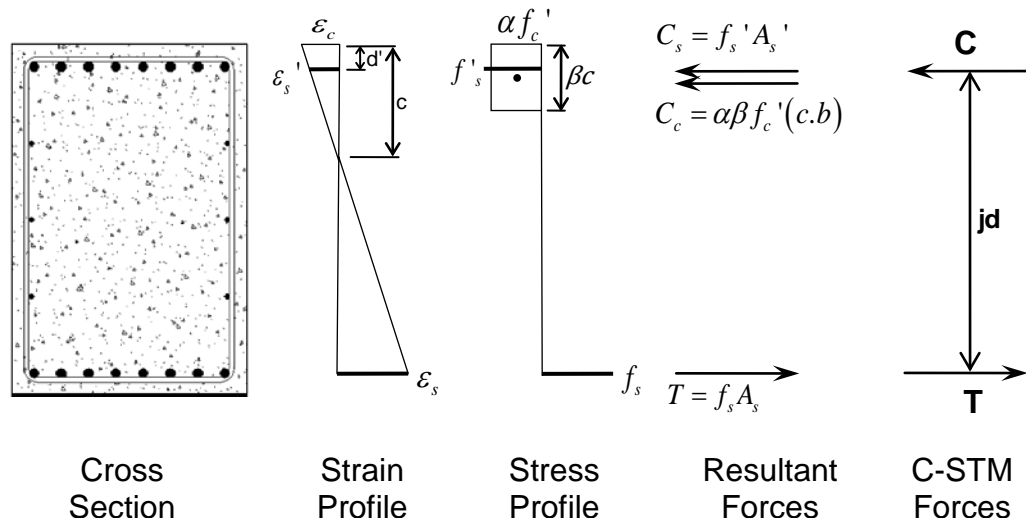
The following presents the theory for defining the top and bottom chord members for doubly and singly reinforced sections using stress block analysis techniques to make this required transformation.

Stress Block Analysis for Doubly Reinforced Beams and Columns

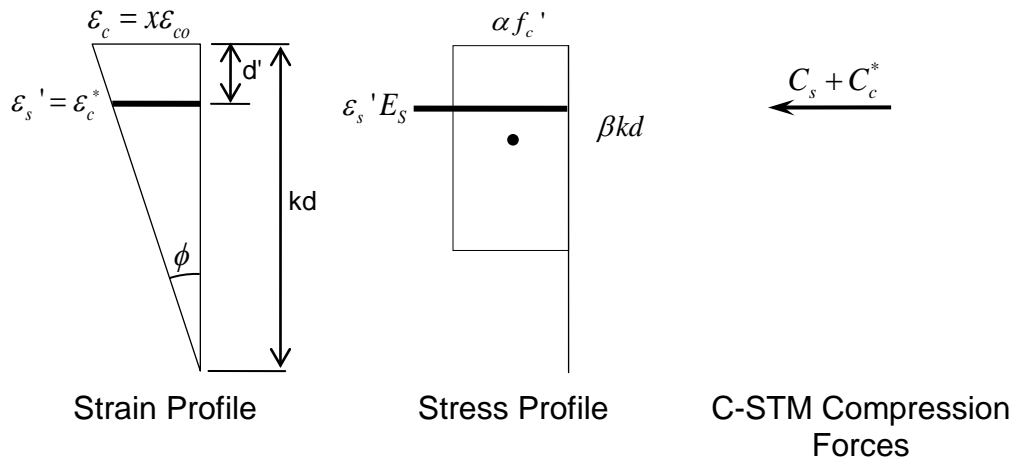
For doubly reinforced sections, it is proposed that the C-STM flexural chord members be aligned with the respective steel centroids so that the internal lever arm is represented as $jd = d - d'$, where d and d' are the respective centroids of the tension and compression steel. A similar approach was used and validated by Kim and Mander (1999) in order to incorporate cyclic behavior. However, because the centroids of the steel compression force (C_s) and the concrete compression force (C_c) may not coincide, it is necessary to adjust the concrete constitutive material properties accordingly so that the transposition of the concrete element force C_c will provide a similar moment in order to satisfy the sectional moment capacity throughout the analysis.

Figure 2.5 (a) shows an elastic stress block analysis performed on a doubly reinforced concrete section assuming plane sections remain plane purely for the purposes of defining the concrete compression force. The neutral axis depth c can be defined such that $c = kd$, where k is the well-known elastic compression zone coefficient for beams given by Eq. (2.13) (Park and Paulay 1975)

$$k = \sqrt{(\rho + \rho')^2 n^2 + 2(\rho + \rho' d'/d)n} - (\rho + \rho')n \quad (2.13)$$



(a) Stress block analysis of a doubly reinforced concrete section after cracking



(b) Transformed stress block for strains measured at compression steel centroid

Figure 2.5: Equivalent stress block analysis for doubly reinforced sections

For column members an additional modification is made to allow for the axial force given by Eq. (2.14) (Arnold 2004).

$$k = \sqrt{\left(\rho + \rho' + \left(\frac{P}{f_c'bd}\right)\left(\frac{f_c'}{f_s}\right)\right)^2 n^2 + 2\left(\rho + \rho'\left(\frac{d'}{d}\right) + \left(\frac{P}{f_c'bd}\right)\left(\frac{f_c'}{f_s}\right)\right)n - \left(\rho + \rho' + \left(\frac{P}{f_c'bd}\right)\left(\frac{f_c'}{f_s}\right)\right)n} \quad (2.14)$$

where d = the effective depth of the beam from the extreme concrete compression fiber to the centroid of the tension steel; d' = the depth from the extreme compression fiber to the centroid of the compression reinforcement; ρ = the ratio of tension reinforcement; ρ' = the ratio of compression reinforcement; n = the modular ratio of steel to concrete; b = the section breadth; f_c' = concrete compression strength; and P = column axial force.

Because the C-STM compression chord member is located at the steel centroid, a transformation of the concrete stress block force C_c is required to convert it to an equivalent C-STM force as shown in Figure 2.5 (b). Section equilibrium requires

$$P = (C_s + C_c^*) - T \quad (2.15)$$

in which $T = A_s E_s \varepsilon_s$ (where A_s = representative area of longitudinal tension steel, and ε_s = tensile steel strain); $C_s = A_s' E_s \varepsilon_s'$ (where A_s' = representative area of longitudinal compression steel, and ε_s' = compression steel strain); and C_c^* = transformed concrete force discussed below. This analysis assumes concrete tensile effects are zero at the ultimate limit state.

The effective concrete strain ε_c^* measured by the C-STM chord member can be defined in terms of the extreme compressive concrete strain using the following strain compatibility relationships:

$$\phi = \frac{\varepsilon_c}{kd} = \frac{\varepsilon_c^*}{kd - d'} = \frac{\varepsilon_s'}{kd - d'} \quad (2.16a)$$

$$\therefore \varepsilon_c^* = \varepsilon_s' = \varepsilon_c \left(1 - \frac{d'}{kd}\right) \quad (2.16b)$$

Hence, the concrete compression force can be expressed in terms of equivalent concrete stress block and related to $\varepsilon_s' = \varepsilon_c^*$ as follows:

$$C_c = \alpha\beta f_c'(kd.b) = \varepsilon_c^* \psi E_c A_c \quad (2.17)$$

where $A_c = kd b$ is the area assigned to the concrete chord element; ψ = a compatibility correction scalar; ε_c^* = concrete compression chord strain; and $\alpha\beta$ = the stress block parameters used to define the equivalent stress block, where α = effective average concrete stress ratio, and β = effective stress block depth factor.

Rearranging Eq. (2.17) and substituting Eq. (2.16b), the compatibility correction scalar can be expressed as:

$$\psi = \frac{\alpha\beta f_c'}{\varepsilon_c^* E_c} = \frac{\alpha\beta}{\left(1 - \frac{d'}{kd}\right) \frac{\varepsilon_c}{\varepsilon_{co}}} \frac{f_c'}{E_c \varepsilon_{co}} = \frac{\alpha\beta}{\left(1 - \frac{d'}{kd}\right)^{xn}} \quad (2.18)$$

in which $x = \varepsilon_c / \varepsilon_{co}$ is the normalized concrete compression strain at the extreme compression fiber; $\varepsilon_{co} = 0.002$; and n is defined as:

$$n = \frac{E_c \varepsilon_{co}}{f_c'} = \frac{5000 \sqrt{f_c'(MPa)} 0.002}{f_c'} = \frac{10}{\sqrt{f_c'(MPa)}} \equiv \frac{120}{\sqrt{f_c'(psi)}} \quad (2.19)$$

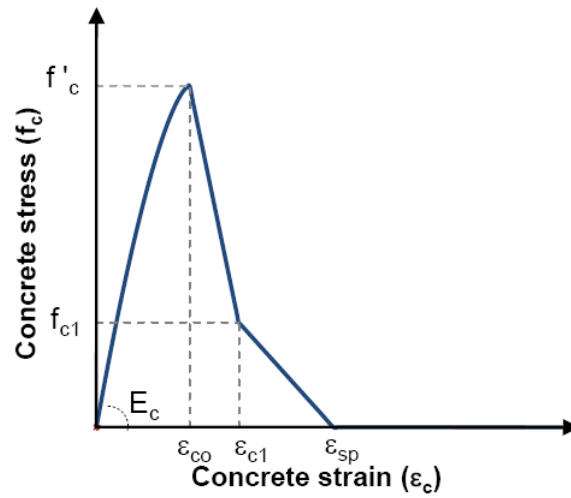
where $E_c = 5000 \sqrt{f_c'(MPa)} = 60000 \sqrt{f_c'(psi)}$ is the initial tangent modulus in accordance with Mander et al. (1988).

Now the only remaining unknown variables in Eq. (2.18) are $\alpha\beta$ and x . The nonlinear relationship between these two stress block variables is shown in Figure 2.6 according to research conducted by Reddiar (2009) (note: concrete strengths are in metric). This shows a linear relationship between $\alpha\beta$ and x up to the coordinates $(x, \alpha\beta) = (0.7, 0.5)$.

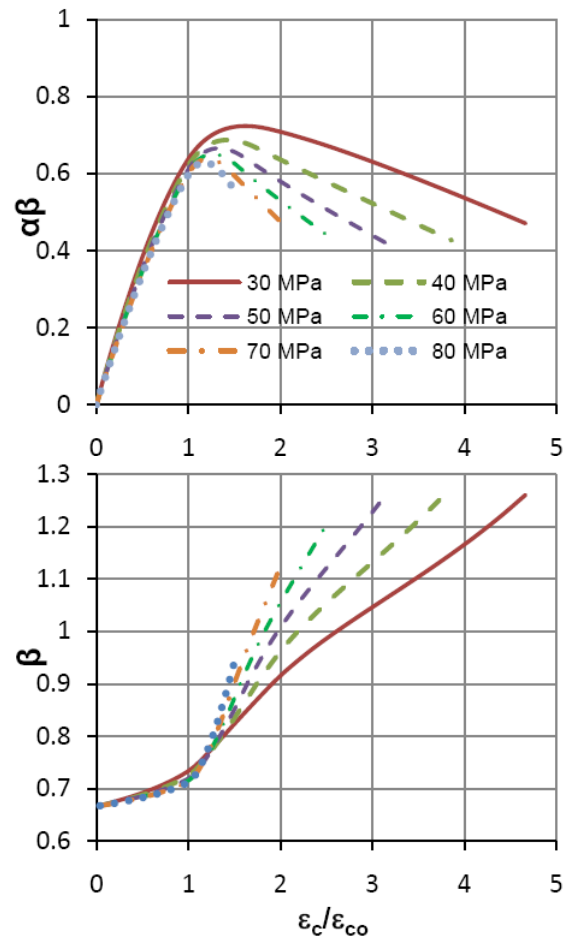
Substituting these coordinates into Eq. (2.18) as well as the expressions defined in Eq. (2.19), the elastic compatibility correction scalar ψ_E can be expressed as:

$$\psi_E = \frac{\sqrt{f_c'(psi)}}{168(1-d'/kd)} \equiv \frac{\sqrt{f_c'(MPa)}}{14(1-d'/kd)} \quad (2.20)$$

The original expression in Eq. (2.17) shows that the force measured in the C-STM concrete is directly related to the compression chord strain ε_c^* , where the concrete stiffness is modified using the elastic compatibility correction scalar.



(a) Stress-strain relationship $f'_c = 60$ MPa



(b) Alpha-Beta and Beta stress block parameters

Figure 2.6: Stress block variables as defined by Reddiar (2009)

$$C_c = \varepsilon_c^* (\psi_E E_c) A_c \quad (2.21)$$

where the axial rigidity assigned to the C-STM concrete element is $EA = \psi_E E_c A_c$.

Further detail of the transformed nonlinear constitutive material relationships applied to the concrete chord members is provided in subsequent sections.

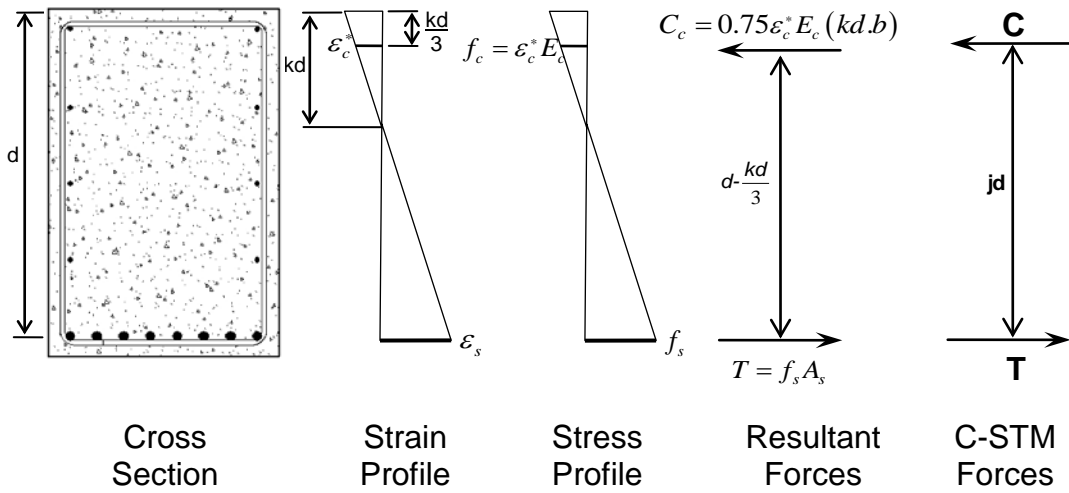
Stress Block Analysis for Singly Reinforced Beams

For singly reinforced beams that do not exceed the elastic limit in the concrete compression stress block, the internal lever arm can be represented using an elastic analysis such that $jd = d - kd / 3$ (as shown in Figure 2.7 (a)). In a similar manner to before, the resultant concrete compression force can be defined as:

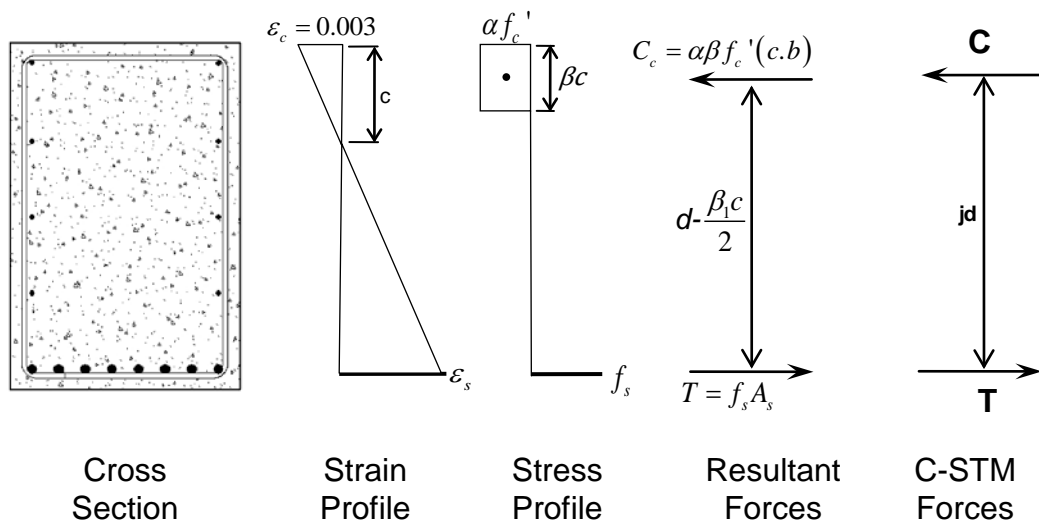
$$C_c = \varepsilon_c^* (\psi_E E_c) A_c = 0.75 \varepsilon_c^* E_c A_c \quad (2.22)$$

where $A_c = kdb$ is the area assigned to the concrete chord element; $\psi_E = 0.75$ is the compatibility correction scalar obtained from the assumed triangular elastic stress block; ε_c^* = C-STM concrete compression chord strain measured at a depth of $kd / 3$ below the extreme compression fiber.

For nodes where compression failure is likely, a more appropriate representation of the internal lever arm may be defined using an ultimate limit state analysis such that $jd = d - \beta_1 c / 2$ (as shown in Figure 2.7 (b)), where β_1 is the normal code-based stress block factor, and c is the neutral axis depth calculated by satisfying section equilibrium.



(a) Stress block analysis of singly reinforced section in service load range



(b) Stress block analysis of singly reinforced section at ultimate limit state

Figure 2.7: Equivalent stress block analysis for singly reinforced sections

For this case, a similar stress block analysis to that conducted for the doubly reinforced case can be used. It is important to note that β_1 is used to approximate the location of the C-STM compression chord member in order to obtain an internal lever arm that is representative of the ultimate limit state. Whereas $\alpha\beta$ is used to approximate the force of the equivalent concrete stress block as the strain increases.

In a similar manner to the derivation of the doubly reinforced concrete stress block, the effective concrete strain ε_c^* measured by the C-STM chord member can be defined as:

$$\varepsilon_c^* = \varepsilon_c \left(1 - \frac{\beta_1}{2} \right) \quad (2.23)$$

Thus the elastic compatibility correction scalar ψ_E can be expressed as:

$$\psi_E = \frac{\sqrt{f_c'}(\text{psi})}{168(1 - \beta_1/2)} \equiv \frac{\sqrt{f_c'}(\text{MPa})}{14(1 - \beta_1/2)} \quad (2.24)$$

2.6 C-STM Truss Geometry and Axial Rigidity Assignments

The C-STM shown in Figure 2.3 (c) can be adapted for any deep beam or disturbed region and modeled using structural analysis software. Each member in the C-STM is comprised of two elements that model the individual behavior of steel and concrete in that member. The two elements are constrained together in order to give the combined steel-concrete response. The C-STM requires the following parameters to be defined in order to model the constitutive behavior of truss members: (i) truss geometry to define

the member force; and (ii) axial rigidities of the steel and concrete elements to define elastic deformations.

Truss Geometry

As previously discussed, the primary difficulty associated with accurate truss modeling is the limitation of selecting a single truss model that captures the full force deformation over a range of both elastic and inelastic response. The truss geometry is defined by first locating the compression and tension chord members in the beam and column members. This is done in accordance with the foregoing section, where the location of the compression chord member varies for doubly and singly reinforced sections.

The horizontal positioning of the boundary nodes is either defined by: (i) an applied load/bearing support (i.e. Node 5 in Figure 2.3 (c) is defined by the centroid of the applied load); or (ii) at the intersecting lines of thrust from the beam and column members (i.e. Node 1 in Figure 2.3 (c) is defined at the intersection of the compression steel in the beam and supporting column). The transverse tension ties in the truss mechanism are then located according to the selected numerical truss as defined in Figure 2.2 (i.e. Nodes 3 and 4 in Figure 2.3 (c) are defined by single-point Gauss quadrature).

Axial Rigidity

For each C-STM truss member, the expected composite steel-concrete response is modeled using separate elements for steel and concrete, respectively. Each element is

assigned elastic axial rigidities as specified in Table 2.2, where the member numbers refer to Figure 2.3 (c). Some comments on Table 2.2 follow.

For tension and compression chord members (row 1 and 2 of Table 2.2), the concrete area is assumed to be the same so that cyclic effects can to be accounted for, if necessary.

Table 2.2: Elastic truss member axial rigidities

Member	Steel Element		Concrete Element		Comments
	E	A	E	A	
2 - 4 4 - 5	E_s	A_s	E_c	$b.kd$	Tension Chord
1 - 3	E_s	A_s'	$\psi_E E_c$	$b.kd$	* Compression Chord
3 - 4	E_s	$N_h A_{sh}$	E_c	$(4c_c + 2d_h)N_h s$	~ Active Hoop steel including tension stiffening effect
1 - 5	—	—	E_c	$\frac{0.375 \eta b_w j d}{\cos \alpha}$	Concrete Strut in Arch Mechanism
1 - 4	—	—	E_c	$\frac{0.5(1-\eta)b_w j d}{\sqrt{0.423 + \tan^2 \alpha}}$	Concrete Strut in Truss Mechanism
3 - 5	—	—	E_c	$\frac{0.5(1-\eta)b_w j d}{\sqrt{0.577 + \tan^2 \alpha}}$	Concrete Strut in Truss Mechanism

$$* \psi_E = \text{strain compatibility coefficient} = \frac{\sqrt{f'_c(\text{psi})}}{168(1-d'/kd)} \equiv \frac{\sqrt{f'_c(\text{MPa})}}{14(1-d'/kd)}$$

In lieu of a more precise analysis it is recommended that $\psi_E = 0.6$

~ $N_h = \text{int}[L/s - 1]$ is the integer part of active hoops in truss mechanism

For transverse truss members (row 3 of Table 2.2), the total area of transverse reinforcement is evaluated as the number of hoops actively participating in the truss mechanism N_h , where $N_h = \text{int}[L/s - 1]$ is the number of hoopsets. Also, the embedment area of concrete for the transverse tie is taken as twice the cover depth (c_c) plus the stirrup hoop diameter (d_h), multiplied over the length of actively participating hoops ($N_h s$), thus defining the area of concrete surrounding the stirrup legs.

For the concrete arch member (row 4 of Table 2.2), the strut width is assumed to have a parabolic stress distribution that is proportional to the depth and length defined by Holden et al (2003) as $W_A = (3/8)jd\sqrt{1+(jd/L)^2}$. This is multiplied by the apportioned arch strut width ηb_w and simplified accordingly to obtain the strut area.

For the concrete truss strut members (row 5 and 6 of Table 2.2), the strut width is defined using the expression derived by Mander et al. (1999) in Eq. (2.7), where the normalized coordinate of the i^{th} integration point x_i is taken as 0.423 and 0.577 (in accordance with Table 2.1) for the concrete elements 1-4 and 3-5, respectively. These are multiplied by the apportioned truss strut width $(1-\eta)b_w$ to obtain the respective strut areas.

2.7 Constitutive Material Relations of Truss Elements

The elastic parameters of the C-STM model are defined by the truss geometry and axial rigidities. In order to define the strength of each truss element, nonlinear constitutive material relationships are applied in accordance with Figure 2.8 and described as follows.

Reinforcing Steel

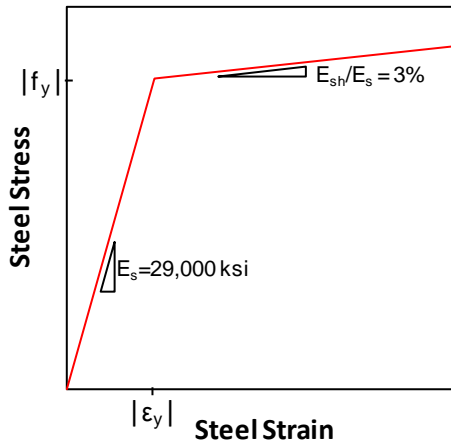
Reinforcing steel (Figure 2.8 (a)) is approximated using a bi-linear stress-strain relationship with 3% strain hardening beyond yielding. Where necessary, a more accurate material model may be applied in order to allow for bond slip or steel fracture.

Diagonal Concrete Struts

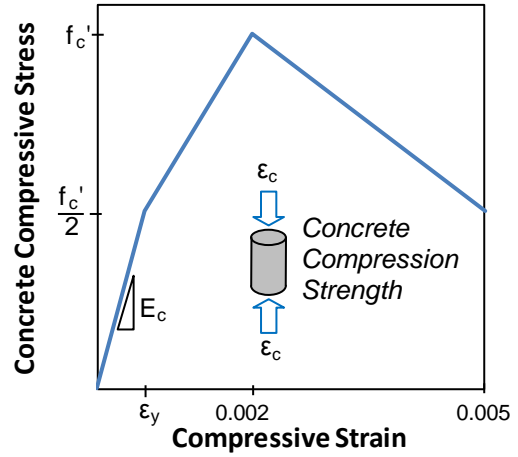
Concrete in compression for the diagonal web compression struts for both the arch and truss mechanisms (Figure 2.8 (b)), is defined by the well-known Mander model (Mander et al. 1988), or suitably approximated using a tri-linear stress-strain relationship as shown.

Concrete Tension Stiffening Effects

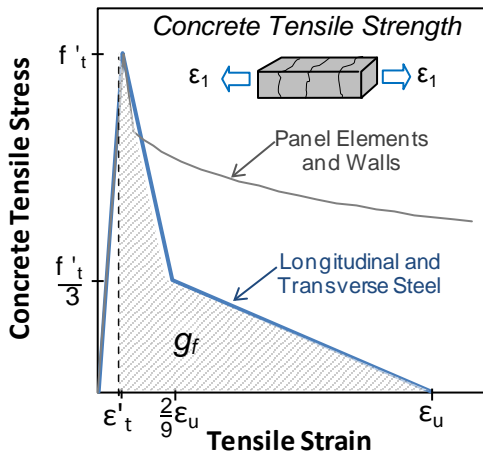
The contribution of concrete tensile strength, referred to as “tension stiffening”, was first observed by Considère (1899). Neither the original compression field theory (Collins 1978) nor conventional strut-and-tie models consider the tensile contribution of concrete,



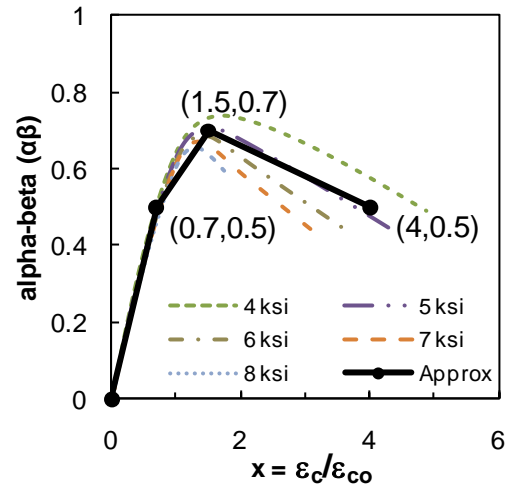
(a) Reinforcing steel



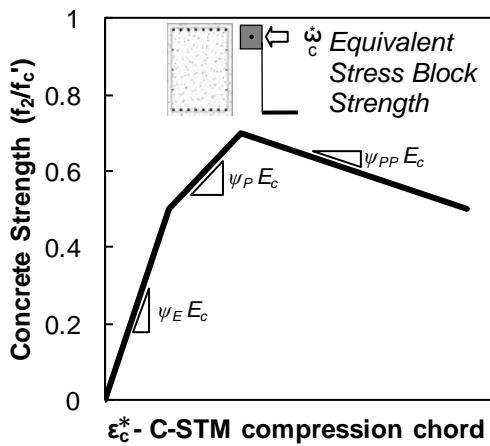
(b) Concrete modeling for web members



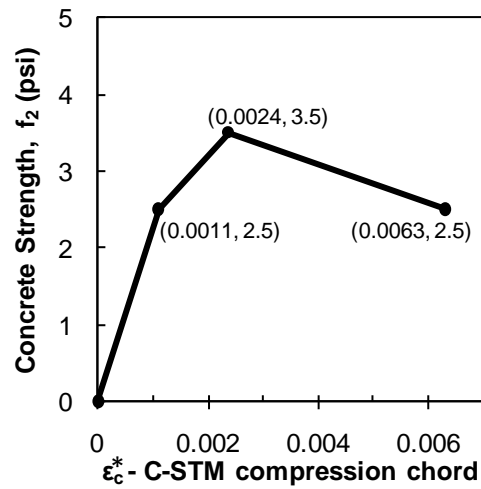
(c) Proposed tension stiffening models



(d) Stress-block parameters for unconfined concrete



(e) Concrete modeling for chord members



(f) Compression chord stress-strain illustration

Figure 2.8: Constitutive stress-strain relationships

thus lower bound solutions are inevitable. It is contended that to provide accurate estimates of real behavior using a full truss model, such a tension-stiffening modification is required.

Assuming strain compatibility between the concrete and steel, the overall member tensile force is simply the summation of the steel and concrete forces for a given strain (Collins and Mitchell 1991; Vecchio and Collins 1986). Thus the combined steel and concrete elements that make up the tension members 2-4-5, and 3-4 in Figure 2.3 (c), intrinsically provide the overall tension stiffened response.

Tension stiffening models vary for different situations and structures, hence the following three approaches are recommended for the C-STM:

- 1) For longitudinal and transverse reinforcing steel bars, tension stiffening is modeled by considering a fracture energy method proposed by Rots et al. (1985) and adopted by Kim and Mander (1999), as shown in Figure 2.8 (c). The fracture energy G_f is defined as the energy required to create one unit area of cracking in which $G_f = h g_f$, where $h = 3d_a$ is the crack band width taken as three aggregate diameters; and $g_f =$ shaded area under the stress-strain softening diagram. The stress-strain relationship is defined using a tri-linear stress-strain relationship given by

$$f_t = E_c \varepsilon_t \quad \text{for} \quad \varepsilon_t \leq \varepsilon_t' \quad (2.25)$$

$$f_t = \frac{f_t'}{3} \quad \text{for} \quad \varepsilon_t = \frac{2}{3} \varepsilon_u \quad (2.26)$$

$$f_t = 0 \quad \text{for} \quad \varepsilon_t = \varepsilon_u \quad (2.27)$$

in which f_t = average concrete tensile stress; ε_t = average concrete tensile strain; ε_t' = strain at peak tensile stress; $f_t' = x\sqrt{f_c'}$ (psi) is used to define the concrete tensile strength, where $x=4$ is typically assumed for standard concrete (Collins and Mitchell 1991), but can be as large as 7.5 for flexural tension members (Reddiar 2009); and ε_u = ultimate tensile strain where stress can no longer be transferred given below

$$\varepsilon_u = \frac{18 G_f}{5 f_t' h} \quad (2.28)$$

Based experimental results, the fracture energy G_f for normal-weight concrete typically ranges from $0.343 - 0.571$ (lbs/in) $\equiv 60 - 100$ (N/m) (Petersson 1980).

Alternatively ε_u may be assumed as the steel yield strain for simplicity.

- 2) In the case of panel and wall structures with a dense network or reinforcing steel, the descending branch model proposed by Vecchio and Collins (1986) may be more appropriate as shown in Figure 2.8 (c). That is,

$$f_t = \frac{\alpha_1 \alpha_2 f_t'}{1 + \sqrt{500 \varepsilon_t}} \quad \text{for} \quad \varepsilon_t > \varepsilon_t' \quad (2.29)$$

where α_1 and α_2 = factors to account for bond characteristics of reinforcement.

- 3) For structures with experimental results, parameterized models can be applied to model the stress-strain relations used for concrete tension stiffening.

Concrete Compression Chord Members

Section 2.5 presents the transformation of the elastic properties for concrete compression chord members in order to modify the concrete resultant force according to the stress block analogy. This theory can be extended to model the full stress-strain constitutive material relations using the stress block parameters derived by Reddiar (2009) shown in Figure 2.6.

The relationship between $\alpha\beta$ and x can be approximated using a tri-linear relationship (shown in Figure 2.8 (d)), thus the full stress-strain relationship for concrete compression chord elements in the C-STM can be obtained through an axis transformation of f_c and ε_c^* , respectively as shown in Figure 2.8 (e). The compatibility correction scalar ψ can be defined for the three tri-linear slopes using the change in coordinates ($\Delta x, \Delta\alpha\beta$), such that:

$$\psi = \frac{\Delta\alpha\beta}{\left(1 - \frac{d'}{kd}\right)\Delta x n} \quad (2.30)$$

$$\text{For } 0 < x \leq 0.7 \quad \psi_E = \frac{(0.5 - 0)}{(1 - d'/kd)(0.7 - 0)} \frac{\sqrt{f_c'(psi)}}{120} = \frac{\sqrt{f_c'(psi)}}{168(1 - d'/kd)} \quad (2.31)$$

$$\text{For } 0.7 < x \leq 1.5 \quad \psi_P = \frac{(0.7 - 0.5)}{(1 - d'/kd)(1.5 - 0.7)} \frac{\sqrt{f_c'(psi)}}{120} = \frac{\sqrt{f_c'(psi)}}{480(1 - d'/kd)} \quad (2.32)$$

$$\text{For } 1.5 < x \leq 4 \quad \psi_{PP} = \frac{(0.5 - 0.7)}{(1 - d'/kd)(4 - 1.5)} \frac{\sqrt{f_c'(psi)}}{120} = -\frac{\sqrt{f_c'(psi)}}{1500(1 - d'/kd)} \quad (2.33)$$

where ψ_E = the initial elastic slope; ψ_P = the slope prior to the peak; and ψ_{PP} = the post peak slope.

For illustrative purposes, assume that $f_c' = 5000$ (*psi*), $E_c = 4030$ (*ksi*); and $d'/kd = 0.25$. The corresponding compatibility correction scalars can be defined as: $\psi_E = 0.56$, $\psi_P = 0.20$; and $\psi_{PP} = -0.06$, thus the coordinates for the equivalent C-STM compression chord stress-strain relationship can be defined below (shown in Figure 2.8 (f)):

$$(\varepsilon_{c1}^*, f_{c1}) = \left(\frac{0.5 f_c'}{\psi_E E_c}, 0.5 f_c' \right) = (0.0011, 2.5) \quad (2.34)$$

$$(\varepsilon_{c2}^*, f_{c2}) = \left(\varepsilon_{c1}^* + \frac{(0.7 - 0.5) f_c'}{\psi_P E_c}, 0.7 f_c' \right) = (0.0024, 3.5) \quad (2.35)$$

$$(\varepsilon_{c3}^*, f_{c3}) = \left(\varepsilon_{c2}^* + \frac{(0.5 - 0.7) f_c'}{\psi_{PP} E_c}, 0.5 f_c' \right) = (0.0063, 2.5) \quad (2.36)$$

The area of the corresponding concrete element is defined as $A_c = kd b$.

2.8 Ultimate Strength and Softening of Constitutive Relations

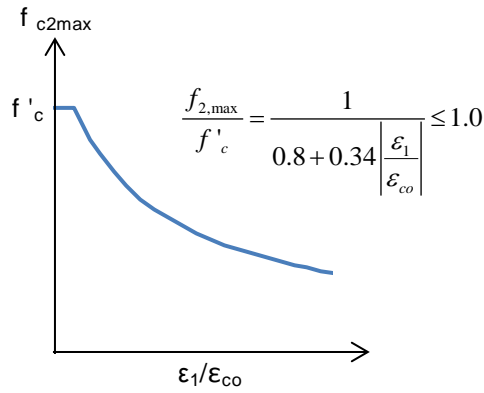
The exact failure mechanism for deep beams or disturbed regions is difficult to define due to unknown (a priori) hierarchy of failure mechanisms; particularly given the fact that shear failure alone can be of four types: diagonal tension, web crushing, nodal failure, or sliding shear. In reality the type of failure is heavily dependent on the member geometry and detailing, and is often a combination of events that lead to the formation of the final collapse mechanism. In the C-STM, steel yielding and concrete crushing is intrinsically accounted for through the material constitutive relationships previously described. However a more thorough post analysis assessment is required in order to assess other possible critical failure mechanisms, further discussed in this section.

Compression Softening

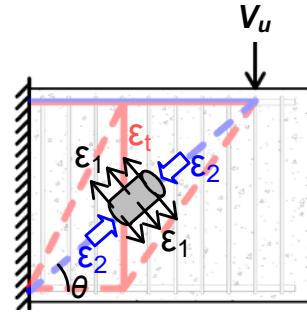
According to Vecchio and Collins (1986) softening of the principal compression concrete struts is due to orthogonal tensile strains in cracked reinforced concrete that can be modeled by the equation:

$$\zeta = \frac{f_{2,\max}}{f'_c} = \frac{1}{0.8 + 0.34 \left| \frac{\varepsilon_1}{\varepsilon_{co}} \right|} \leq 1.0 \quad (2.37a)$$

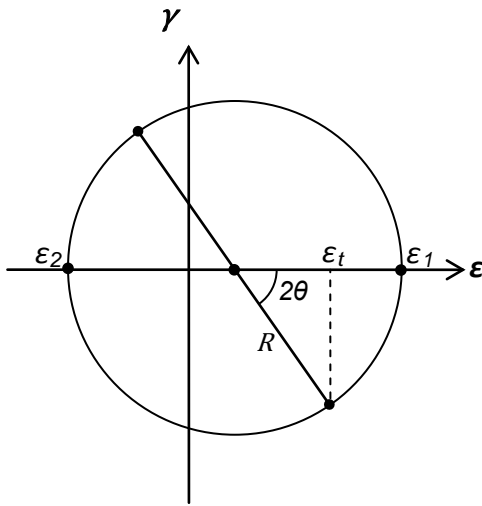
where ζ = the softening coefficient; $f_{2,\max}$ = the “softened” concrete strength shown in Figure 2.9 (a); ε_{co} = is the principal compression strain typically taken as 0.002; and ε_1 = is the principal tensile strain acting perpendicular to compression strut.



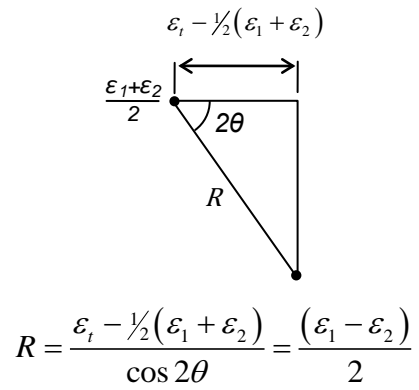
(a) Compression softening



(b) Illustrative application of compression softening



(c) Mohr's circle



(d) Radius

Figure 2.9: Mohr's circle for defining the principal tensile strain

Eq. (2.37a) can be conveniently recast as

$$\zeta = \frac{f_{2,\max}}{f'_c} = \frac{1}{1 + \left\langle \frac{\varepsilon_1 - 0.0012}{3\varepsilon_{co}} \right\rangle} \quad (2.37b)$$

where $\langle \bullet \rangle$ are Macaulay brackets; and the value 0.0012 can be thought of as a fracture strain such that when $\varepsilon_1 > 0.0012$ the concrete softens.

Figure 2.9 (b) illustrates the compression softening effects acting on the diagonal corner-to-corner arch strut. As ε_1 is difficult to assess directly, particularly in commercial software (SAP2000), it can be inferred by assuming out-of-plane compatibility such that ε_1 is proportional to the transverse tie strain ε_t . Hence, if the compressive axial strain of a strut ε_2 and the transverse tie strain ε_t acting across the strut are known, then the principal tensile strain ε_1 can be determined using Mohr's circle, as shown by the transformation in Figure 2.9 (c). Solving the expression derived from the radius R for ε_1 gives

$$\varepsilon_1 = |\varepsilon_2| \left(\tan^2 \theta + \frac{|\varepsilon_t / \varepsilon_2|}{\cos^2 \theta} \right) \quad (2.38)$$

in which $\theta =$ the diagonal strut angle relative to the longitudinal direction.

Thus, in terms of Eq. (2.37b), the compression softening coefficient can be rewritten as

$$\zeta = \frac{f_{2,\max}}{f'_c} = \frac{1}{1 + \left\langle \frac{C_\varepsilon |\varepsilon_2| - 0.0012}{3\varepsilon_{co}} \right\rangle} \quad (2.39)$$

where C_ε = a principal tensile strain constant defined as

$$C_\varepsilon = \tan^2 \theta + \frac{|\varepsilon_t / \varepsilon_2|}{\cos^2 \theta} \quad (2.40)$$

To evaluate C_ε , the ratio of $\varepsilon_t / \varepsilon_2$ can be determined from an elastic analysis with no tension stiffening effects where C_ε remains constant. Modified stress-strain relations are then found from the modified ascending branch of a power-type stress-strain curve proposed by Mander (1983) and given by

$$f_c = \zeta f'_c \left(1 - \left(1 - \frac{\varepsilon_2}{\zeta \varepsilon_{co}} \right)^n \right) \quad (2.41)$$

where $n = E_c \varepsilon_{co} / f'_c$. This softens both the concrete stress and strain according to the secant stiffness. As an example, consider the case of $\varepsilon_t / \varepsilon_2 = 2.1$, and $\theta = 38^\circ$. From Eq. (2.40) $C_\varepsilon = 4$, and from Eq. (2.39) $\zeta = 1 / \left(1 + \left\langle 666.7 |\varepsilon_2| - 0.2 \right\rangle \right)$. This result is now applied to Eq. (2.41) and plotted in Figure 2.10.

The softened stress-strain relationship can then be applied to the constitutive material model for the diagonal compression struts. The analysis is then re-run to provide the response that includes the effects of the softened diagonal struts.

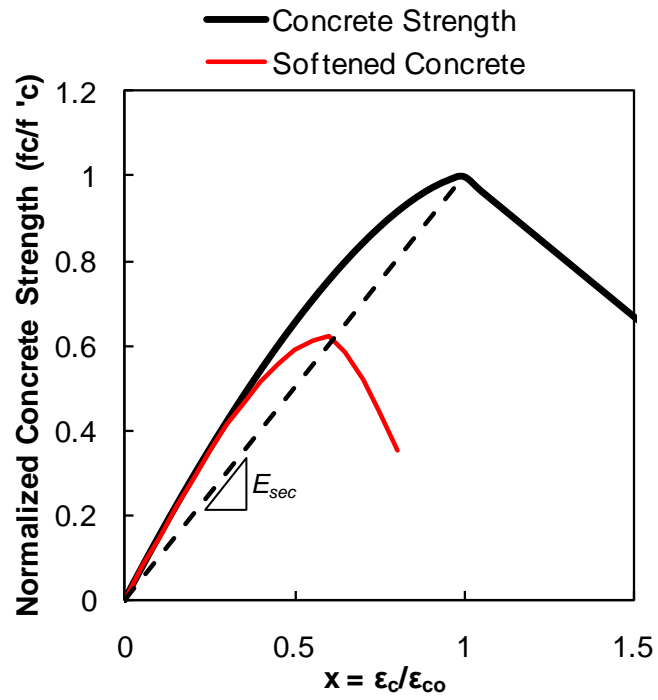


Figure 2.10: Illustration of concrete softening

Strut-and-Tie Strength Checks

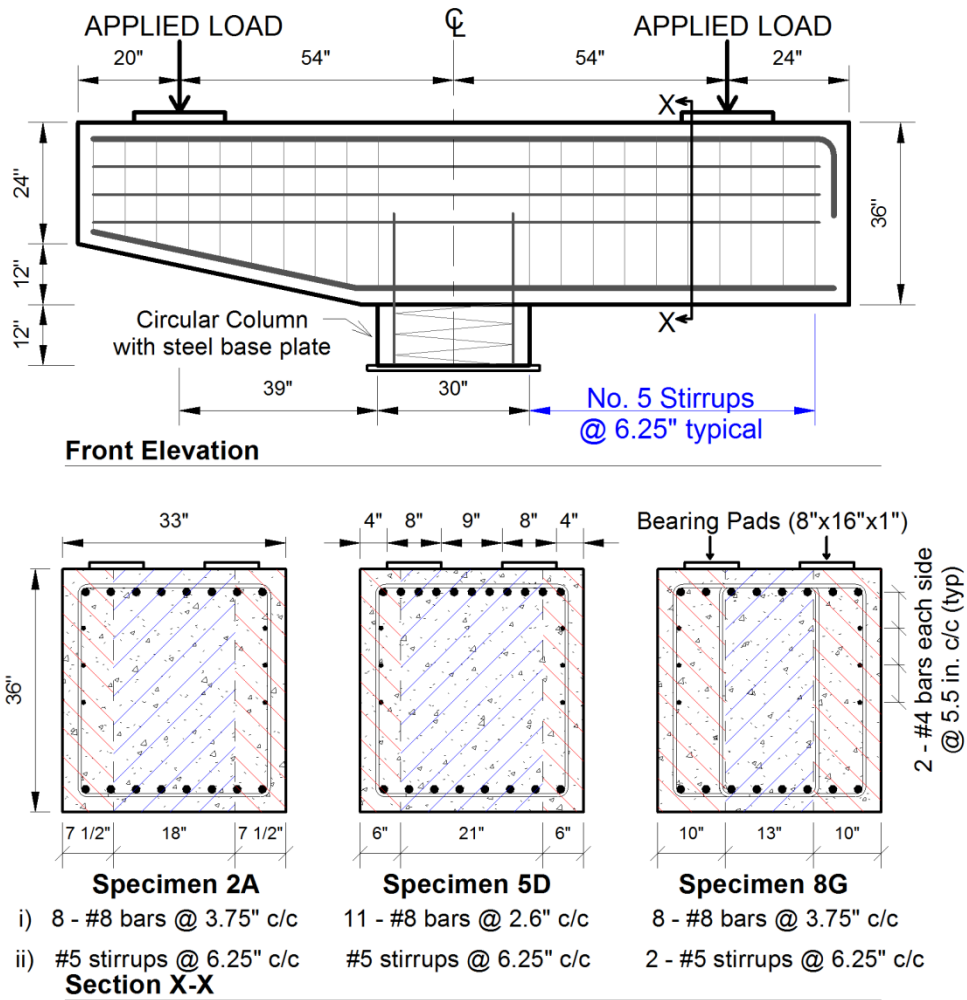
Strut-and-tie modeling predisposes itself to defining failure as either: yielding of reinforcing ties, crushing of a strut, anchorage failure of reinforcing ties, or nodal failure. The first two failure modes are accounted for with the constitutive material models, however other failure modes need to be checked in a post analysis assessment. The member forces in the C-STM can be used to check that the force does not exceed the strength defined using conventional STM design procedures for anchorage and nodal failures.

2.9 Experimental Verification

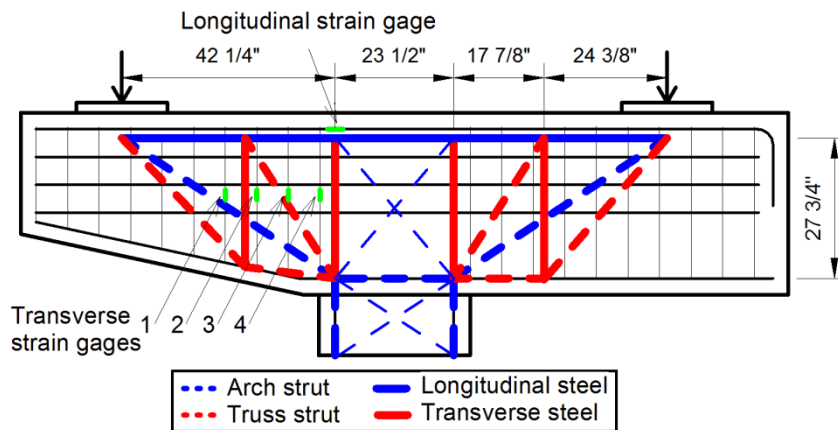
The proposed C-STM was used to predict the force-deformation response and internal strain behavior of previously tested reinforced concrete bridge bent caps (Bracci et al. 2000; Powanusorn and Bracci 2006a; Powanusorn and Bracci 2006b; Young et al. 2002). This study is used to verify the accuracy of the proposed C-STM and demonstrate how the C-STM can be applied to reinforced concrete structures. The model was implemented using standard commercial nonlinear structural analysis software (SAP2000 1995).

Bracci et al. (2000) investigated the causes of excessive cracking in deep reinforced concrete bent caps. The specimens were full-scale models of prototype bents used in Texas that developed cracking near the column-to-bent cap region under service loading. Three out of 16 specimens were selected herein for modeling verification; the selection was based on a variety of transverse to longitudinal reinforcement ratios and clarity of reported results. Figure 2.11 shows the general details of the selected specimens.

Figure 2.11 (a) presents the reinforcing layout and cross-sections of the three specimens, along with their corresponding distribution breadths of “Arch” (inner fill) and “Truss” (outer fill) action. Each cross-section specifies the longitudinal and transverse reinforcement used in each specimen. All bents had compression reinforcement consisting of 8 – #8 bars and a specified cover concrete depth of 2.25 in.



(a) Front elevation and sections of specimens used for validation



(b) C-STM of Bent Cap showing selected strain gages

Figure 2.11: RC-Bent cap model used to verify C-STM

The measured yield strength of the longitudinal (#8) and transverse (#4) steel was $f_y = 65 \text{ ksi}$. Specimen 5D had a larger amount of longitudinal steel resulting in a higher contribution of arch action; conversely, Specimen 8G had twice the amount of transverse reinforcement resulting in a higher contribution of truss action, as shown in Figure 2.4.

Figure 2.11 (b) illustrates the C-STM used to analyze each specimen overlaid with the reinforcement details. Also shown is the location of the longitudinal and transverse strain gages used to compare experimental vs. predicted results. The modeling procedure of the C-STM and parameters are defined in Appendix A.

Table 2.3 shows the measured 28 day concrete strengths and the factors used to calculate the arch breadth scalar, η . No test day strength results were provided hence the 28 day strength was assumed for each analysis.

Table 2.3: Concrete strengths and arch breadth scalar

Specimen	2A	5D	8G
$f'_{28} \text{ (ksi)}$	6.2	5.5	5.3
ρ_T / ρ_L	0.408	0.314	0.816
L/jd	1.52	1.50	1.52
η	0.555	0.625	0.384

General observations reported during testing were as follows: 1) flexural cracking initiated near the column face of the bent cap around 100 kips; 2) at approximately 160 kips the vertical flexural cracks began to incline toward the column support; 3) with increased loading, inclined flexure-shear cracks initiated, propagated, and widened while the original flexural cracks stabilized; 4) ultimate failure was very

sudden and typically occurred along a shear plane, extending from the load point inclined toward the column support (Bracci et al. 2000). These experimental results serve as the basis for the initial verification of the C-STM analysis.

C-STM Analysis Results

Figure 2.12 presents results of the nonlinear response as predicted by C-STM analysis for Specimen 2A. These results are compared with experimentally observed longitudinal and transverse reinforcement results, and the overall force-deformation response. Here, a chronological breakdown of the progression of nonlinear behavior is used to illustrate the corresponding member stress-strain relationships as they develop during the computational modeling. It should be noted that the C-STM concluded that the responses of each end were within 3% of each other despite their geometric differences, hence only the cantilevered end is reported from the C-STM analysis.

LC = Longitudinal cracking (see graphs in row 1 of Figure 2.12) first occurs in the longitudinal concrete elements when the member stress exceeds the concrete tensile strength f_t' , thus indicating vertical flexural cracking in the top chord. As the force increases, the longitudinal tension stiffened member's exhibit tension softening effects where the concrete between cracks still have some ability to contribute in resisting tensile strains.

TC = Transverse cracking (see graphs in row 2 of Figure 2.12) then occurs in the tension stiffened transverse truss elements. This correlates to the diagonal shear cracking observed as a result of the flexure-shear interaction.

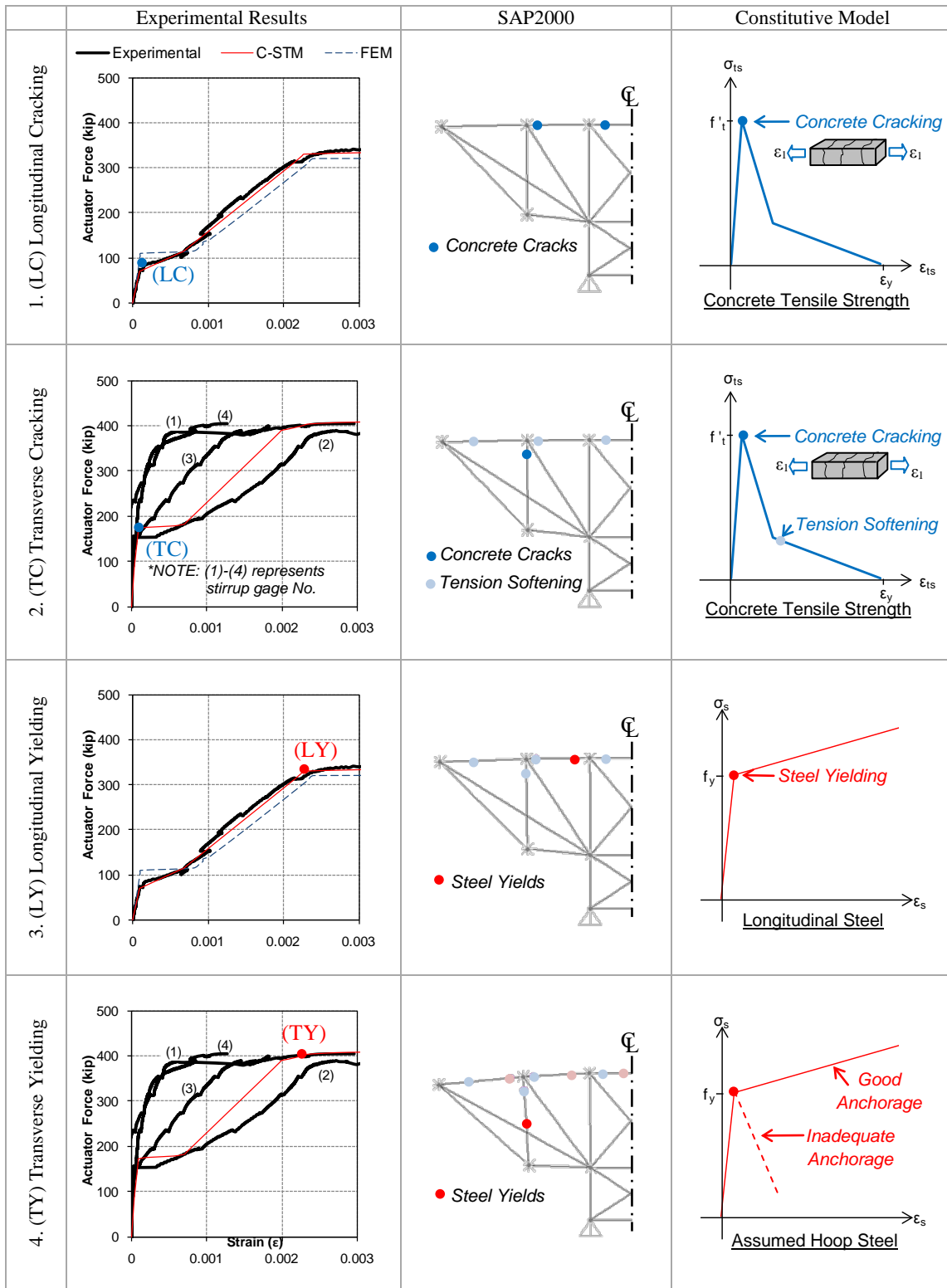


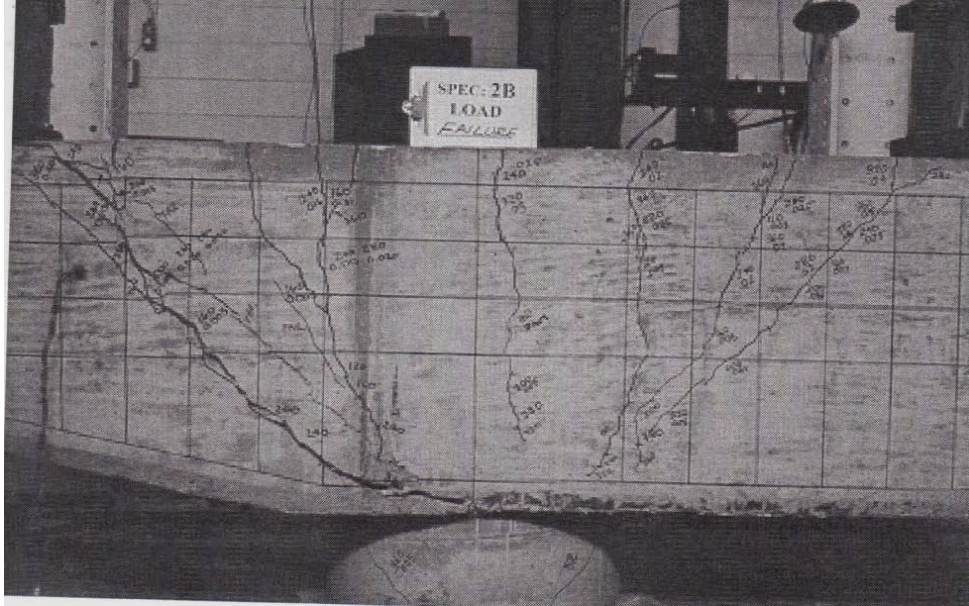
Figure 2.12: Progression of nonlinear behavior for Specimen 2A

LY = Longitudinal steel yielding (see graphs in row 3 of Figure 2.12) occurs when the reinforcing steel yield stress f_y is exceeded, and correlates to the flexural moment capacity of the member.

TY = Transverse steel yielding (see graphs in row 4 of Figure 2.12) may occur if the member has insufficient transverse reinforcement and correlates to the widening of the inclined shear cracks. Post-yield behavior of transverse reinforcement is governed by the anchorage of the hoops: if open 90° hooks or U-bars are used then loss of anchorage may occur at high strains; if closed 135° hooks are used then a full post-yield behavior may be assumed. Here open hooks were used thus a loss of anchorage is assumed after yielding.

The ultimate collapse mechanism formed along the main diagonal corner-to-corner shear plane as shown in Figure 2.13 (a). In order to predict this failure mechanism, a post-analysis investigation was conducted and concluded that the corner-to-corner arch strut was prone to a compression softening failure. This was determined through the following steps:

1. The principal tensile strain was evaluated using Eq. (2.38) based on the strains in the compression arch strut ε_2 and transverse steel ε_t .
2. The “softened” concrete strength is then calculated using Eq. (2.37b), thus defining the struts capacity.



(a) Experimental photo of Specimen 2A at failure

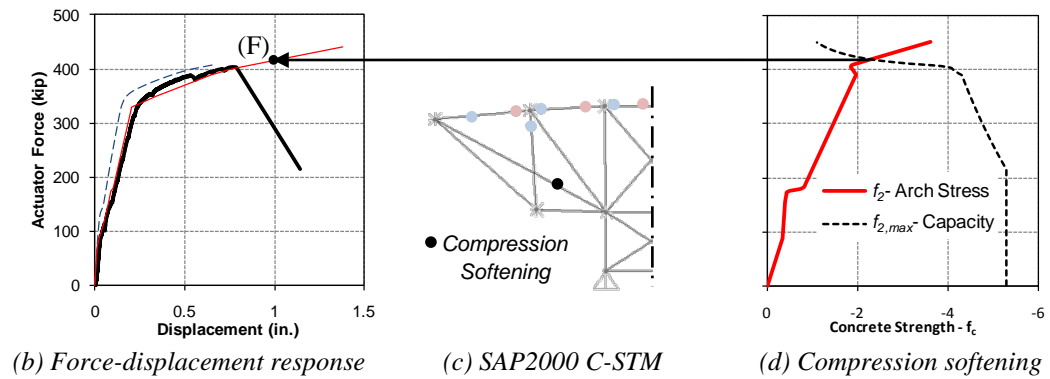


Figure 2.13: Compression softening failure of Specimen 2A

3. The stress in the strut is defined as $f_2 = \varepsilon_{ci} E_c$ in accordance with the stress-strain profile (alternatively $f_2 = F_{ci} / A_{ci}$ can be used in the elastic region), thus defining the struts demand.
4. The demand and capacity lines are then plotted against the actuator load for every analysis time step as shown in Figure 2.14 (d). The intersection of the two lines defines when compression softening effects are critical, and can be projected onto the force-displacement diagram to predict the ultimate failure load (Figure 2.14 (b))

The drastic change in slope of the capacity line (at approximately 400 kips) is due to the onset of transverse steel yielding, thus showing the rapid deterioration of the arch strut confinement. This analysis was in good agreement with the observed ultimate load.

Figure 2.14 presents a summary of experimental versus theoretical results for the overall force-deformation, longitudinal, and transverse responses of Specimens 5D and 8G. The longitudinal and transverse force vs. strain diagrams (column (b) and (c) of Figure 2.14 respectively) identifies the nonlinear behavior in a similar manner to Figure 2.12. It is interesting to note that the C-STM provided a closer approximation of the elastic stiffness than the FEM proposed by Bracci et al. (2000). However the predicted response tended to be a little stiffer than the experimental response for Specimen 5D and 8G.

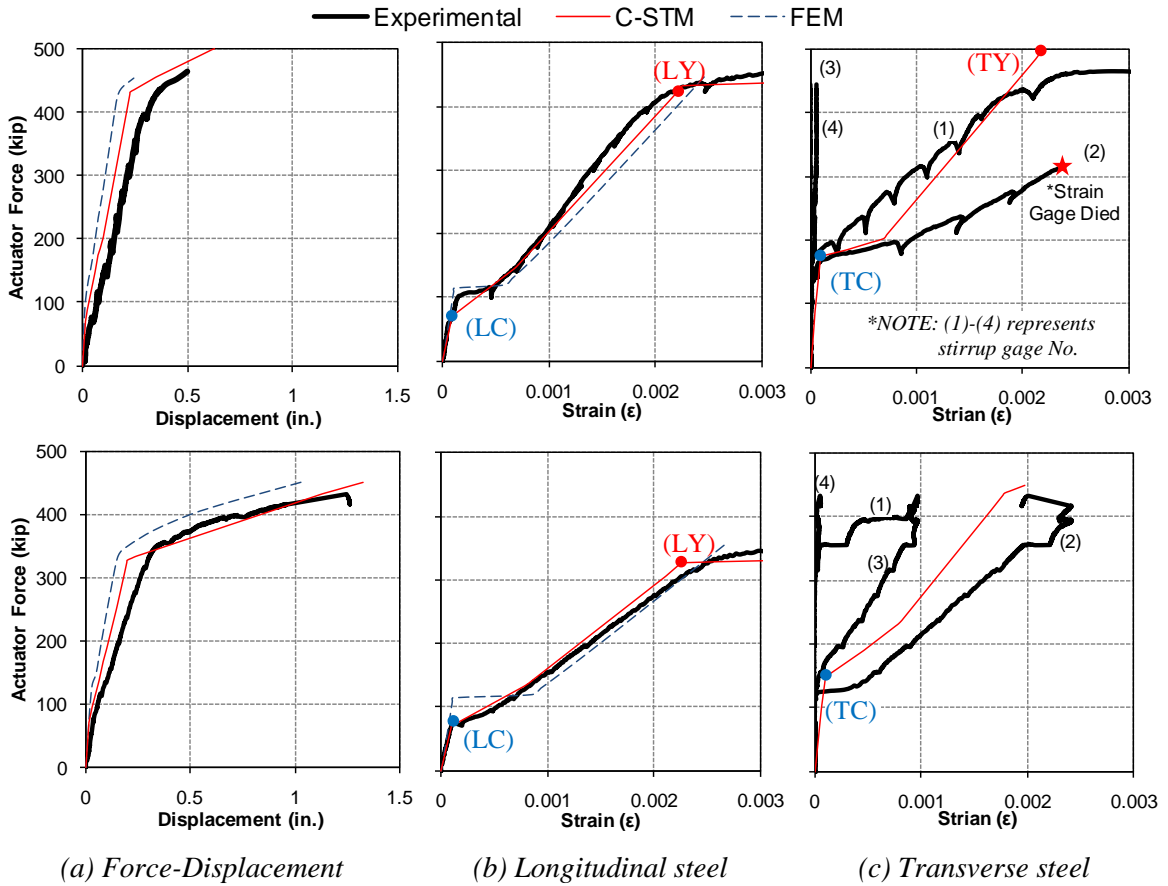


Figure 2.14: Experimental vs. analytical results for Specimen 5D (top row) and 8G (bottom row), where (LC) – Longitudinal Cracking; (TC) – Transverse Cracking; (LY) – Longitudinal Yield; (TY) – Transverse Yield

The longitudinal steel response (column b of Figure 2.14) shows good agreement with the experimental response capturing both cracking and yield strengths well. The transverse steel response (column c of Figure 2.14) also shows good agreement with the experimental response, considering that the C-STM provides an averaged response of the overall transverse behavior. Stirrup 2 (third stirrup from the column face) consistently had the highest experimental strain response and is the closest stirrup to the vertical tension tie approximated by the C-STM. The initially vertical response observed in the transverse steel gages prior to diagonal or shear cracking is a result of tension stiffening effects in the transverse stirrups. This phenomenon was accurately modeled using the C-STM.

2.10 Discussion

The C-STM provided an accurate representation of each specimen's behavior in terms of overall force-deformation, internal strains, and the progression of nonlinear behavior. The C-STM also provides promising results to demystifying the internal stress and strain fields of highly cracked reinforced concrete structural elements, particularly in relation to using the composite arch and truss mechanisms to model the interaction of flexure and shear. The C-STM provides a minimalist computational analysis, with only 12 nodes (24 degrees of freedom) and a computation time less than two minutes, without sacrificing modeling accuracy as shown in this verification study. In comparison the FEM analysis consisted of 2968 nodes (8900 DOF).

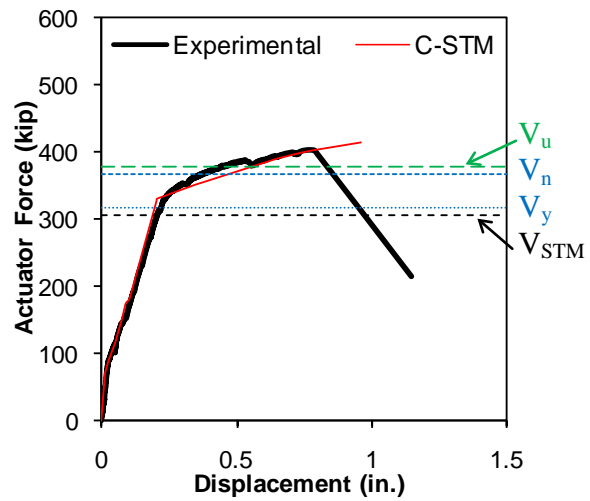
For the purpose of comparison, Figure 2.15 shows the force-deformation responses of each specimen overlaid with code-based prediction based on:

- Flexural bending theory at the first yield moment (M_y) of the longitudinal steel, $V_y = M_y / a$, where $a = 39 - in =$ the span between the applied load and critical section
- Flexural bending theory at the nominal ultimate moment (M_n) capacity, $V_n = M_n / a$
- Sectional shear $V_U = A_{sh} f_y d / s + 2 \sqrt{f'_c} b_w d$ (*psi units*)
- Strut-and-Tie Model (V_{STM}) predictions based on the AASHTO LRFD (2008) Bridge Design Specifications.

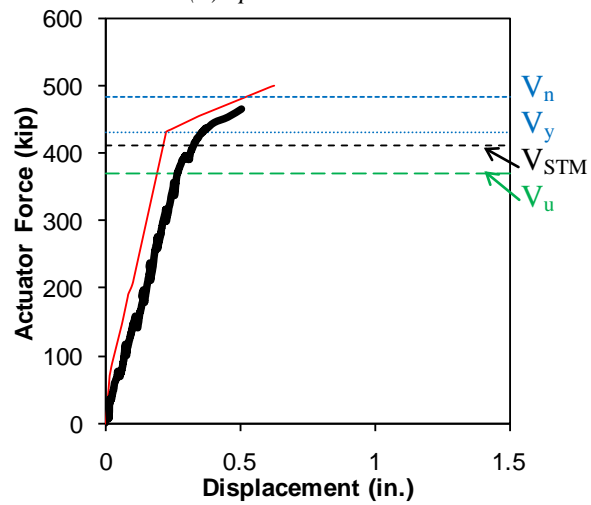
N.B. The exact calculations for each case can be found in Appendix D.

Interestingly, the separate flexural (V_y) and shear (V_u) capacities can be used together to provide some insight into flexural-shear interaction and its hierarchy, whereas STM gives no clues. Specimen 2A yields first in the longitudinal reinforcement, followed by a loss of shear capacity in the post-yield response as a result of compression-softening in the arch strut. Specimen 8G had additional transverse steel relative to 2A, thus confining the arch strut and allowing a ductile response.

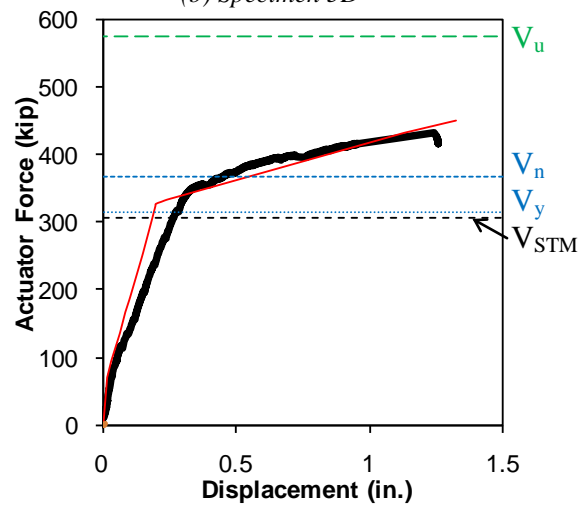
The STM analysis was conducted without any reduction factors and was based on the maximum nodal stress conditions defined in the AASHTO LRFD (2008) Bridge Design Specifications. Yielding of the longitudinal reinforcement governed the



(a) Specimen 2A



(b) Specimen 5D



(c) Specimen 8G

Figure 2.15: Flexure, shear, and STM strength comparison

maximum design shear force; hence similar results for flexural yield and STM were obtained with STM consistently lower. As post yield behavior is not considered in force based predictions, the reserve capacity subsequent to longitudinal yielding was not accounted for when assessing the ultimate load.

This discussion illustrates that when present conventional strength-based analysis techniques are used alone, they are unable to provide satisfactory insight into the expected behavior to identify failure modes and their progression along with any reserve capacity. The C-STM serves as a straight-forward method to remedy this shortcoming.

Finally, this chapter has presented the C-STM in the form of a generic cantilevered beam that uses a rational approach to defining the truss geometry and element area assignments. The intention of chapter is to provide a fundamental understanding of computational truss modeling so that the methodology can then be applied to modeling the response of other reinforced concrete structures. The correct implementation of the C-STM is at the discretion of the Engineer; hence good engineering judgment is required to apply the C-STM principles to the task at hand. For unique details that are not specifically addressed in this thesis, it is recommended that a sensitivity analysis is conducted by changing one parameter at a time in order to determine how critical that particular parameter is.

2.11 Chapter Closure

This Chapter presented a compatibility based strut and tie model for the shear analysis of reinforced concrete D-regions, specifically applied to bridge pier caps. A progressive development of the modeling parameters required to construct the C-STM was presented. The proposed C-STM was used to analyze previous experimental testing to validate the modeling approach in comparison with code-based analysis techniques.

Based on the research presented in this Chapter, the following conclusions can be drawn:

1. By considering equilibrium, compatibility, and nonlinear constitutive laws of cracked reinforced concrete members, the C-STM serves as an advanced method of analysis that can predict with suitable accuracy the force-deformation response of D-regions and deep beams. Additionally, insights into internal member strains and the hierarchy of failure mechanisms can be calculated.
2. The C-STM was applied to large-scale experimental bridge cap specimens and showed good agreement between the experimental and predicted response was observed.
3. Using stress-block theory, a rational solution to modeling the combined response of steel and concrete in compression chord members is proposed. This approach also enables the nonlinear behavior of the concrete compression stress block and steel in compression to be modeled.
4. The C-STM is a minimalist computational method of analysis that can be implemented into commercial available structural nonlinear analysis software such

as SAP2000. This provides consulting engineers with a supplementary design tool that can be used to accurately assess the force-deformational response and nonlinear behavior of D-regions and deep beams.

5. When modeling truss action, any defensible numerical integration scheme can be adopted to size and locate the truss elements. However, if strut crushing is expected, a convergence study may be warranted to accurately capture failure.

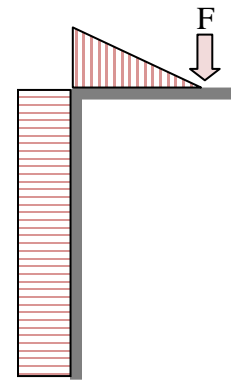
CHAPTER III

EXPERIMENTAL AND ANALYTICAL INVESTIGATION OF REINFORCED CONCRETE BRIDGE BENTS

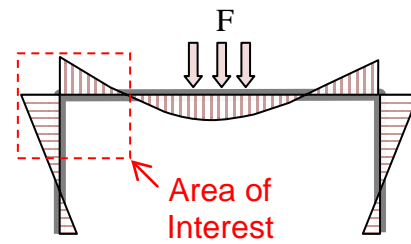
3.1 Chapter Scope and Research Motivation

Over the past decade, the structural longevity of a large number of reinforced concrete bridge bent caps has been compromised as a result of premature concrete deterioration. Figure 3.1 shows two bridge bents indicating signs of distress in the disturbed (D-) regions. The *cantilever bent* (San Antonio, TX) shown in Figure 3.1 (a), exhibits flexural cracking on the tension fiber of the column and one large shear crack propagating from the applied load to the internal knee joint indicated by the staining patterns shown as white dotted lines. The *straddle bent* (Houston, TX) shown in Figure 3.1 (b), exhibits distinct shear cracks through the beam and beam-column joint indicated by the white dotted lines.

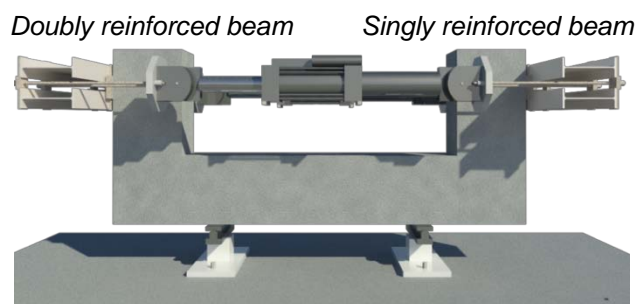
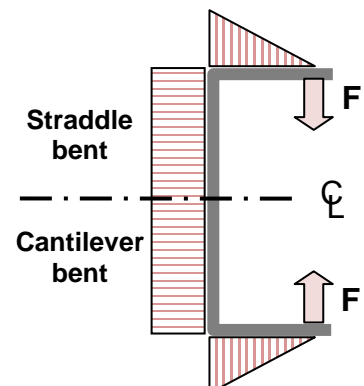
In order to assess the structural integrity of such structures, a thorough understanding of the structural behavior in the disturbed regions is required. Current code design methods are purely force-based approaches that are conservative lower bound solutions (AASHTO, 2008; and ACI 318-08). Hence they are not appropriate for modeling the complex behavior of D-regions as a means of assessing the degradation in strength. Clearly it is desirable to have an advanced method of analysis that can be adopted by practicing engineers and implemented as a means of assessing the structural nonlinear behavior of reinforced concrete bridges and D-regions.

(a) *Cantilevered bent*

Schematic BMD

(b) *Straddle bent*

Schematic BMD

*C-Specimen seated on column sections for experimental purposes*(c) *Experimental C-Specimen*Schematic BMD
(Rotated 90°)**Figure 3.1: Prototype bridge bents and the evolution of the experimental specimen**

This research presents an experimental investigation on the structural performance of large-scale reinforced concrete specimens specifically designed to replicate typical bridge bents currently used in practice. The advanced compatibility-strut and tie model (C-STM) described and verified in the preceding chapter is used to assess the force-deformation response, as well as the nonlinear internal flow of stress that eventually leads to the ultimate collapse mechanism.

3.2 Experimental Investigation

Representative Prototypes to be Physically Modeled

Figure 3.1 shows the two bridge bents selected as the basis for designing the specimens to be tested in this research based on current bridge structures typically used in Texas. Cantilever bents (Figure 3.1 (a)) are typically designed with minimal compression steel using strut-and-tie design methods, hence a similar *singly reinforced beam* was considered in the specimen design. Straddle bents (Figure 3.1 (b)) typically have more compression steel at the column/pier face due to the positive and negative moments in the beam section, hence a *doubly reinforced beam* was considered accordingly.

Experimental Design

The experimental specimens in this research were designed as a “C” shape sub-assembly such that two large-scale bridge bent components were placed back-to-back so they could be tested as a self-reacting system as shown in Figure 3.1 (c). This provided an axis of symmetry at the specimen’s centerline. The C-specimens had a constant cross-section of 3ft deep and 2ft wide, that was symmetrical with the exception

of the beam compression steel. More specifically the physical model scale factors representing the singly reinforced cantilevered bent and the doubly reinforced straddle bent were approximately 0.5 and 0.75, respectively.

Reinforcement Details

Reinforcing details of the C-Specimen are shown in Figure 3.2. The reinforcement layout was scaled to replicate the cantilever and straddle bents described previously. The longitudinal reinforcement consisted of 10 No. 8 bars running continuously around the outside and hooked at the end of each beam. The singly reinforced beam (*S*) had 2 No. 8 straight compression bars for construction purposes. The doubly reinforced beam (*D*) had symmetrical compression and tension reinforcement.

The longitudinal beam distribution steel (distributed along the beam web) consisted of 3 sets of No. 4 straight bars equally spaced. Transverse beam reinforcement consisted of closed stirrups with a center-to-center spacing of 4.5-in. starting at the column face. The longitudinal column distribution steel consisted of 5 sets of No. 8 bars equally spaced. Transverse column reinforcement had overlapping No.4 stirrups spaced 4.5-in. centers. The beam-column joint (herein referred to as the joint) was reinforced with 4 No.4 U-bars at 8-in. centers continuing from the transverse beam reinforcement.

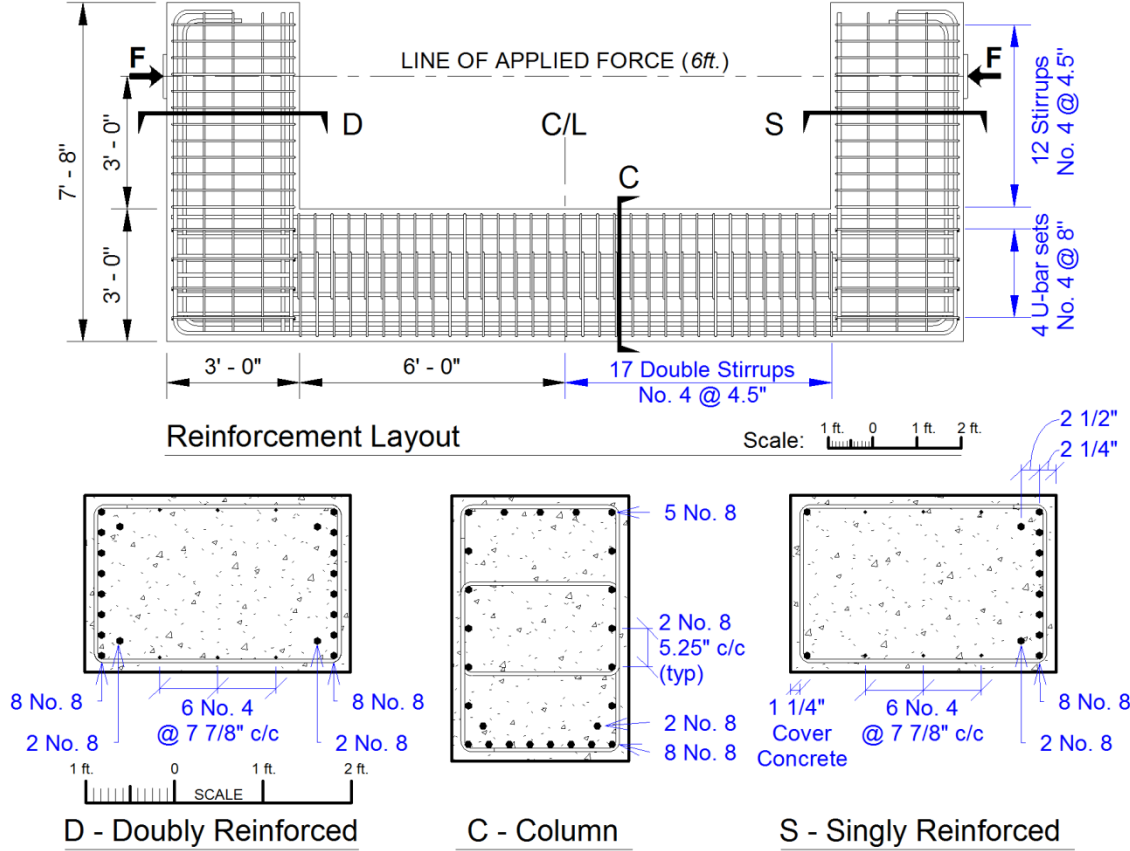


Figure 3.2: Reinforcement details

Materials

The concrete mix used in this research was custom batched using aggregates containing high silica content, and sodium hydroxide to accelerate premature concrete deterioration mechanisms. This did not affect the performance of the control specimen as it was maintained in a controlled lab environment unexposed to water. Measured compressive strength of standard 4 x 8 in. concrete cylinders at 28 days and at the time of the test are presented in Table 3.1

Table 3.1: Mechanical properties of concrete

Beam	f'_c (ksi)	E_c (ksi)	f'_t (ksi)	f'_{s-t} (ksi)
28 day	4.5	3850	0.3	0.3
Test	5.4	4260	0.45	0.57

Concrete tensile strengths were obtained using two test methods: (i) embedded bar tensile (*t*) test; and (ii) splitting tensile (*s-t*) test. Further details of the tested material properties may be found in Appendix E along with steel coupon test results.

The steel properties were taken as an average of three coupon tests providing an average yield stress and strain of 65 *ksi*, and 0.0024, respectively, with a post-yield strain-hardening of modulus of 3% of the elastic stiffness.

3.3 Experimental Testing

This section describes the experimental test setup, procedure, loading history, and instrumentation layout (both internal and external) for the control specimen.

Test Setup

The C-Specimen was designed as a self-reacting system concurrently representing two bridge bent types, with potentially two comparative results obtained from one sub-assembly. Figure 3.3 shows a detailed plan and elevation of the experimental test setup. For experimental convenience, the specimens were oriented so that the column was placed horizontally while the cantilevered beams were oriented vertically. The column was seated on two hinge supports located a distance of $D/2$ from the beam face. Equal and opposite loads were applied to the beams at a distance of 3 ft. from the column face using two 220 Kip MTS (model 244.51S) actuators placed in parallel. The actuators were connected to header beams using 1 3/8" diameter high strength Dywidag bars, and were operated using servo hydraulic control (displacement control). A third actuator operated in force control was placed between the 220 kip actuators and maintained at 100 kips in order to provide a total capacity of 540 kips.

In order to maximize the performance of the C-Specimen, one end was "protected" using external post-tensioning to prevent yielding of the longitudinal steel and minimize cracking, thus focusing the other end as the principal "test" subject. In this way two "tests" could be performed on the one specimen as discussed in subsequent sections. As shown in Figure 3.3, the protection consisted of two 1-3/8-in. high strength (DYWIDAGTM) high alloy thread-bars, eccentrically positioned 12-in. from the beam centerline towards the tension steel and post tensioned to a total axial load of 300 kips. This was designed to reduce the strain in the tension steel and minimize cracking.

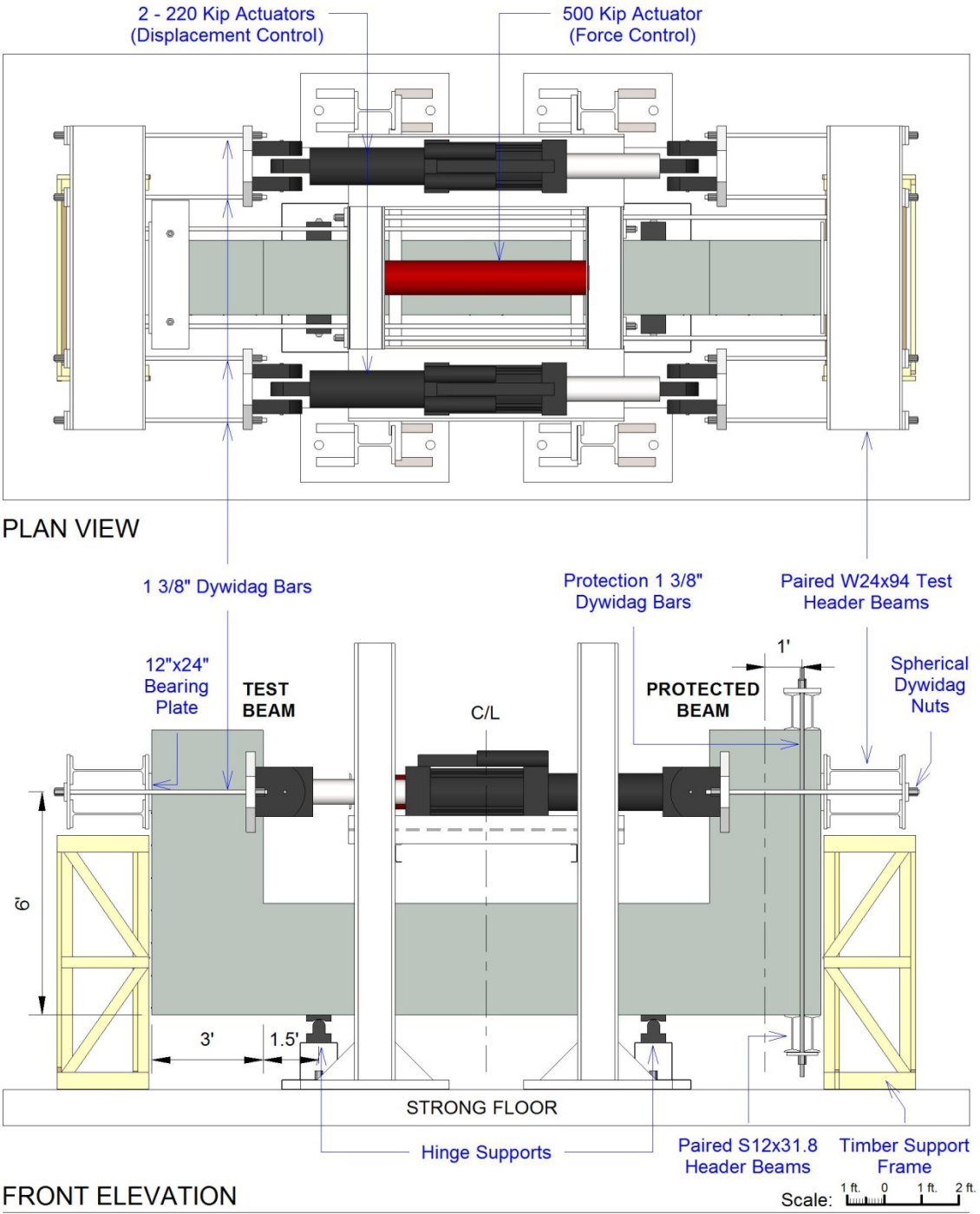


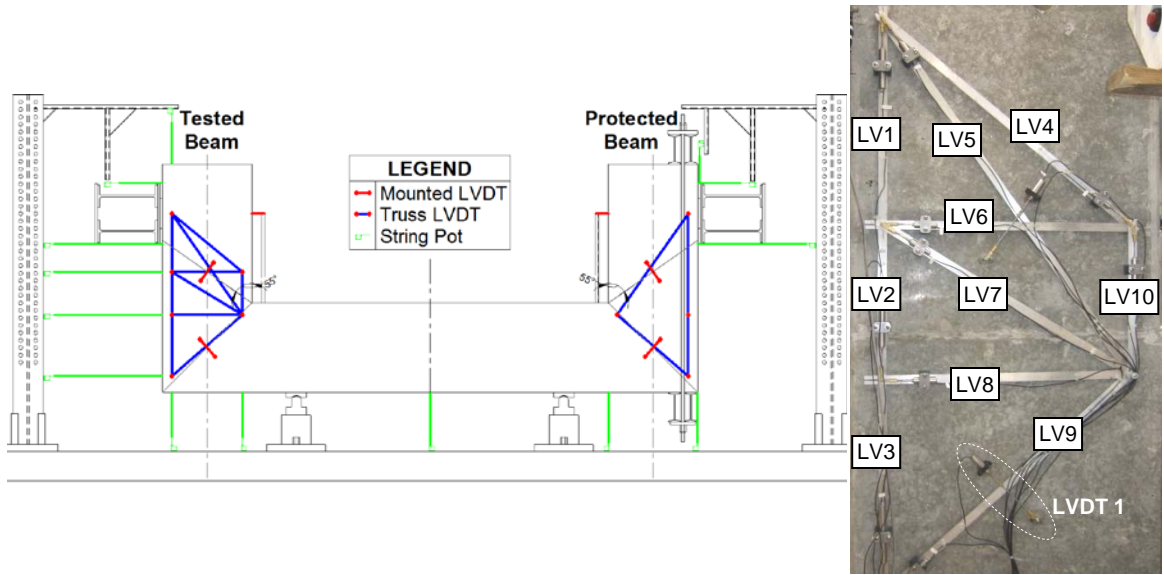
Figure 3.3: Details of the experimental setup

Instrumentation

One objective of the experiment was to investigate the specimen's structural performance and model the overall force-deformation behavior by means of a compatibility strut-and-tie model. It was therefore deemed necessary to monitor the internal and external response accordingly. Figure 3.4 shows the external and internal instrumentation layout plans used to obtain experimental results that could be used to compare analytical modeling results. Specimens were externally instrumented using linear variable differential transformers (*LVDT's*), string pots (*SP*), internally instrumented using strain gages (*SG*) attached to steel, and embedded concrete gages (*KM*).

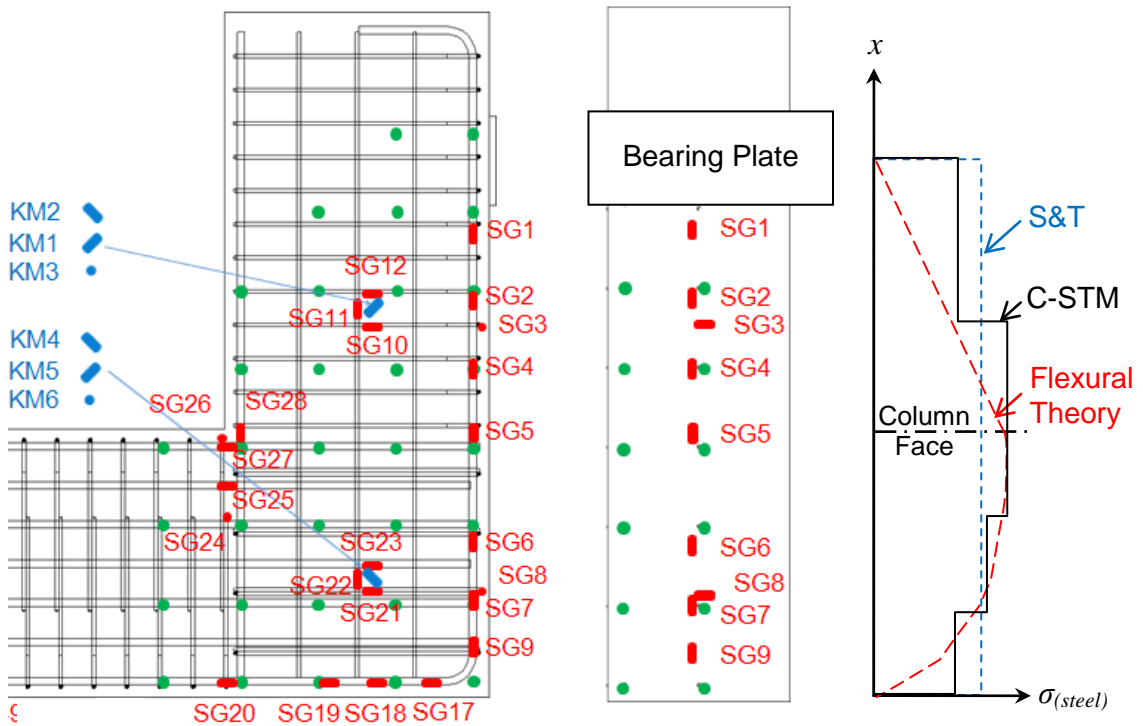
The global displacement at the applied load was obtained by taking an average of the measured displacements above and below the header beam. The drift of the beam relative to the column was measured using two LVDT's mounted to a rigid column that was fixed to the surface of the column and offset from the beam face 3 in. The overall deflected shape was obtained by externally mounted string pots secured to external reaction columns or mounted on the strong floor.

Experimental deformations associated with the analytical C-STM members where measured using LVDT's mounted to aluminum truss members that were connected between node points as shown in Figure 3.4 (b). This consisted of 10 members with 6 node points for the tested beam, and 4 members with 4 node points for the protected beam each labeled as LV#. Embedded DEMEC points defined each



(a) External instrumentation layout

(b) LVDT truss setup



(c) Internal instrumentation elevation

(d) End elevation

(e) Longitudinal stress

Figure 3.4: Specimen instrumentation

node point and were connected with aluminum members that had pinned-slotted end connections in order to measure deflections.

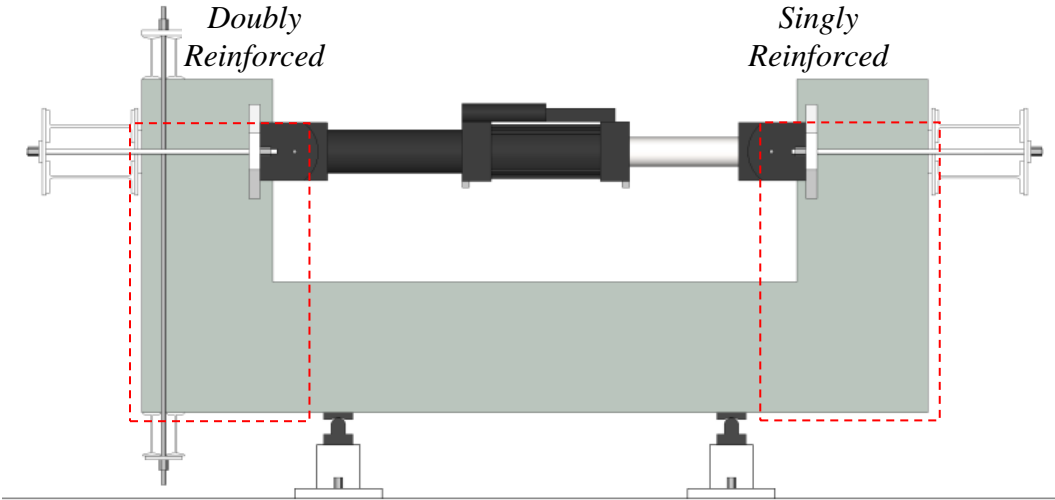
Crack widths or inferred principal tensile strains perpendicular to the corner-to-corner arch struts in the beams and joints were measured with 4 LVDT's mounted perpendicular to the expected crack angles (55° and 45° in the beam and joint respectively) with a 9" gage length.

In order to provide insight into the internal deformation strains, an assortment of strain gauges were affixed to rebars at locations shown in Figure 3.5 (c) and (d) (N.B. to distinguish between the doubly reinforced and singly reinforced beams, a suffix of *D* or *S* is used subsequent to the strain gage number, respectively). To measure the strain in the corner-to-corner concrete struts of the beam and joint regions, concrete gages were embedded at the center of the cross section and oriented in the three principal directions relative to the arch strut.

Test Procedure and Loading History

The experiment was conducted in two Phases in order to assess the performance of both cantilevered beams of the specimen through the effective use of post-tensioning, as depicted in Figures 3.5 to 3.7.

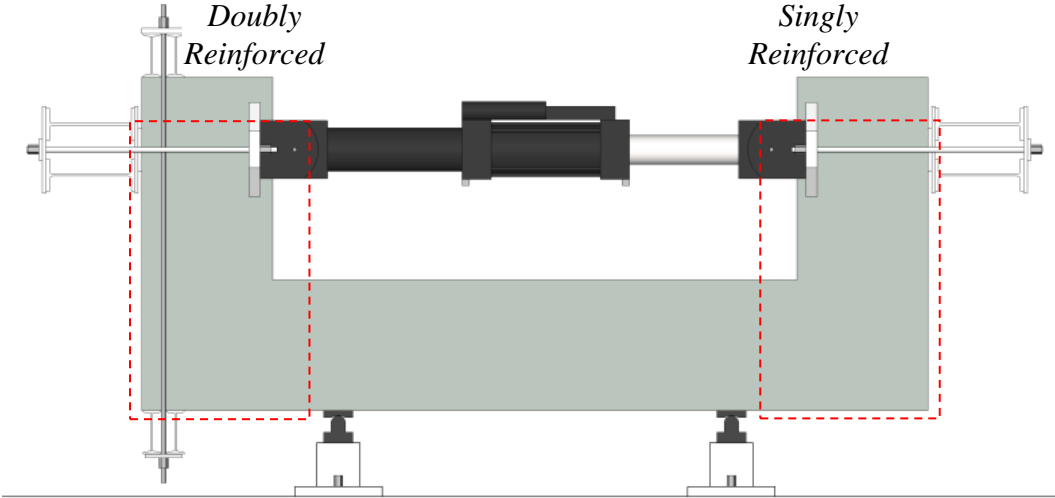
Phase I focused on the virgin performance of the singly reinforced beam, where the doubly reinforced beam was protected using post tensioning (*PT*). An applied service



(a) Doubly reinforced beam

(b) Singly reinforced beam

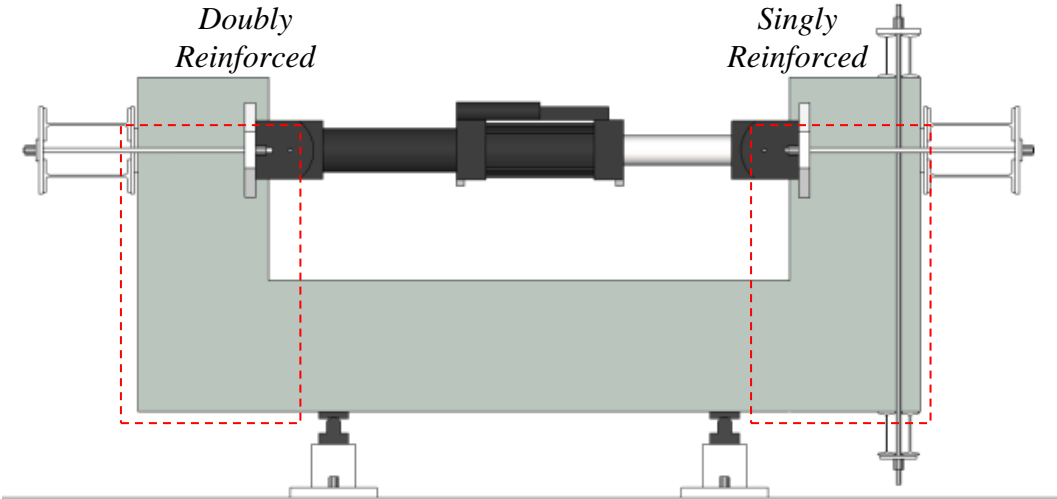
Figure 3.5: PHASE I – Serviceability loading (200 kip)



(a) Doubly reinforced beam

(b) Singly reinforced beam

Figure 3.6: PHASE I – Yield (440 kip)



(a) *Doubly reinforced beam*



(b) *Singly reinforced beam*

Figure 3.7: PHASE II – Ultimate load at (474 kip)

load of 200 kips was initially applied, held for approximately 2 hours to take measurements, and then unloaded. The specimen was then reloaded to yield (440 kip).

Phase II focused on the pre-cracked performance of the doubly reinforced beam until the ultimate failure load, where the singly reinforced beam was strengthened via the application of post-tensioning to the beam.

3.4 Test Results and Discussion

Figures 3.5 to 3.7 show experimental test photos of the control specimen at the conclusion of phases I and II, highlighting the primary crack patterns. Experimental observations during testing were reported as follows.

Experimental Observations

Phase I – Tested Beam region: Flexural cracking was first observed at 110 kips shortly followed by flexural cracks in the column. Distinct diagonal cracking in the joint was observed at approximately 170 kips. Diagonal cracking through the beam slowly propagated when held at 200 kips. Upon reloading to 440 kips, existing cracks in the beam and joint propagated towards the internal knee joint (CCC node) with the largest crack width observed in the beam of 0.05 in. at a load of 440 kips.

Phase I – Protected Beam region: Flexural cracking was first observed in the column at approximately 120 kips shortly followed by diagonal cracking in the joint propagating from the post-tensioning header beam to the internal knee joint. One hair

line crack was observed in the beam column face at 200 kips. A distinct diagonal crack in the beam formed at approximately 360 kips with a crack width of 0.02 in.

Phase II: Due to the pre-cracked state of both beams, existing cracks propagated with the formation of a few new cracks in the joint and beam at higher loads. At 440 kips the largest diagonal cracks in the beam and joint was approximately 0.025 in. and 0.035 in., respectively. The ultimate failure mechanism occurred in the tested beam-column joint along the main corner-to-corner diagonal in a sudden collapse. The maximum applied force was 474 kips.

The applied post tensioning successfully protected the longitudinal reinforcement from prematurely yielding by offsetting the measured strain to approximately zero at the applied service load of 200 kips. This not only protected the beam from yielding, but also delayed concrete cracking, thus resulting in a stiffer response as seen in the force-displacement responses below.

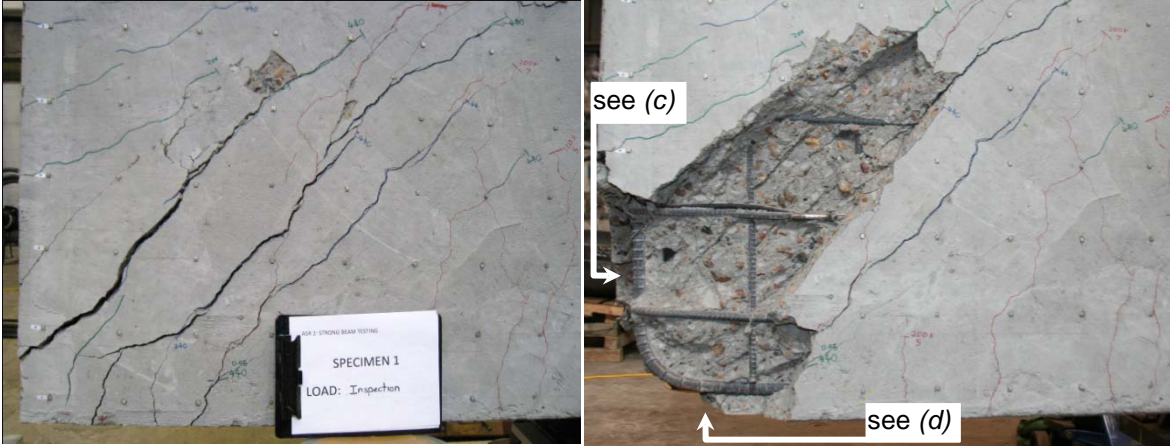
Failure Assessment

The failure mechanism was classified as a brittle joint shear failure. Evidently, failure was initially triggered by concrete softening of the joint corner-to-corner diagonal strut (arch action), thus redistributing the force to the transverse reinforcement in the joint (truss action). Because the joint was under-reinforced, this redistribution of force to the truss mechanism further intensified the arch compression softening. The brittle nature of the failure was attributed to the insufficient confinement of the transverse U-bars used in the joint due to the lack of 135-degree hooks. The initiation of concrete cover cracking

resulted in a loss of bond in the U-bars thus allowing a complete collapse (failure) mechanism to form. This failure proposition is validated with experimental and analytical results discussed in subsequent sections.

The joint reinforcement consisted of 4 U-bars and straight longitudinal distribution steel from the beam and column that were not anchored sufficiently well to confine the core concrete. U-bar and other open hook type reinforcement details do not form a complete load path in the structure as they rely on bond strength provided by the cover concrete to transfer the force. Under the high-strain overload conditions imposed, the cover concrete (due to spalling) typically provides very little, if any, restraint. This reduces the ability of the U-bars to provide confinement and ultimately results in a very rapid and brittle collapse mechanism. It is not uncommon to specify this type of detailing in bridge structures particularly in non-seismic regions. Such a failure could easily be inhibited by specifying a fully enclosed perimeter hoop with 135-degree anchorage hooks.

Figure 3.8 shows the joint failure before and after removal of the loose and spalled concrete. Upon closer examination, sufficient debonding was observed around the U-bars, and signs of pullout were evident from the direction of the steel ties (Figure 3.8 (c)) as a result of the cover concrete spalling (verifying that previously discussed). Out-of-plane splitting/bursting in the joint was also observed by the crack patterns on the exterior face of the column along with bulging of the U-bars (Figure 3.8 (d)).



(a) Failure in joint

(b) Removal of loose and spalled concrete



(c) Debonding of transverse U-bars

(d) Exterior face of column showing bulging of U-bars

Figure 3.8: Experimental photos of failure mechanism

Behavior and Code Force-based Predictions

Figure 3.9 presents the force versus overall displacement response for both the singly and doubly reinforced cantilever beams, where a thick black line represents the tested response and a thin light line represents the “protected” response. The experimental response is overlaid with code-based prediction based on:

- Flexural bending theory at the first yield moment (M_y) of the longitudinal steel, $V_y = M_y / a$, where $a = 36 - in$ = the distance between the applied load and critical section
- Flexural bending theory at the nominal ultimate moment (M_n) capacity, $V_n = M_n / a$
- Sectional shear $V_U = A_{sh} f_y d / s + 2 \sqrt{f'_c} b_w d$ (*psi units*)
- Strut-and-Tie Model (V_{STM}) predictions based on the AASHTO LRFD (2008) Bridge Design Specifications.

N.B. The exact calculations for each case can be found in Appendix D.

From these code-based predictions, one is led to believe that this bridge specimen is shear-critical in the beam because both V_u and V_{STM} are smaller than V_y . This observation is quite deceptive; clearly a more insightful analysis method is needed. This is now the subject of the following section.

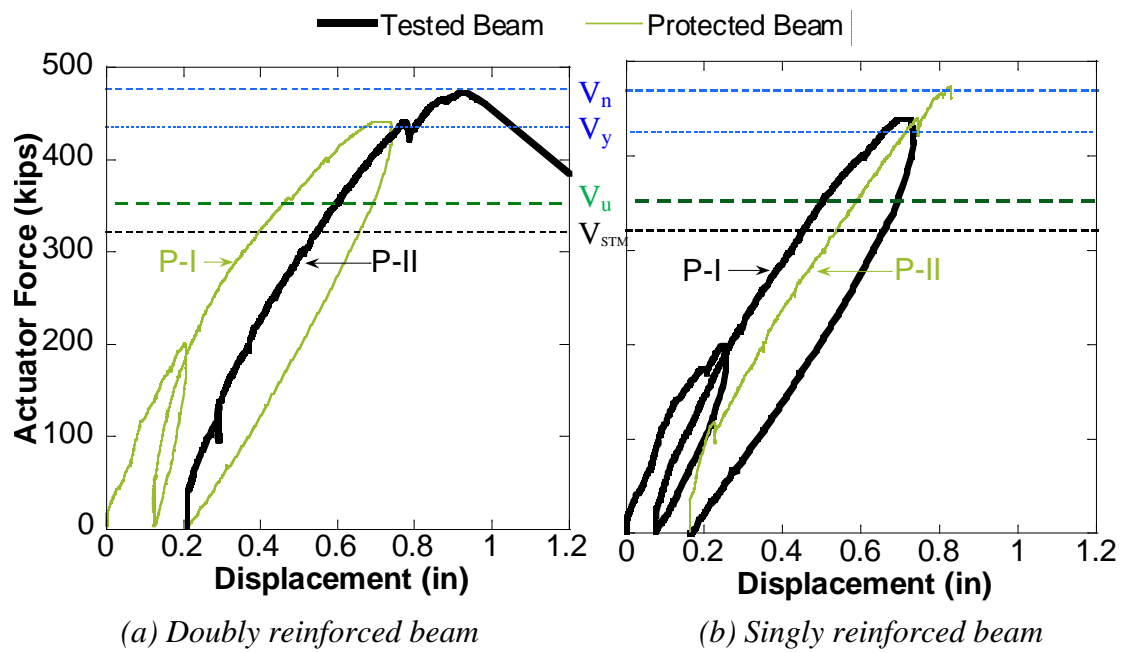


Figure 3.9: Force vs. overall displacement in conjunction with code based predictions

3.5 Compatibility-based Strut and Tie Application

The compatibility based strut and tie model (C-STM) proposed in Chapter II was adopted as an advanced means of analyzing the C-Specimens force-displacement response and internal strain behavior.

C-STM Model

Figure 3.10 shows the C-STM overlaid with the reinforcing steel of C-Specimen. The C-STM was constructed using the techniques developed in Chapter II, where a detailed explanation of the truss geometry, member sizes, and constitutive material models is appended in Appendix B. To simulate the experimental test setup as accurately as possible, initial loads (shown as *PT* in Figure 3.10) were applied to the tension chord members of the protected beam in order to replicate post-tensioning effects in accordance with Phase I and Phase II testing.

The cantilevered beams were modeled using a single-point Gauss quadrature model. The joint were modeled using a two-point model where the transverse ties were aligned with the U-bar reinforcement to provide a more exact representation of the reinforcement. Phase II was modeled using a reduced concrete tensile strength f'_t in order to allow for the pre-cracked concrete state; however, the bilinear tension softened response shown in Figure 2.8 (c) remained the same.

The results of the C-STM are directly compared to the experimental response and were used to provide a detailed interrogation of the force-deformation and nonlinear response behavior.

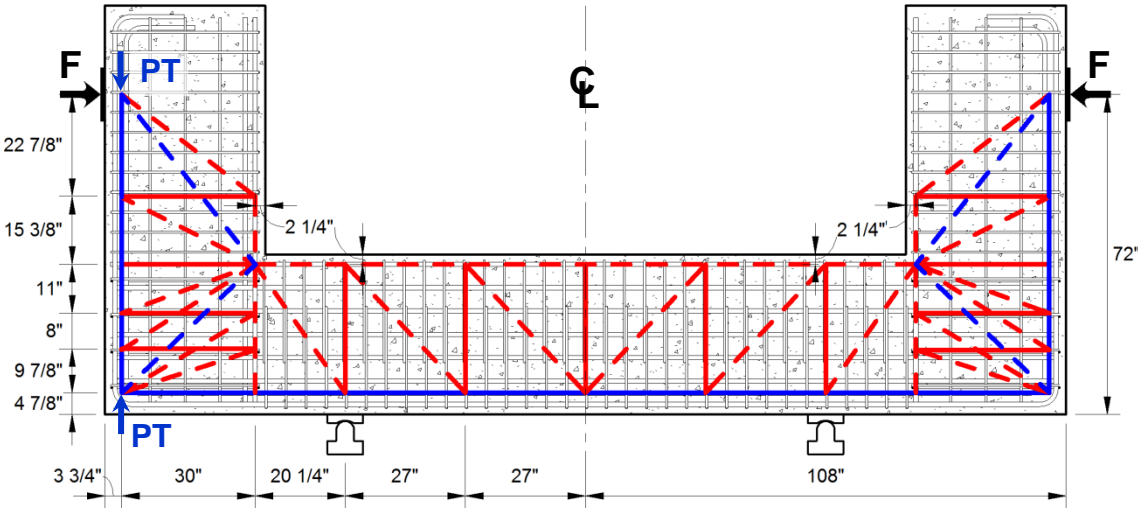


Figure 3.10: Applied C-STM of C-Specimen – Phase I modeling

Force-displacement Response

Figure 3.11 overlays the predicted response using the C-STM (thin red line) with the experimental force versus overall displacement response (thick black line) shown in Figure 3.9. For clarity, the two phases of testing are shown separately in order to clearly distinguish between the protected and tested responses. Columns (a) and (b) refer to the doubly and singly reinforced beam responses, and rows 1 and 2 refer to testing Phases I and II, respectively. The C-STM prediction models well both the protected and tested response of both beams. The initial tension-stiffening effects observed are also captured well by the C-STM.

Figure 3.12 shows a similar comparison of the beam-only response that is measured with respect to the column. The drift is defined as the percentage of displacement relative to the top of the column section divided by the beam length ($L = 36 \text{ in.}$). Good agreement between the experiment and the C-STM is evident.

Appendix C presents a comprehensive comparison of the experimental results and C-STM predictions, focusing on critical sections of the C-Specimens.

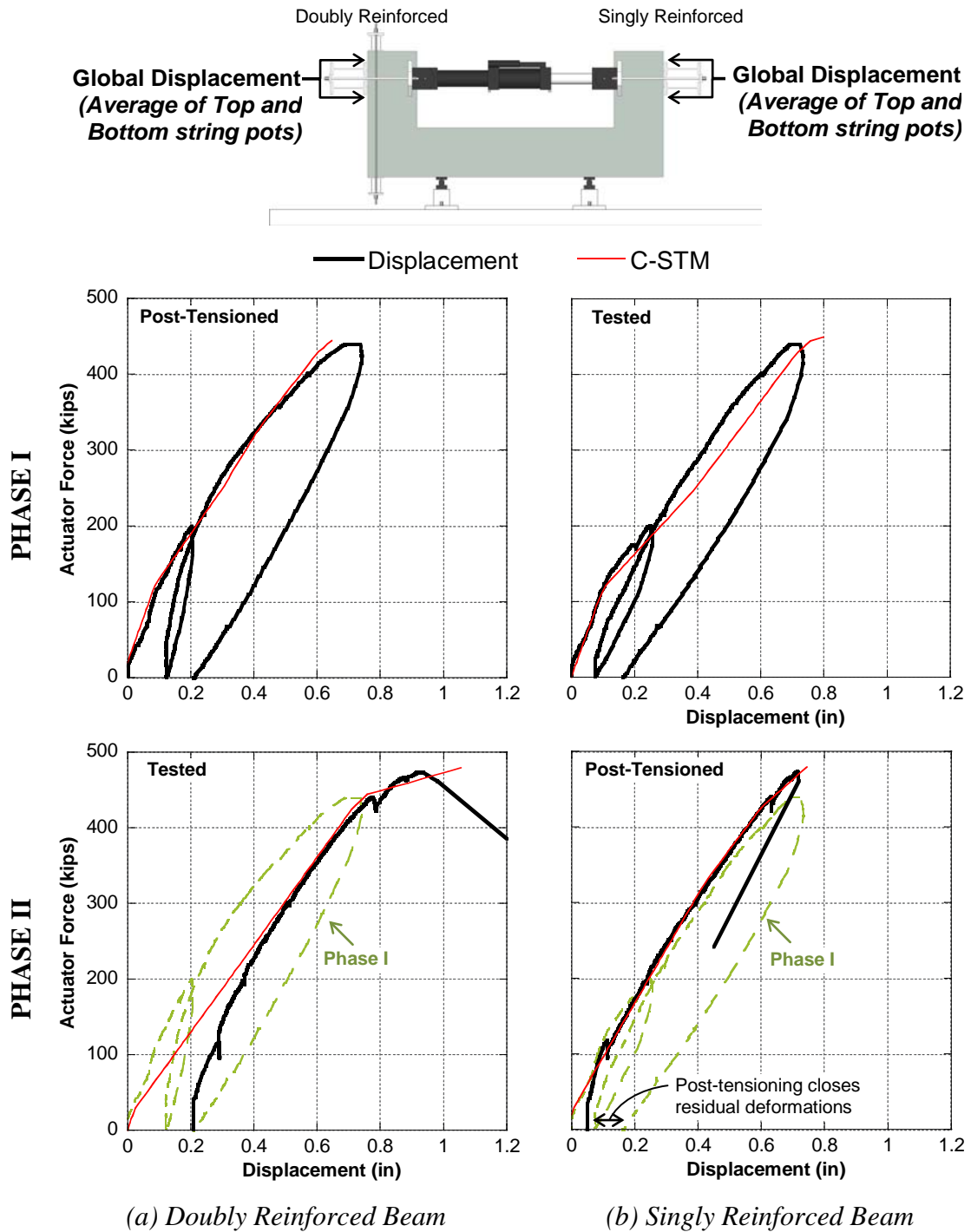


Figure 3.11: Global force-deformation behavior

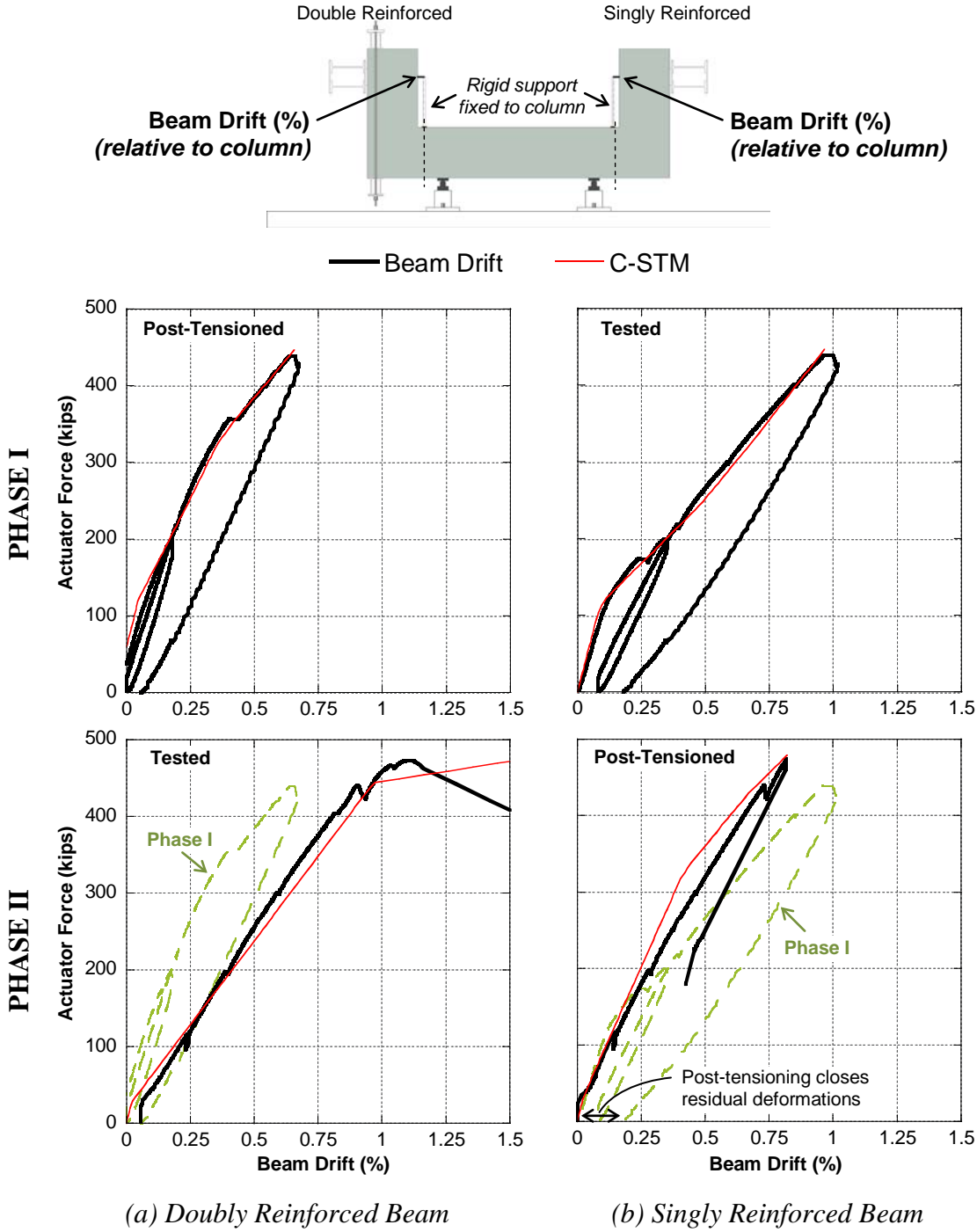


Figure 3.12: Beam only (drift) response

Internal Behavior of the Specimen

Figures 3.13 and 3.14 present the development of nonlinear behavior in the C-STM with increasing levels of force. The predicted behavior is compared with experimentally observed instrumental results. The notation in the left-hand column first describes the type of nonlinear mechanism in parentheses (a description of each follows), followed by the member it refers to (e.g. beam, joint or column). The instrumentation used for each graph is labeled in the bottom corner of each graph and can be referred to in Figure 3.4.

The first nonlinear mechanism is concrete cracking of the concrete truss elements as shown in Figure 3.13. Subsequent nonlinear mechanisms are shown in Figure 3.14 consisting of concrete chord and arch inelastic compression, followed by steel yielding. The progression of nonlinear behavior can be described as follows.

LC = Longitudinal Cracking (see graphs in row 1 & 2 of Figure 3.13) first occurred in the beam, shortly followed by the column. This is when the member stress exceeds the concrete tensile strength f_t' , thus initiating flexural cracking in the beam at the column face, and along the column respectively. Tension softening refers to the concrete's ability to resist tensile strains after the development of the primary cracks.

TC = Transverse Cracking (see graphs in row 3 and 4 of Figure 3.13) then occurred in the transverse concrete elements, starting in the beam column joint and then in the beam element. This corresponds with diagonal shear cracking observed as a result of the flexure-shear interaction and is in agreement with experimental observations.

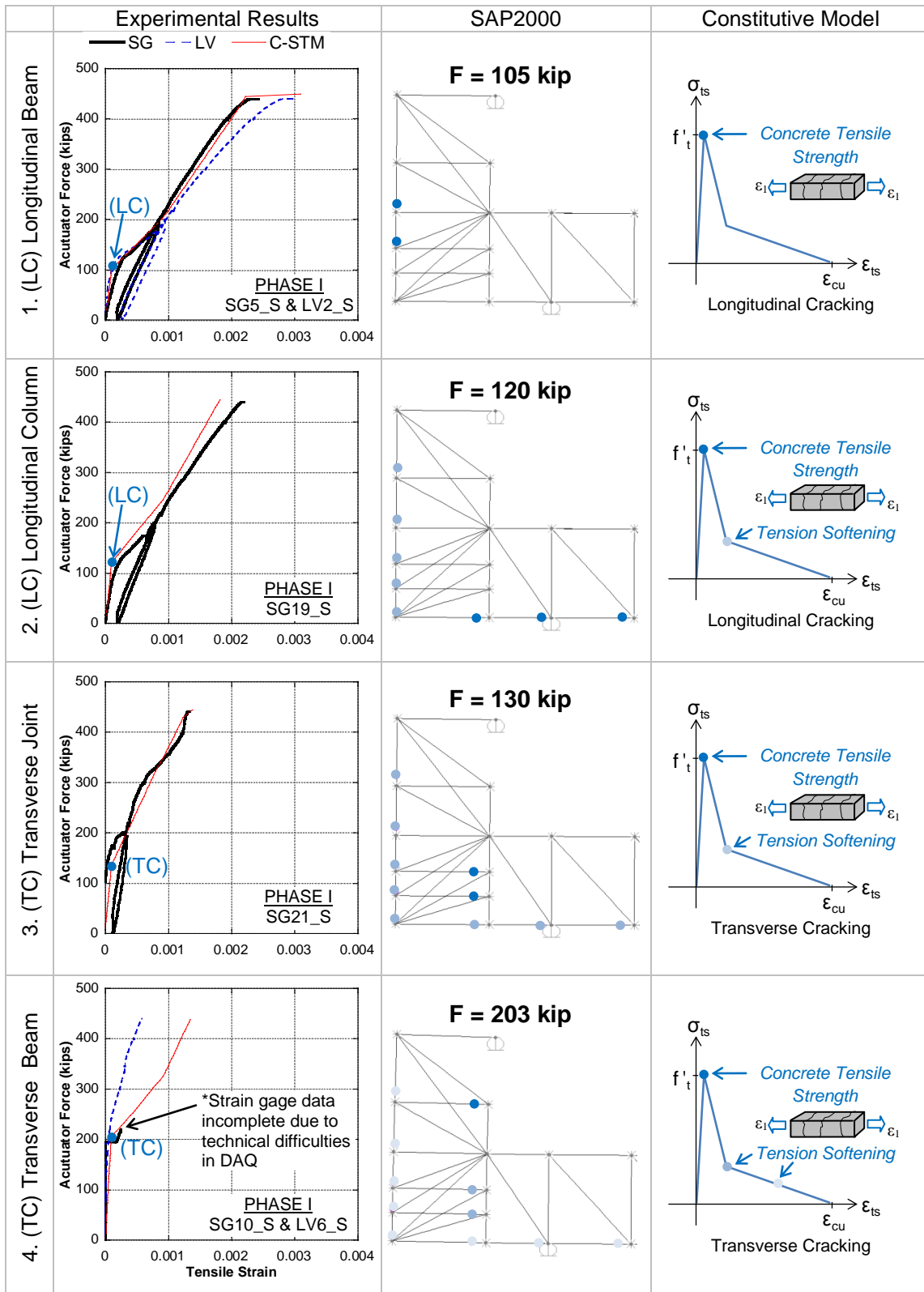


Figure 3.13: Nonlinear response and early concrete cracking effects

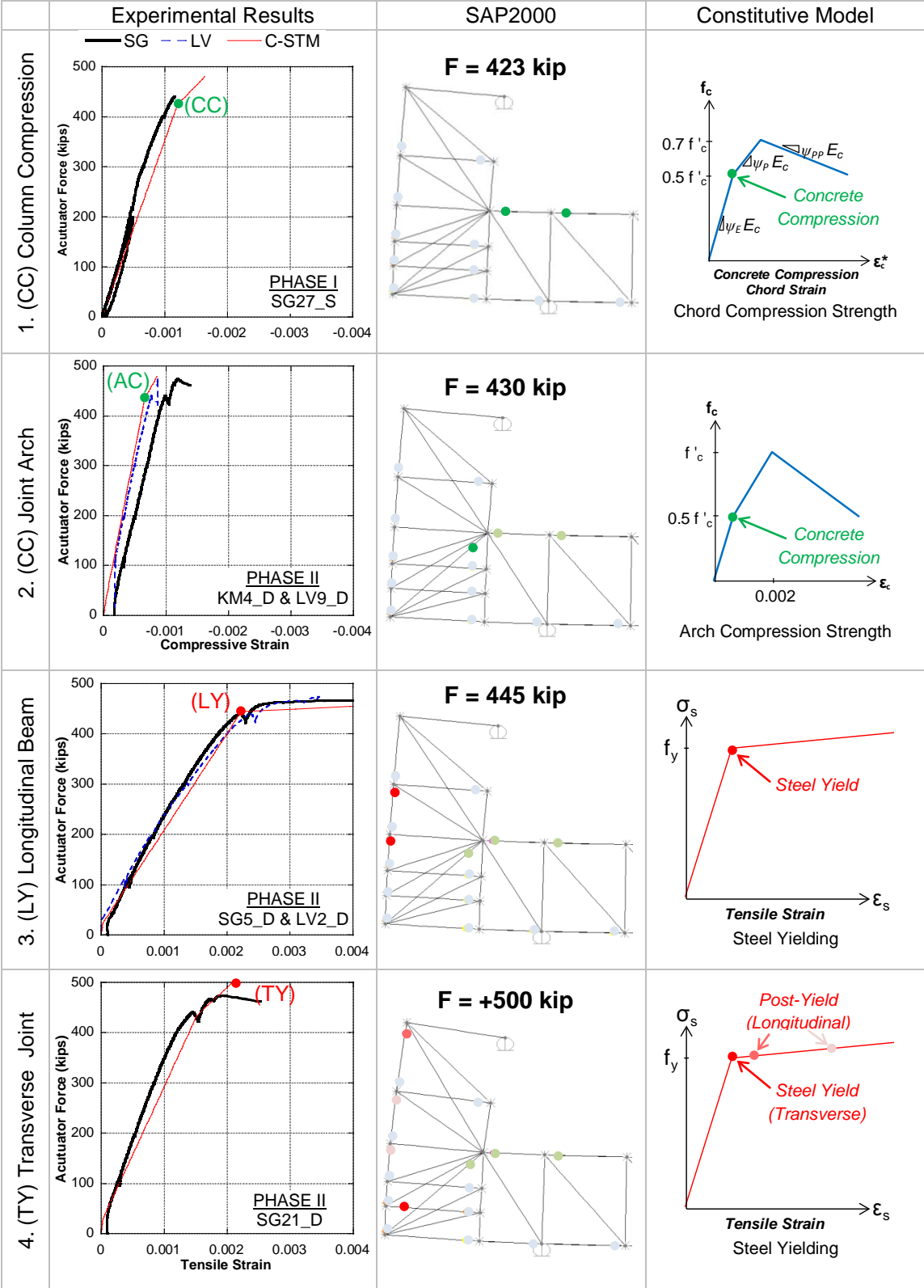


Figure 3.14: Nonlinear concrete and steel response

CC = Chord Compression (see graph in row 1 of Fig. 3.14) occurred in the column compression chord elements indicating that the concrete had exceeded the elastic limit as specified in Section 2.5. It is evident that the C-STM prediction agrees well with the strain gage observations located on the column compression steel at the beam face.

AC = Arch Compression (see graph in row 2 of Fig. 3.14) shortly followed in the joint arch (corner-to-corner diagonal strut) which also indicated that the concrete had exceeded the elastic limit (defined as $0.5f'_c$) where a reduction in stiffness commenced. The predicted response is in good agreement with the embedded strain gages and the external LV truss member response. The drop in response at 440 kips corresponds to a pause in loading. However, following the pause, a definite change in stiffness was observed upon reloading that agrees with the C-STM prediction.

LY = Longitudinal Yielding (see graph in row 3 of Fig. 3.14) occurred in the longitudinal beam reinforcement when the stress exceeds the specified yield stress f_y . The C-STM prediction agreed well with the steel strain gage response of $SG5_D$ (located at the column face), and the corresponding $LV2_D$ truss member response.

TY = Transverse joint steel Yielding (see graph in row 4 of Fig. 3.14) in the joint U-bars were the next member in the C-STM to respond nonlinearly. Although this was not so accurately predicted by the initial analysis, what is important to note is the change in the elastic slope observed at 430 kips (before yielding at +500 kips) in both the predicted and experimental response. This clearly is not a result of yielding as the measured strain was approximately half the yield strain. Instead the change in slope

corresponds to the softening of the arch strut (as indicted by *CC* in row 2 of Fig 3.14). As the arch strut softens, more force is transferred into the truss mechanism as a result of the displacement compatibility requirements between the arch and truss mechanism. This observation is validated by the experimental strain gage located on the second U-bar in the joint (*SG21_D*). This observed softening of the joint arch (corner-to-corner strut) is further intensified by companion orthogonal tensile strain (ϵ_I), eventually resulting in ultimate failure which is discussed further as follows.

Failure Mechanism

Figure 3.15 presents the post analysis investigation conducted to check compression softening failure in accordance with Section 2.8. The joint arch strut was determined to be the critical element that was prone to compression softening failure as illustrated by Figure 3.13 (a). The inferred principal tensile strain ϵ_1 was calculated from the C-STM using the obtained strains from the arch and the transverse ties in the joint using Eq. (2.38). Figure 3.13 (b) compares the predicted ϵ_1 with the experimental results obtained from the embedded concrete gage (*KM5_D*) and *LVDT 1* mounted with a 9-in. gage length orthogonal to the corner-to-corner strut as shown in Figure 3.4 (b). The inferred tensile strain agrees well with the corresponding surface gage *LVDT 1*. However, the embedded concrete gage had a higher measured internal tensile strain that eventually exceeded the capacity of the gage. This higher tensile strain could either be indicative of

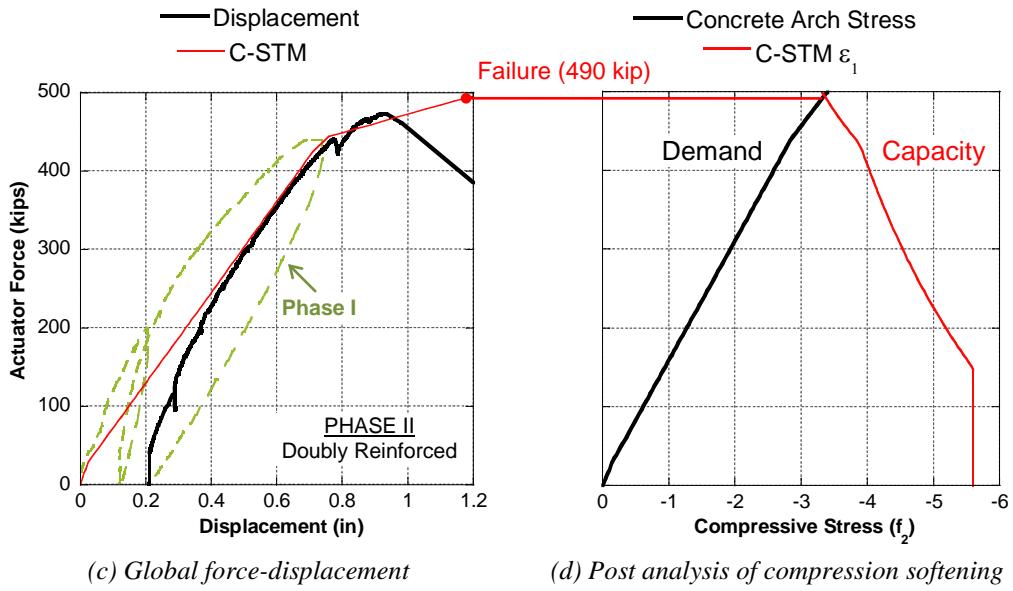
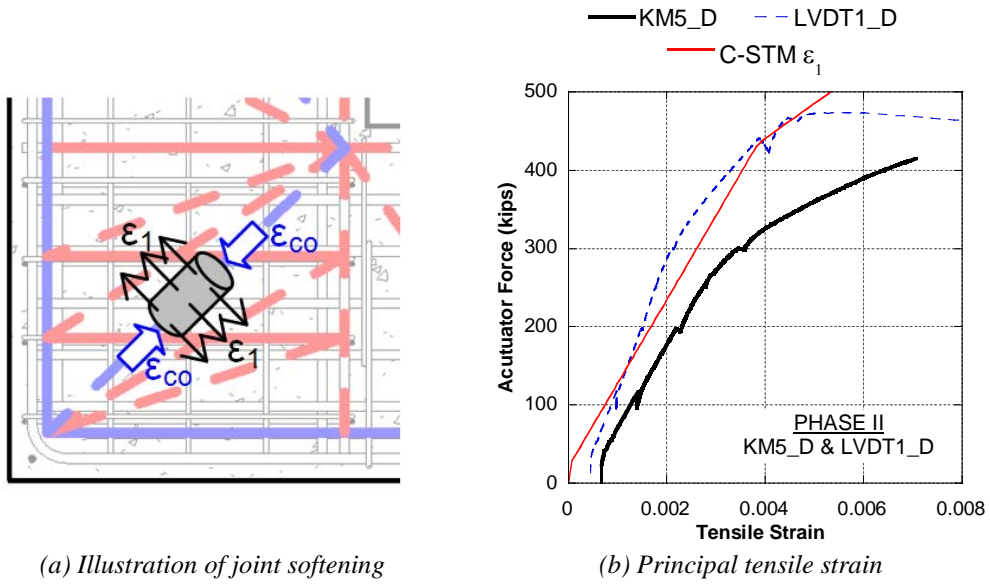


Figure 3.15: Failure analysis of compression softening effects

greater tensile strains in the concrete core, or a discrete crack crossing the gage resulting in higher strains.

Figure 3.15 (d) shows the compression softening results of Eq. (2.37b) using the principal tensile strains defined by the C-STM, thus defining the capacity of the concrete as a function of ε_1 with respect to the actuator load. The demand line was defined using strain in the joint arch strut (experimentally verified in row 2 of Figure 3.14) to calculate the concrete arch stress with respect to the actuator load. Hence, the intersection of the two lines indicates the ultimate failure load. For Phase II, this was determined as 490 kips ($1.03 F_{exp}$) as indicated by the horizontal lines projected back onto the force-displacement plot in Figure 3.15 (c).

Although the C-STM ε_1 agreed well with the experimental results prior to ultimate, it over-predicted the failure response because it does not account for the softening of the concrete strut strain prior to failure as indicated by the change in slope at approximately 460 kips in Figure 3.15 (b). Hence, in order to accurately model this, a second analysis would need to be run with the concrete strut stress-strain relationships adjusted according to the softening effects.

Discussion of Interaction between Arch and Truss Action

A common trend was observed between the analytical and experimental results related to the interaction of force transfer between arch and truss action. Figure 3.16 presents the analytical and experimental results obtained for selected truss members shown in Figure 3.16 (a).

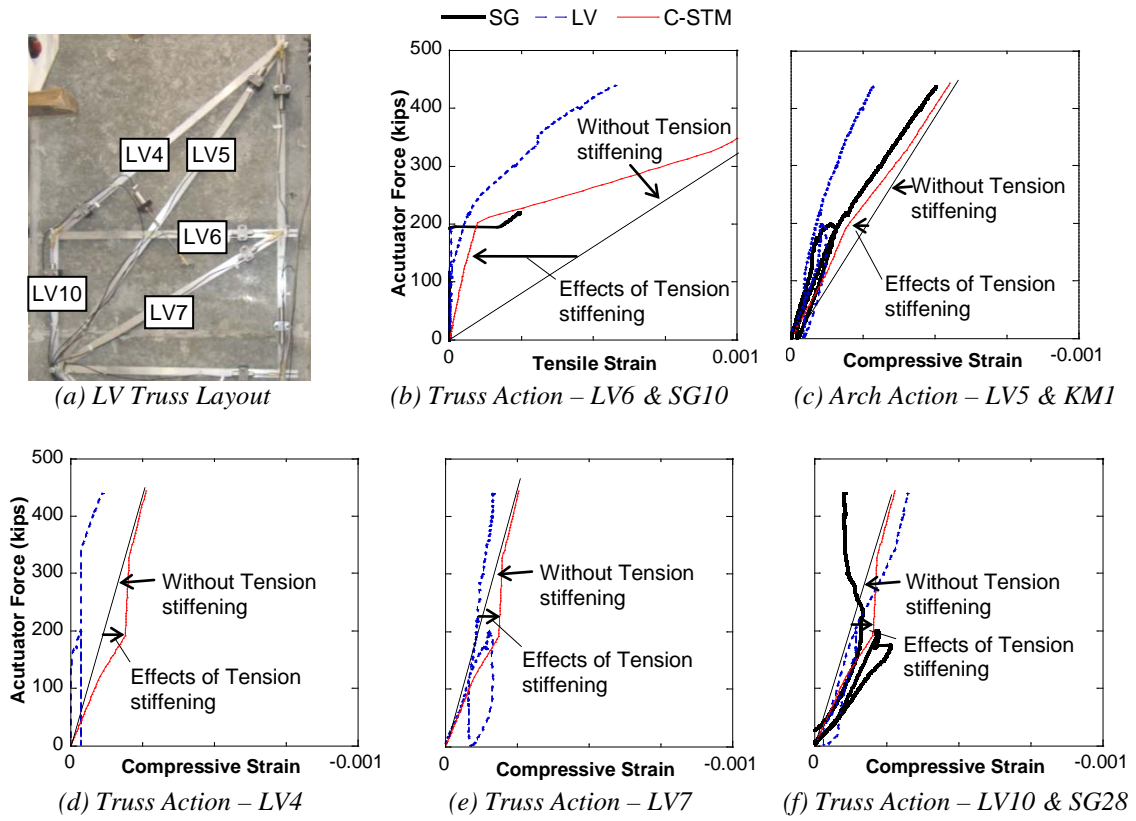


Figure 3.16: Interaction of arch and truss action

The arch and truss mechanism can be thought of as two shear resisting springs acting in parallel and constrained by displacement compatibility. The force transferred into each mechanism from an applied load is thus going to be function of the mechanisms stiffness. For example, the truss mechanism is initially stiffer due to concrete tension stiffening of the transverse ties, hence it attracts more force relative to the arch mechanism. Once the transverse concrete element cracks, the stiffness of the truss mechanism reduces, thus redistributing more force into the arch mechanism. This is observed in graphs (b) to (f) of Figure 3.14, where each plot shows the analytical C-STM predictions with and without tension stiffening, overlaid with the corresponding experimental results.

Figure 3.14 (b) shows the response for the transverse tension tie in the truss mechanism where diagonal flexure-shear cracking was observed by the sudden change in slope at approximately 200 kips.

Figure 3.14 (c) shows the response of the diagonal corner-to-corner arch mechanism. A distinct change in slope is observed at approximately 200 kip that represents the redistribution of force from the truss mechanism to the arch mechanism after transverse cracking occurs.

Figures 3.14 (d), (e), and (f), show an equivalent but converse observation to the arch mechanism. Initially, the diagonal concrete struts (LV4 and LV7) and the compression chord member (LV10) in the truss mechanism showed a greater rate of force transferred to the members due to tension stiffening effects. This is evident by the initially higher strains observed when compared to that without tension stiffening before

transverse cracking occurred at 200 kip. Subsequent to transverse cracking, the change in response represents the force being transferred into the arch mechanism due to reduced stiffness of the truss mechanism.

This interaction of arch and truss action further verifies the compression softening observation described in the previous section. In this case, the loss of corner-to-corner arch stiffness (due to compression softening effects) resulted in a greater transfer of force into the truss mechanism. However, because the joint was under-reinforced and the transverse U-bars were unable to sustain yield strains due to the lack of proper anchorage (including no 135-degree hooks), this in turn caused major distress to the corner-to-corner joint strut eventually resulting in a system failure.

3.6 Chapter Closure

This chapter presented an experimental and analytical investigation on the shear strength of large-scale reinforced concrete bridge bents. The experimental specimens were designed to replicate current bridges in Texas, where an increasing need to accurately assess the structural integrity of the structure is required. Code-based analysis techniques and an advanced Compatibility based Strut-and-Tie Model (C-STM) were used to assess the experimental specimen's response.

Based on the research described in this chapter, the following conclusions can be drawn:

1. The near full scale C-specimens tested in this experimental research provided an accurate representation of the shear-flexure performance associated with deep beams

and disturbed regions, and provided some insight into the internal stress and strain fields. Based on scaled reinforcing details of the representative cantilevered and straddle pier bents, the joint was insufficiently reinforced to confine the main diagonal corner-to-corner concrete strut and a brittle failure mechanism ensued as a result of inadequate detailing. Recommendations for exterior beam-column joint reinforcement detailing includes: providing transverse reinforcement in both beam and column directions to sufficiently confine the core concrete; and using well-anchored perimeter hoops (with 135-degree hooks).

2. Code-based shear analysis under-predicted the specimens response and provides inadequate detailing for designing against the observed brittle failure mechanism, thus presenting a need for a more advanced method of analysis. To which the proposed C-STM presents itself as an advanced analysis tool that can be adopted and implemented by practicing structural engineers.
3. The C-STM provided an accurate representation of the structures force-deformation response, providing a detailed evaluation of the internal nonlinear behavior that was verified through experimental instrumentation. A thorough interrogation of the ultimate failure mechanism was also accurately modeled.

CHAPTER IV

SUMMARY, CONCLUSIONS AND RECOMMENDATIONS

4.1 Summary

This research has primarily focused on the development of a compatibility-based strut-and-tie model (C-STM) for the purpose of analyzing the complex shear-flexure behavior associated with deep beams and disturbed regions. In addition to the normal strut-and-tie force equilibrium requirements the model accounts for non-linear material behavior through displacement compatibility using inelastic constitutive laws for reinforced concrete. The model was implemented into the widely used commercial structural analysis software SAP2000. As such it is ideally suited for design checks routinely conducted by practicing bridge engineers.

The proposed C-STM focuses particularly on the behavior of reinforced concrete bridge piers through an applied experimental investigation of previously conducted research. Additionally, an experimental investigation was conducted on a near-full scale subassembly representing two distinctive types of bridge pier construction in Texas – namely, cantilever (hammerhead) bents and straddle (frame) bents. The C-STM was also applied and compared to the experimental results, where good agreement between the two was observed.

4.2 Conclusions

Based on the research presented in this thesis, the following major conclusions may be drawn

1. The proposed *Compatibility-Strut and Tie Model* serves as an advanced method of analysis that can predict with suitable accuracy the force-deformation response of both D- and B- regions, deep beams, and beam columns. By considering equilibrium, compatibility, and nonlinear constitutive laws of cracked reinforced concrete members, insights into internal nonlinear member strains and the hierarchy of failure mechanisms can be assessed with reasonably good accuracy. The C-STM was verified by analyzing the behavior of large-scale experimental bridge cap specimens, where good agreement between the experimental and predicted response was observed.
2. The near full scale C-specimens tested in this experimental research provided an accurate representation of the shear-flexure performance associated with deep beams and disturbed regions, and provided some insight into the internal stress and strain fields. Code-based analysis under predicted the specimens response and brittle failure mechanism, whereas the applied C-STM provided an accurate representation of the specimen's force-deformation response, providing a detailed evaluation of the internal nonlinear behavior that was verified through experimental instrumentation.
3. The C-STM is a minimalist computational method of analysis that can be implemented into commercial available structural nonlinear analysis software such as SAP2000. This provides both consulting and state bridge design engineers with a

supplementary analysis tool that can be used to augment the design process and accurately assess the force-deformation response and nonlinear behavior of bridge piers with stocky members and/or large disturbed regions.

4.3 Recommendations and Future Work

The developed C-STM in this research lays a pathway for further research to be conducted in the following two areas of interest: (i) implementing the effects of cyclic loading in C-STM; and (ii) modeling the effects of aging and material deterioration specifically the effects of ASR/DEF on the performance of bridge piers. These are discussed as follows.

Modeling of Cyclic Loading

The effect of cyclic loading on C-STM performance is considered to be the first challenge to be undertaken. Although much work in this direction has been done by Kim and Mander (1999; 2000a; 2000b), there are some new features, discovered as part of this research, that need to be implemented. Specifically the concrete softening of the arch/struts requires proper treatment under cyclic loading, and the interaction of concrete and steel in the compression chord member. The approach should first be validated against cyclic quasi-static tests and the extended into the time domain to conduct non-linear time history analysis similar to the approach used by To et al. (2009).

Cyclic loading effects can be modeled through the successful application of nonlinear material stress-strain relationships that consider the cyclic unloading reverses

using appropriate hysteresis models. In order to model reversal loading, symmetrical diagonal concrete struts are required in order to allow for the transfer of compression through the web in both loading directions. This can be achieved in SAP2000 through the application nonlinear link elements that encompass hysteretic models, where the back-bone of the stress-strain relationship can be inputted by the user. The alternative nonlinear frame hinge elements provided in SAP2000 were found to be sensitive and somewhat difficult to apply when modeling the hysteretic behavior of non-symmetrical stress-strain curves (i.e. concrete stress-strain compression and tension effects).

Modeling of Concrete Deterioration

The ingress of moisture that accelerates physical-chemical concrete deterioration mechanisms such as Alkali Silica Reaction (ASR) and Delayed Ettringite Formation (DEF) are typically the main causes of premature deterioration in modern reinforced concrete structures. These mechanisms induce internal swelling strains that potentially result in concrete cracking, loss of bond, internal excessive steel strains, thus reducing the concrete's compression and tensile strength, and elastic stiffness.

The following two methods are proposed as preliminary methods of modeling premature concrete deterioration when using C-STM techniques:

1. The deterioration of concrete strength and stiffness can be altered through the assigned member axial rigidities and the specified nonlinear constitutive material models. A preliminary investigation is provided below in Figure 4.1, where the

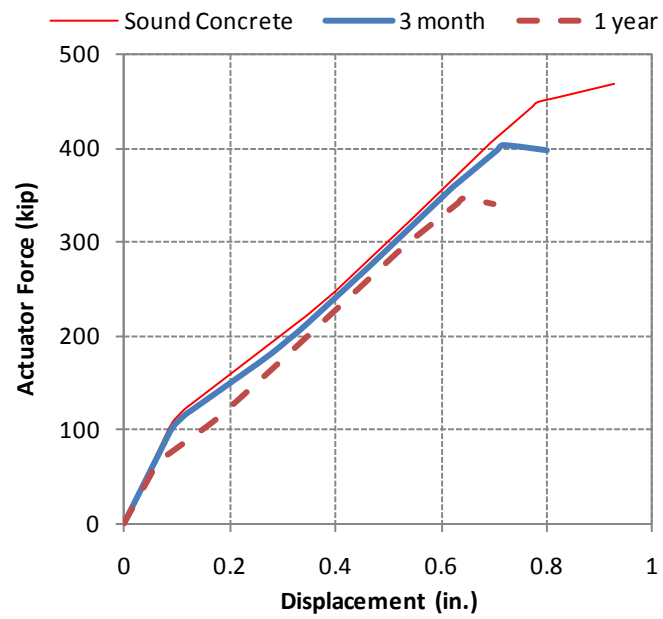


Figure 4.1: Illustrative force-deformation response of deteriorated concrete

concrete material parameters for the C-Specimen discussed in Chapter was altered according to Table 4.1.

Table 4.1: Illustrative deteriorated concrete strengths

	Sound Concrete	3 months Deterioration	1 year Deterioration
f'_c (ksi)	5.6	4.9	4
E_c (ksi)	4265	3990	3620
f'_t (ksi)	0.425	0.3	0.24
Failure Load (kips)	469	400	345

2. Deterioration of ASR/DEF is typically a function of the expansion strains that arise over time. Now suppose ε_{ASR} = the deteriorated expansion strain, then the compression softening equation Eq. (2.37b) could simply be modified by adding in the deterioration expansion, thus

$$\zeta = \frac{f_{2,\max}}{f'_c} = \frac{1}{1 + \left\langle \frac{\varepsilon_{ASR} + \varepsilon_1 - 0.0012}{3\varepsilon_{co}} \right\rangle} \quad (2.37b)$$

This equation implies that when $\varepsilon_{ASR} > 1200\mu\varepsilon$, the concrete is already subject to softening without load induced strains, hence this would further decrease the capacity of the diagonal concrete struts. To validate the accuracy of this relationship, experimental research into the deteriorated performance of concrete cylinders could be conducted as a function of the swelling strain.

REFERENCES

- AASHTO. (2008), *AASHTO LRFD Bridge Design Specifications and Commentary*, 3rd Ed., American Association of State Highway and Transportation Officials, Washington, DC.
- ACI Committee 318. (2008), "Building Code Requirements for Structural Concrete (ACI 318-08) and Commentary," American Concrete Institute, Farmington Hills, MI.
- ASCE-ACI Committee 445 on Shear and Torsion, (1998). "Recent approaches to shear design of structural concrete." *Journal of Structural Engineering*, (124)12, 1375-1417.
- Alcocer, S. M., and Uribe, C. M. (2008). "Monolithic and cyclic behavior of deep beams designed using strut-and-tie models." *ACI Structural Journal*, 105(3), 327-337.
- Arnold, D. M. (2004). "Development and experimental testing of a seismic damage avoidance designed beam to column connection utilising draped unbonded post-tensioning," M.S. thesis, University of Canterbury, Christchurch, New Zealand.
- Bracci, J. M., Keating, P. B., and Hueste, M. B. D. (2000). "Cracking in RC bent caps." Research Report, 1851-1, Texas Transportation Institute, Texas A&M University. College Station.
- Collins, M. P. (1978). "Towards a rational theory for RC members in shear." *ASCE J Struct Div*, V. 104(4), 649-666.
- Collins, M. P., Bentz, E. C., and Sherwood, E. G. (2008). "Where is shear reinforcement required? Review of research results and design procedures." *ACI Structural Journal*, 105(5), 590-600.
- Collins, M. P., and Mitchell, D. (1980). "Shear and torsion design of prestressed and non-prestressed concrete beams." *Journal - Prestressed Concrete Institute*, 25(5), 32-100.

- Collins, M. P., and Mitchell, D. (1991). *Prestress Concrete Structures*, Prentice Hall, Englewood Cliffs, N.J., 1991.
- Considère. (1899). "Influence des armatures métalliques sur les propriétés des mortiers et bétons (The influence of imbedded metal on the properties of mortar and concrete)." *Le Génie Civil*, 34(15), 229-233.
- Dilger, W. (1966). "Veränderlichkeit der Biege- und Schubsteifigkeit bei Stahlbetontragwerken und ihr Einfluß auf Schnittkraftverteilung und Traglast bei statisch unbestimmter Lagerung." Deutscher Ausschuss für Stahlbeton, Heft 179, Berlin, Germany.
- Drucker, D. C. (1961). *On structural concrete and the theorems of limit analysis*, International Association for Bridge and Structural Engineering (IABSE). Zürich, Abhandlungen 21.
- FIP-Commission 3. (1996), "Practical Design of Structural Concrete," SETO, distributed by *fib*, London, UK.
- Holden, T., Restrepo, J., and Mander, J. B. (2003). "Seismic performance of precast reinforced and prestressed concrete walls." *Journal of Structural Engineering*, 129(3), 286-296.
- Hsu, T. T. C. (1994). "Unified theory of reinforced concrete-a summary." *Structural Engineering and Mechanics*, 2(1), 1-16.
- Hsu, T. T. C. (1996). "Toward a unified nomenclature for reinforced-concrete theory." *Journal of Structural Engineering*, 122(3), 275-283.
- Hwang, S.-J., Lu, W.-Y., and Lee, H.-J. (2000). "Shear strength prediction for deep beams." *ACI Structural Journal*, 97(3), 367-376.
- Kim, J. H., and Mander, J. B. (1999). "Truss modeling of reinforced concrete shear-flexure behaviour." Technical Report MCEER - 99-0005, University at Buffalo, New York.

- Kim, J. H., and Mander, J. B. (2000a). "Cyclic Inelastic Strut-Tie Modeling of Shear-Critical Reinforced Concrete Members." *American Concrete Institute*, SP 193, 707-728.
- Kim, J. H., and Mander, J. B. (2000b). "Seismic detailing of reinforced concrete beam-column connections." *Structural Engineering and Mechanics*, 10(6), 589-601.
- Kim, J. H., and Mander, J. B. (2005). "Theoretical shear strength of concrete columns due to transverse steel." *Journal of Structural Engineering*, 131(1), 197-199.
- Kim, J. H., and Mander, J. B. (2007). "Influence of transverse reinforcement on elastic shear stiffness of cracked concrete elements." *Engineering Structures*, 29(8), 1798-1807.
- Kuo, W. W., Cheng, T. J., and Hwang, S. J. (2010). "Force transfer mechanism and shear strength of reinforced concrete beams." *Engineering Structures*, 32(6), 1537-1546.
- MacGregor, J. G. (1992). *Reinforced Concrete: Mechanics and Design*, Prentice-Hall, Inc.
- Mander, J. B. (1983). "Seismic design of bridge piers," Ph.D thesis, University of Canterbury, New Zealand
- Mander, J. B., Priestley, M. J. N., and Park, R. (1988). "Theoretical stress-strain model for confined concrete." *Journal of Structural Engineering*, 114(8), 1804-1826.
- Marti, P. (1985). "Basic tools of reinforced concrete beam design." *Journal of the American Concrete Institute*, 82(1), 46-56.
- Marti, P. (1999). "How to treat shear in structural concrete." *ACI Structural Journal*, 96(3), 408-414.
- Mau, S. T., and Hsu, T. T. C. (1987). "Shear strength prediction for deep beams with web reinforcement." *ACI Structural Journal*, 84(6), 513-523.

- Mitchell, D., and Collins, M. P. (1974). "Diagonal compression field theory - a rational model for structural concrete in pure torsion." *ACI Structural Journal*, 71, 394-408.
- Mörsch, E. (1909). *Concrete-Steel Construction*, McGraw-Hill, New York, 1909, 368 pp.
- Park, R., and Paulay, T. (1975). *Reinforced Concrete Structures*, John Wiley and Sons, New York.
- Paulay, T. (1971a). "Coupling beams of reinforced concrete shear walls." *Journal of the Structural Division*, 97(3), 843-862.
- Paulay, T. (1971b). "Simulated seismic loading of spandrel beams." *Journal of the Structural Division*, 97(9), 2407-2419.
- Petersson, P. E. (1980). "Fracture energy of concrete: Practical performance and experimental results." *Cement and Concrete Research*, 10, 91-101.
- Powanusorn, S., and Bracci, J. M. (2006a). "Behavior of reinforced concrete members prone to shear deformations: part I - effect of confinement." *ACI Structural Journal*, 103(5), 736-46.
- Powanusorn, S., and Bracci, J. M. (2006b). "Behavior of reinforced concrete members prone to shear deformations: Part II - Effect of interfacial bond stress-slip." *ACI Structural Journal*, 103(5), 747-753.
- Reddiar, M. K. M. (2009). "Stress-strain model of unconfined and confined concrete and stress-block parameters," M.S. thesis, Texas A&M University, College Station.
- Ritter, W. (1899). "Die Bauweise Hennebique (The Hennebique system)". *Schweizerische Bauzeitung* (Zürich), 1899.
- Rots, J. G., Nauta, P., Kusters, G. M. A., and Blaauwendraad, J. (1985). "Smearred crack approach and fracture localization in concrete." *Heron*, Delft, Netherlands, 30, 1-48.

- Salem, H. M., and Maekawa, K. (2006). "Computer-aided analysis of reinforced concrete using a refined nonlinear strut and tie model approach." *Journal of Advanced Concrete Technology*, 4(2), 325-336.
- SAP2000. (1995). *SAP2000, Advanced 14.0.0*. Computer and Structures, Inc, Berkeley, CA.
- Schlaich, J., Schaefer, K., and Jennewein, M. (1987). "Toward a consistent design of structural concrete." *PCI Journal*, 32(3), 74-150.
- Sritharan, S., and Ingham, J. M. (2003). "Application of strut-and-tie concepts to concrete bridge joints in seismic regions." *PCI Journal*, 48(4), 66-90.
- Thürlimann, B., Marti, P., Pralong, J., Ritz, P., and Zimmerli, B. (1983). "Application of the theory of plasticity to reinforced concrete (Anwendung der plastizitätstheorie auf stahlbeton)." Institute of Structural Engineering, ETH Zürich.
- To, N. H. T., Ingham, J. M., and Sritharan, S. (2001). "Monotonic nonlinear strut-and-tie computer models." *Bulletin of the New Zealand Society for Earthquake Engineering*, 34(3), 169-190.
- To, N. H. T., Ingham, J. M., and Sritharan, S. (2002). "Strut-and-tie computer modelling of reinforced concrete bridge portal frames." *Bulletin of the New Zealand Society for Earthquake Engineering*, 35(3), 165-189.
- To, N. H. T., Ingham, J. M., and Sritharan, S. (2003). "Strut-and-tie computer modelling of reinforced concrete bridge joint systems." *Journal of Earthquake Engineering*, 7(4), 581-590.
- To, N. H. T., Sritharan, S., and Ingham, J. M. (2009). "Strut-and-tie nonlinear cyclic analysis of concrete frames." *Journal of Structural Engineering*, 135(10), 1259-1268.

- Vecchio, F. J., and Collins, M. P. (1986). "The modified compression-field theory for reinforced concrete elements subjected to shear." *Journal of the American Concrete Institute*, 83(2), 219-231.
- Young, B. S., Bracci, J. M., Keating, P. B., and Hueste, M. B. D. (2002). "Cracking in reinforced concrete bent caps." *ACI Structural Journal*, 99(4), 488-498.
- Yun, Y. M. (2000). "Nonlinear strut-tie model approach for structural concrete." *ACI Structural Journal*, 97(4), 581-590.
- Zhu, R. R. H., Wanichakorn, W., Hsu, T. T. C., and Vogel, J. (2003). "Crack width prediction using compatibility-aided strut-and-tie model." *ACI Structural Journal*, 100(4), 413-421.

APPENDIX A

IMPLEMENTATION OF COMPUTATIONAL C-STM

This Appendix describes how to implement the proposed Compatibility-Strut and Tie Model (C-STM) using structural analysis software. Because of its commercial availability and nonlinear capabilities, SAP2000 was selected in this research to model the C-STM. The cantilevered beam presented in the convergence study of Chapter II (shown in Figure A.1 (a)) is presented as an example to define the step-by-step procedure used to construct the C-STM. Each section refers to the theory presented in Chapter II, demonstrating how each step is carried out in SAP2000. A design application concludes this appendix where this step-by-step procedure is applied to the reinforced concrete cantilevered bent caps presented in Section 2.9

A.1 Proportion C-STM Truss Members (Section 2.6)

The basic premise for computational truss modeling is to use *truss elements* which are only capable of sustaining either axial tensile or compressive loads. Thus each structural member must be assigned an appropriate elastic axial rigidity EA from which member stiffness k_i is assembled

$$k_i = \frac{EA}{L} \quad (\text{A-1})$$

where E = elastic material modulus; A = cross sectional area of assumed prismatic member; and L = member length.

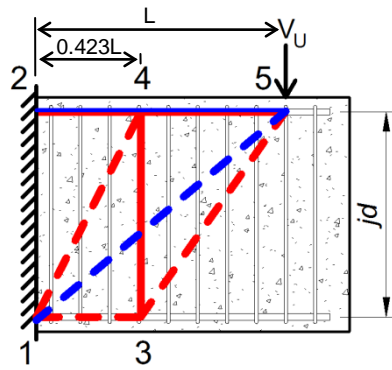
Step 1. Assign Node Points

Referring to Figure A.1 (a), for doubly reinforced sections the tension and compression chord members 2-4-5 and 1-3, are vertically located at the respective steel centroids. The horizontal positioning of the truss node points (nodes 3 and 4) are positioned according to the single-point Gauss quadrature truss model. Each node is then assigned the appropriate constraints based on the boundary conditions.

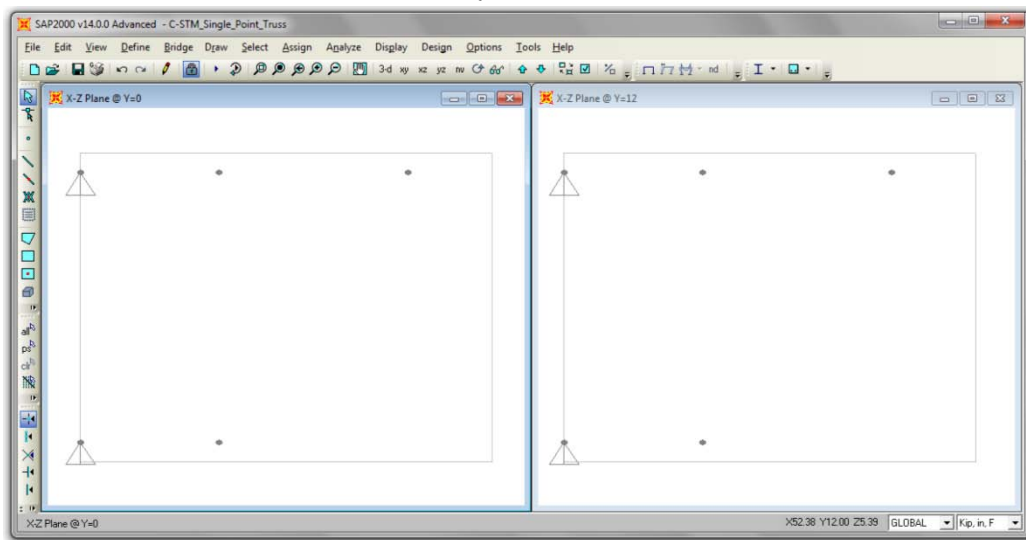
The steel and concrete components of the C-STM can be modeled using separate elements that are constrained together to give the combined steel-concrete member response. In order to model this, two trusses are required: one for steel and one for concrete. Hence the nodal geometry is replicated in the out of plane axis in order to create two separate trusses as shown in Figure A-1 (b) and (c). Parallel nodes are then constrained together using *equal constraints* in order to satisfy displacement compatibility between the steel and concrete truss node points.

Step 2. Assign Steel and Concrete Elements

Steel and concrete truss elements (referred to as *Frame Sections* in SAP2000) are then drawn with pinned-end conditions as shown in Figure A-1 (d) and (e). Table A-1 is used to define the stiffness and axial area for each steel and concrete element associated with each C-STM member, referred to in Section 2.6.

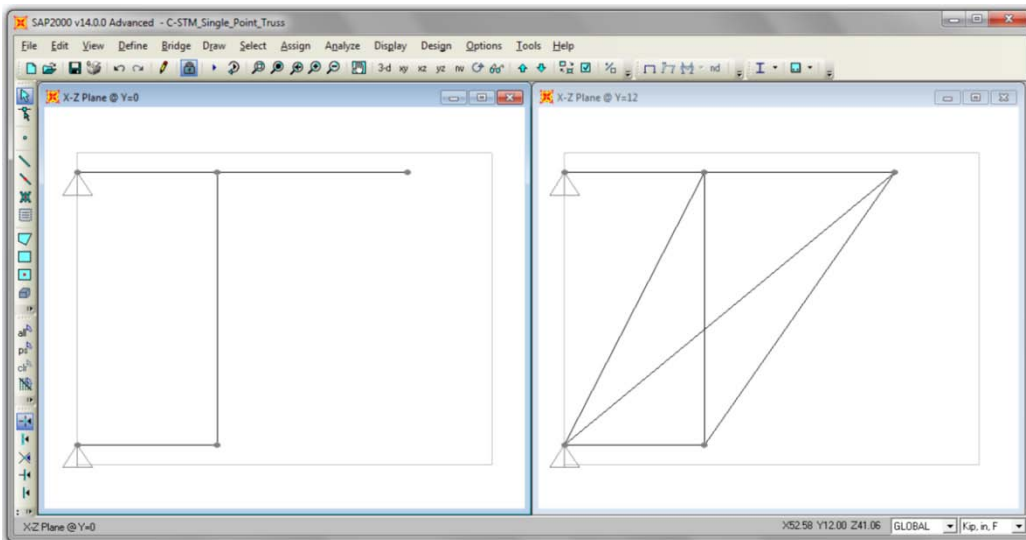


(a) C-STM of cantilevered beam



(b) Steel nodes

(b) Concrete nodes



(d) Steel elements

(e) Concrete elements

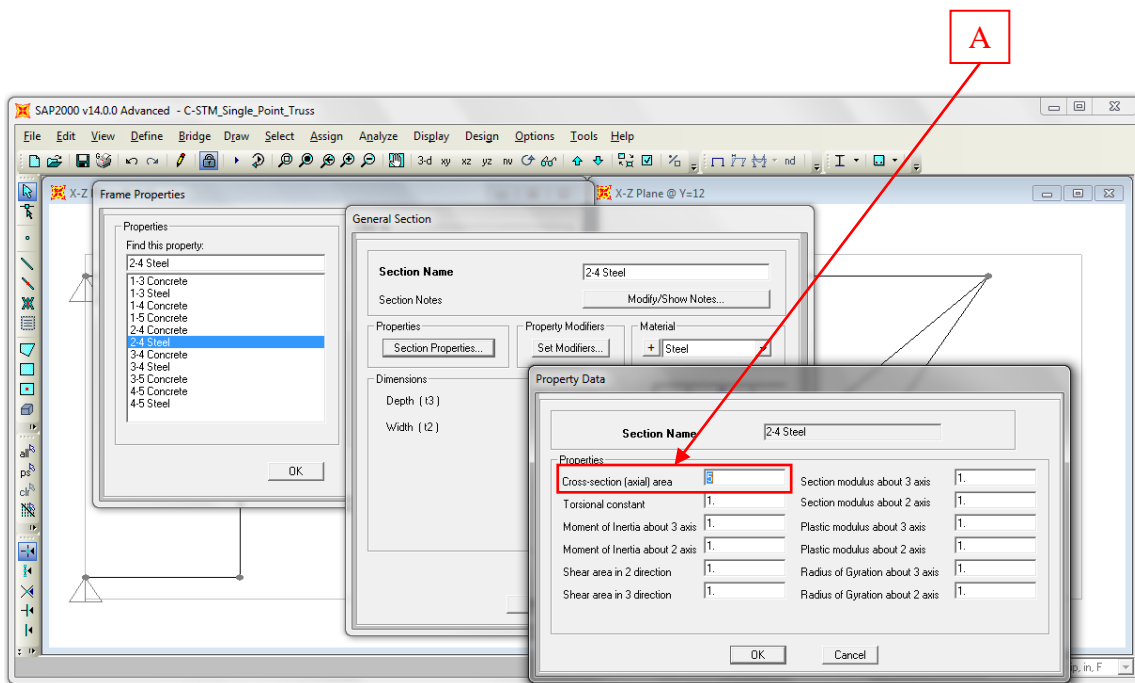
Figure A-1: Node and element construction in SAP2000

Table A-1: Elastic truss member axial rigidities

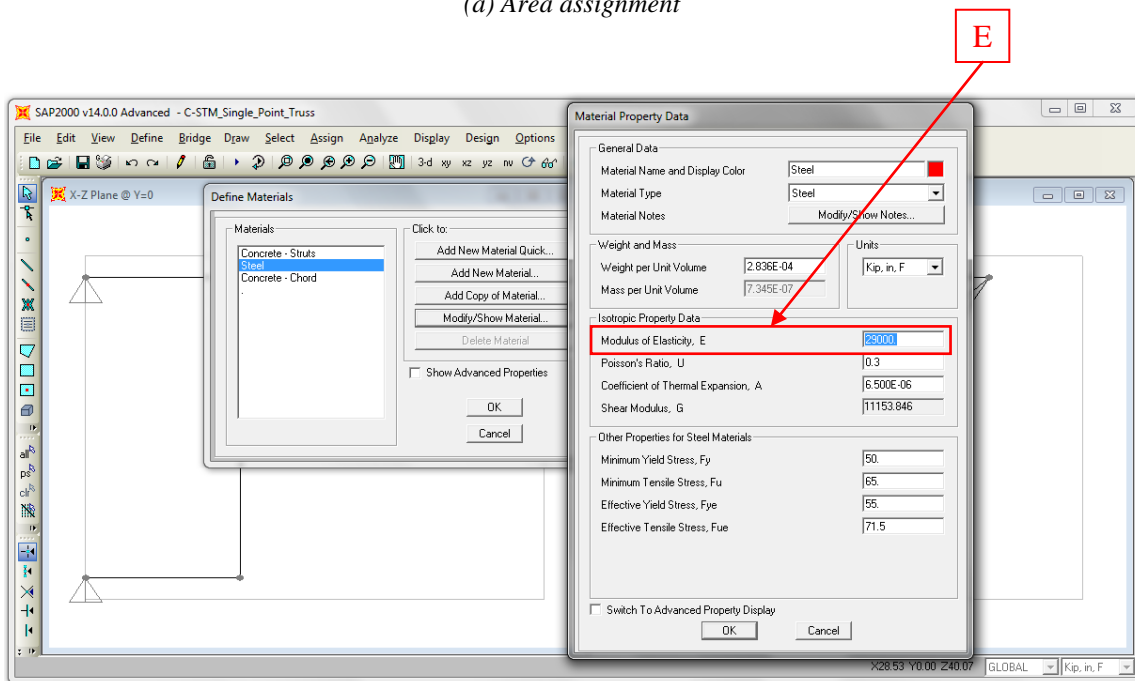
Member	Steel Element		Concrete Element		Comments
	E	A	E	A	
2 - 4 4 - 5	E_s	A_s	E_c	$b.kd$	Tension Chord
1 - 3	E_s	A_s'	$\psi_E E_c$	$b.kd$	Compression Chord
3 - 4	E_s	$N_h A_{sh}$	E_c	$(4c_c + 2d_h)N_h s$	Active Hoop steel including tension stiffening effect
1 - 5	-	-	E_c	$\frac{0.375 \eta b_w j d}{\cos \alpha}$	Concrete Strut in Arch Mechanism
1 - 4	-	-	E_c	$\frac{0.5(1-\eta)b_w j d}{\sqrt{0.423 + \tan^2 \alpha}}$	Concrete Strut in Truss Mechanism
3 - 5	-	-	E_c	$\frac{0.5(1-\eta)b_w j d}{\sqrt{0.577 + \tan^2 \alpha}}$	Concrete Strut in Truss Mechanism

Element areas are defined in the *Frame Properties* form, and are assigned as the *Cross-sectional (axial) area* as shown in Figure A-2 (a). Individual properties can be defined for each concrete and steel element, and then assigned to the appropriate elements.

Element stiffness's is defined in the *Define Materials* form, and are assigned as the Modulus of Elasticity as shown in Figure A-2 (b). This is defined as the material property, and is assigned to the appropriate steel and concrete members. Note that a minimum of three materials should separately be defined: Steel, Concrete struts, and Concrete chord members.



(a) Area assignment



(b) Stiffness assignment

Figure A-2: Area and stiffness assignments

A-2. Constitutive Material Relations of Truss Elements (Section 2.7)

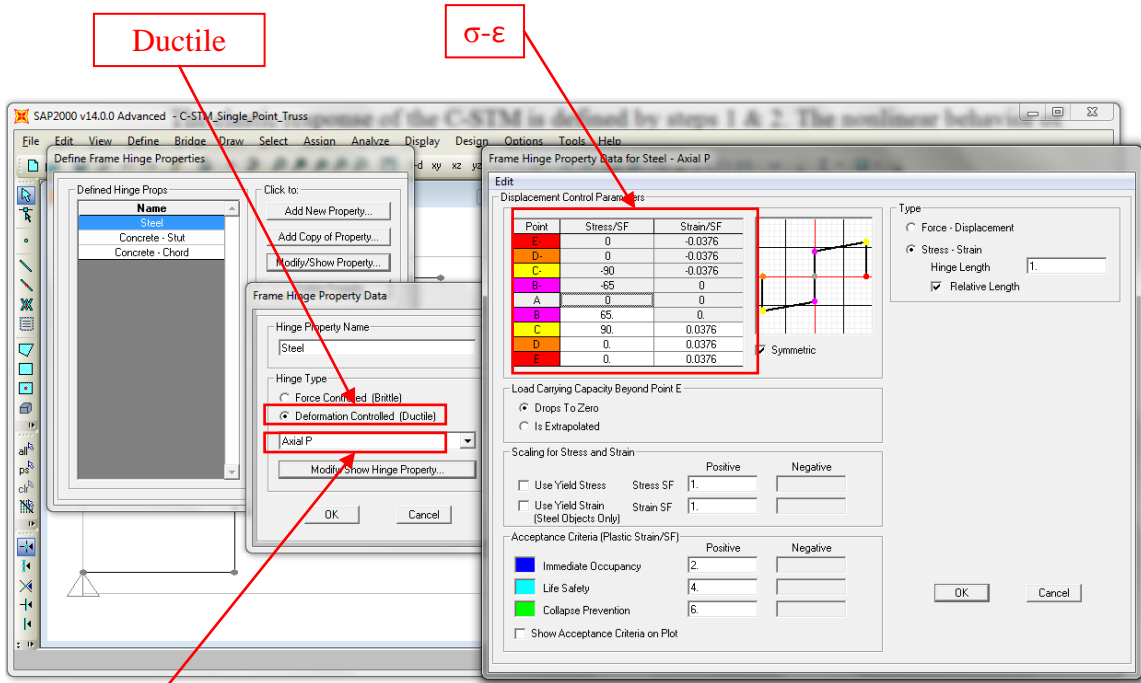
Step 3. Assign Nonlinear Constitutive Material Relationships.

The elastic response of the C-STM is defined by steps 1 & 2. The nonlinear behavior of the elements can be modeled using *Frame Hinges*. Frame hinges define the plastic stress-strain (or force-axial displacement) relationships after the maximum allowed elastic stress (or force) is exceeded in an element. Note: Hinge properties in SAP2000 define only the plastic behavior of the hinge. The elastic behavior of the frame element is determined by the frame section (and hence material properties) assigned to the element.

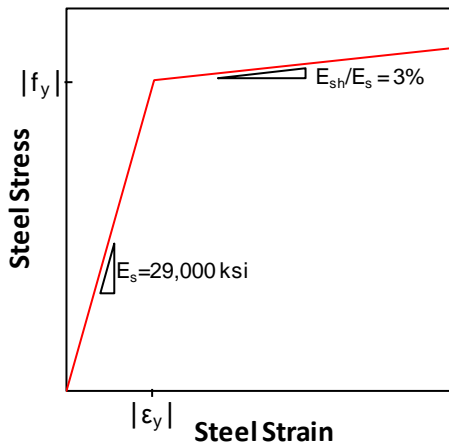
Frame hinges are defined in the *Define Frame Hinge Properties* form as shown in Figure A-3 (a). In order to define the plastic stress-strain relationship, *Ductile* and *Axial* hinges should be specified, thus leading to the *Frame Hinge Property Date – Axial P* form where the stress-strain back-bone curve can be defined. Figures A-3 (b) and (c) show the stress-strain relationships and corresponding plastic hinge relationships used to model steel in accordance with Figure 2.8.

Additional examples of stress-strain and corresponding plastic hinge relationships for concrete struts, concrete chord members, and concrete tension stiffening effects are provided in Figure A-4.

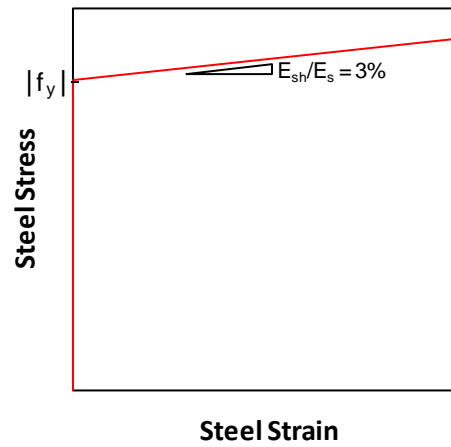
Nonlinear frame hinges are then assigned to the respective steel and concrete elements, thus defining the C-STM nonlinear behavior.



(a) Frame Hinge form

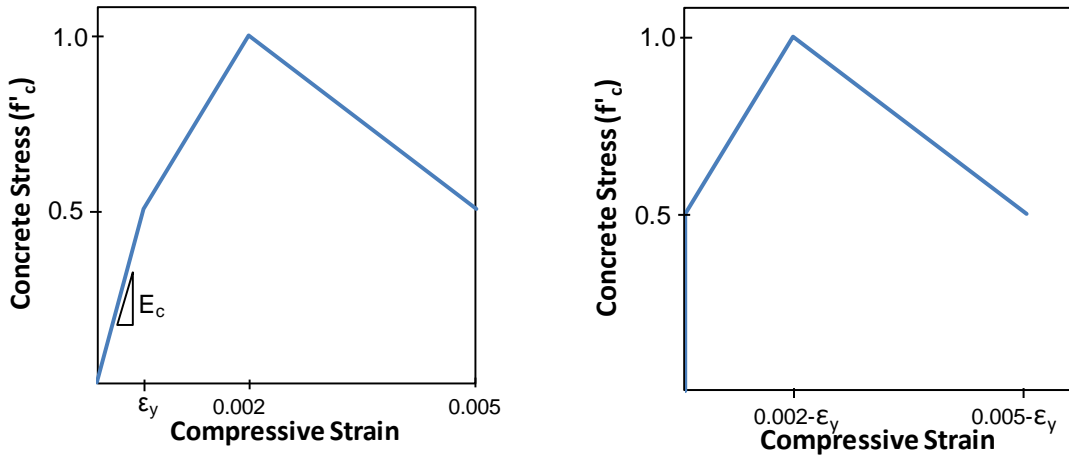


(b) Bilinear stress-strain relations for steel

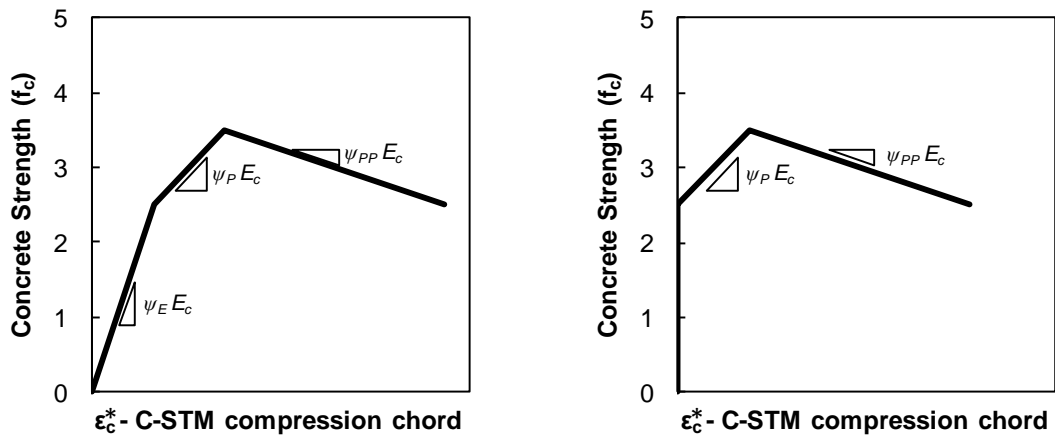


(a) Plastic stress-strain relation for steel

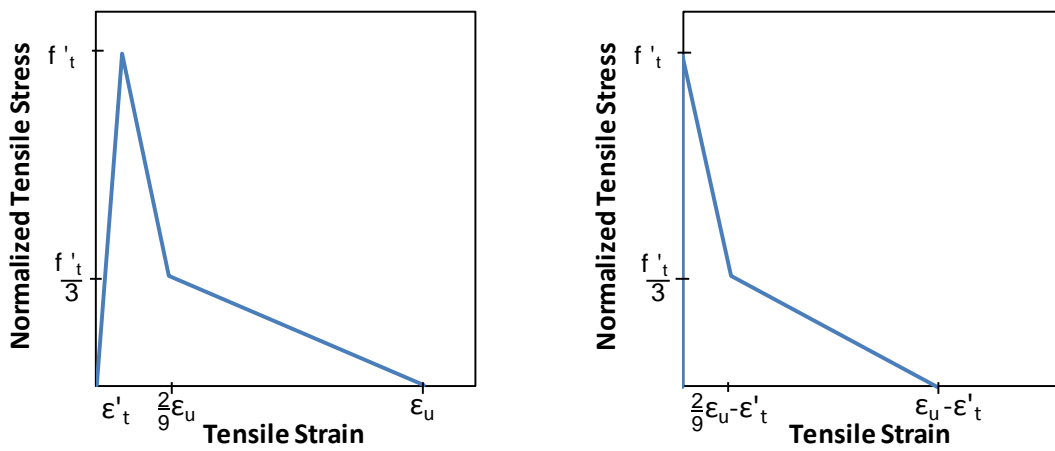
Figure A-3: Nonlinear frame hinge assignment for steel



(a) Concrete compressive struts



(b) Concrete compressive chord elements



(c) Concrete tension stiffening

Figure A- 4: Frame Hinge form

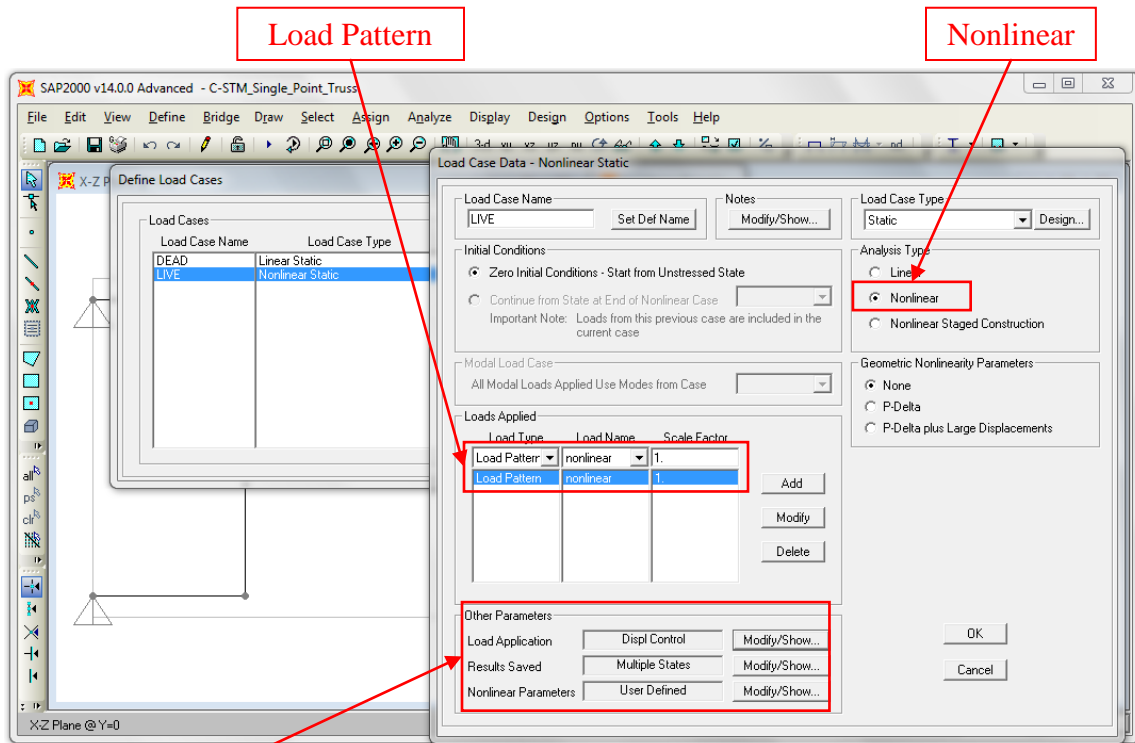
A-3 Assigning Loads and Running C-STM

Step 4. Assign Load Cases

Load cases are first defined in the *Define Load Pattern* form, and are then assigned to the appropriate nodes as either a force or displacement. Load cases are defined in the *Define Load Cases* form, as shown in Figure A-5 (a). The load case type typically used in this research was a Static-Nonlinear analysis. The desired load patterns are selected in the *load pattern* input tab. The other parameters inputs define the following: loading control either specified as *load* or *displacement* control; incremental step size; results saved at final load or incremental load steps; and other nonlinear parameters.

Step 5. Run Analysis

The analysis can now be run for the desired load cases as inputted by the user. Once complete, the user can progressively step through the deformed shape to see the formation of nonlinear behavior as shown in Figure A-5 (b).

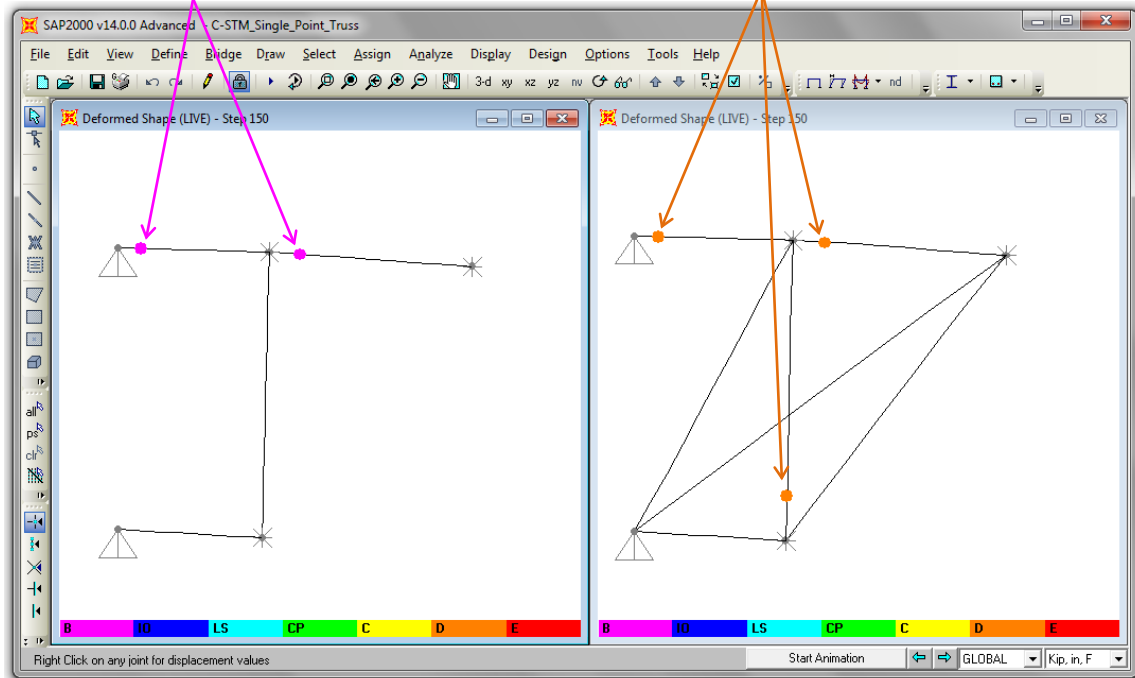


(a) Defining load cases

Other Parameters

Steel Yielding

Concrete Cracking



(b) Deformed shape showing formation of frame hinges

Figure A- 5: Defining and running load cases

A-4 Ultimate Strength and Softening of Constitutive Relations (Section 2.8)

Step 6. Post Analysis Investigation

Axial forces, displacements, and other output parameters can then be exported as an excel spreadsheet so that a post analysis investigation can be conducted. The axial force in each member can be individually assessed in order to make sure that the force does not exceed any other stress conditions (i.e. anchorage failure, nodal crushing, concrete softening, etc).

In order to model compression softening effects, the strain of the compression struts and transverse tension ties is required. Because element strains are not given as an output in SAP2000, an alternative means of defining the strain is required. This can be done using one of the following techniques:

1. The element strain can be defined in terms of the element force divided by the axial rigidity as shown below

$$\varepsilon = \frac{F}{EA} \quad (\text{A-2})$$

where EA is constant in the elastic range, hence this can only be applied prior to nonlinear behavior.

2. For members that reach nonlinear deformations, the elastic range of strain is defined using the method above. The plastic strain is obtained from the frame hinge output files. These are typically defined as element force vs. displacement relationships, hence the displacement can be divided by the length to obtain strain.

3. Alternatively to the previous methods, a third truss called the strain-meter truss, can be defined in parallel to the steel and concrete trusses in a similar fashion to Step 1, such that each node is constrained accordingly. Truss elements with a unit axial rigidity (i.e. $EA = 1$) can be drawn between the desired nodes as *Strain Members* so that the (small) force resisted is equal to the strain as shown in Eq. (A-2). This will provide the composite steel-concrete axial strain associated between the selected two node points. Note: this method was verified in this research using the previously mentioned methods providing identical comparisons for vertical and horizontal members, however some discrepancies were found in diagonal members with highly nonlinear behavior.

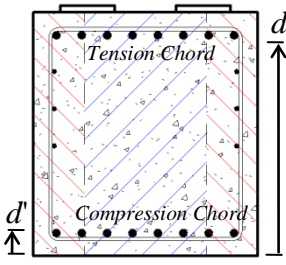
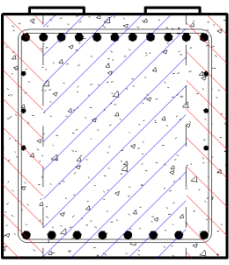
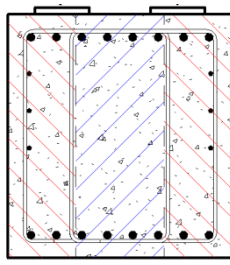
A-5 Design Application: C-STM for Reinforced Concrete Bridge Caps

A design application of the C-STM modeling parameters used to analyze the structural response of the reinforced concrete bridge baps tested by Bracci et al. (2000) is given in this section. The step-by-step procedure presented in the foregoing is used to construct the C-STM as follows.

Step 1. Assign Node Points

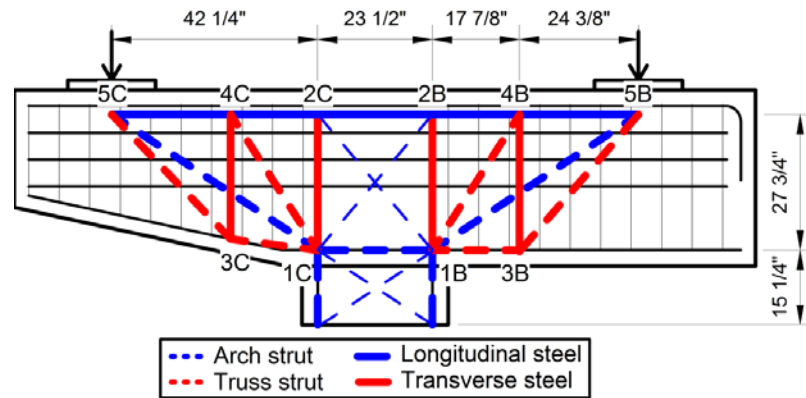
Table A-2 shows the cross-section parameters used to define the effective steel centroids for the three specimens selected in this research: specimen 2A, 5D, and 8G. All sections are doubly reinforced, hence the vertical positioning of the tension and compression chord members were located at the respective steel centroids.

Table A-2: Effective steel centroids for tension and compression chord members

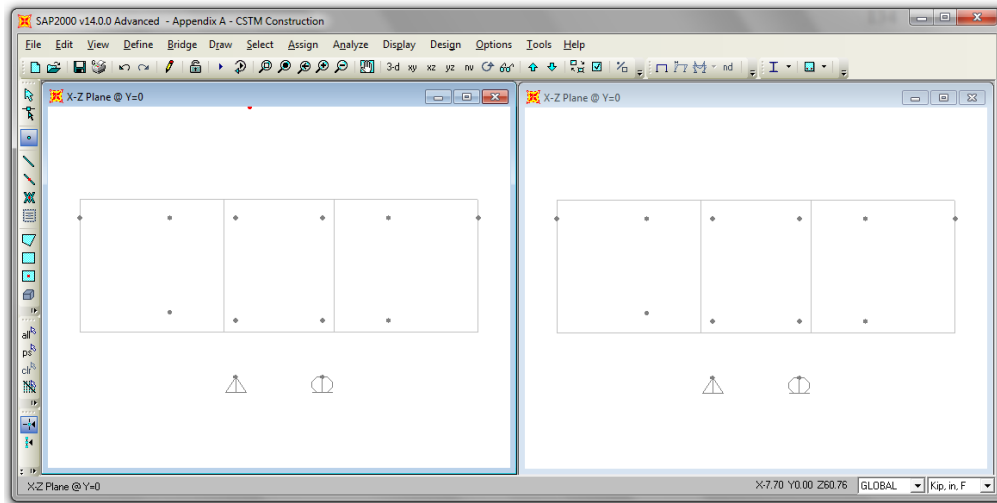
SPECIMEN	2A	5D	8G
CROSS-SECTION			
Tension Chord	8-#8 Bars 3 sets of 2-#4	11-#8 Bars 3 sets of 2-#4	8-#8 Bars 3 sets of 2-#4
d (in)	31.00	31.43	31.00
A_s (in ²)	7.46	9.82	7.46
Compression Chord	8-#8 Bars	8-#8 Bars	8-#8 Bars
d' (in)	3.25	3.25	3.25
A_s' (in ²)	6.28	6.28	6.28
Internal Lever Arm (jd)	27.76	28.18	27.76

The representative areas of reinforcement for the tension chord were defined as the sum of longitudinal steel and three sets of web distribution steel for tension. The compression chord was defined as the compression longitudinal steel. The internal lever arm of the column support was taken as the internal diameter of the longitudinal reinforcement, $jd = 30 - (2 \times 3.25) = 23.5 - in$.

Figure A-6 (a) shows the outline of the C-STM overlaid with the reinforcing details of specimen 2A. The top and bottom chord members were first drawn using the values in Table A-2. For the tapered cantilever, it was assumed that the compression chord followed the same profile as the taper. The two vertical chord members from the

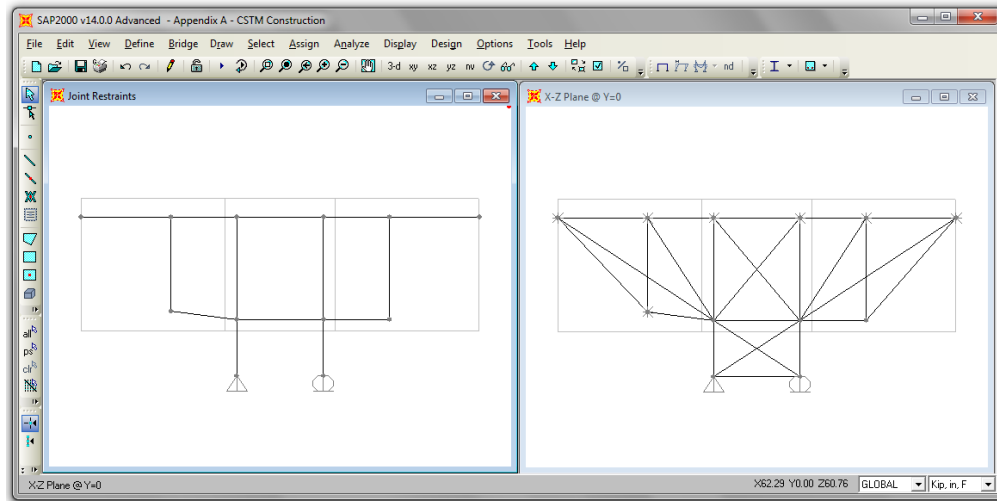


(a) C-STM of Specimen 2A, where C – Cantilever and B – Beam



(b) Steel nodes

(c) Concrete Nodes



(d) Steel elements

(e) concrete elements

Figure A-6: Specimen 2A node and element construction

column where then drawn, thus defining the length of the cantilevered C-STM beam as 42.25-in. with an internal lever arm of 27.75-in. The horizontal positioning of the truss node points was defined according to the single-point Gauss quadrature model, where $L_1 = 0.423L_{beam}$ is the distance from the column to the vertical transverse tie, hence $L_1 = 0.423 \times 42.25$ -in. = 17.87 -in. Figure A-6 (b) and (c) show the assigned node points for the steel and concrete trusses, respectively.

Step 2. Assign Steel and Concrete Elements

To expedite the construction of the C-STM, the material properties and element axial areas (defined below) were defined first so that they could be directly applied when assigning members. Once each element axial rigidity was defined, steel and concrete element members were then assigned between their appropriate node points using pinned-end connections as shown in Figure A-6 (d) and (e).

Three material types were required to be defined for the following C-STM members: steel, concrete, and modified chord concrete. Table A-3 shows the material properties used for each type, where $f_t' = 4\sqrt{f_c'(psi)}$ is the concrete tensile strength used by Bracci et al. (2000); $E_c = 57000\sqrt{f_c'(psi)}$ is the concrete elastic modulus; $k = \sqrt{(\rho + \rho')^2 n^2 + 2(\rho + \rho' d'/d)n} - (\rho + \rho')n$ is the elastic compression depth defined by Eq. (2.13); and $\psi_E = \sqrt{f_c'(psi)} / (168(1 - d'/kd))$ is the concrete chord compatibility correction scalar defined by Eq. (2.20).

Table A-3: Material properties for steel, concrete and concrete chord members

Material Type	Parameter	Specimen		
		2A	5D	8G
Steel	f_y (ksi)	65	65	65
	E_s (ksi)	29000	29000	29000
Concrete	f_c' (ksi)	6.2	5.5	5.3
	f_t' (ksi)	0.32	0.30	0.29
	E_c (ksi)	4490	4225	4150
Concrete Chord	ρ	0.00729	0.00947	0.00729
	ρ'	0.00614	0.00606	0.00614
	n	6.46	6.86	6.99
	k	0.245	0.281	0.252
	ψ_E	0.82	0.70	0.74
	$\psi_E E_c$ (ksi)	3680	2960	3070

Before defining the area assignments, the arch breadth scalar η was defined in order to apportion the contribution of arch and truss action according to Eq. (2.9). Table A-4 shows the longitudinal and transverse reinforcement ratios and other parameters used to define the respective arch and truss widths. Using the above mentioned parameters, the axial areas were defined using the equations shown in Table A-1. Table A-5 shows the final calculated properties of the truss member axial rigidities for Specimen 2A.

Table A-4: Arch breadth scalar

Specimen	2A	5D	8G
No. of hoops	<i>1</i>	<i>1</i>	<i>2</i>
A_{sh}	<i>0.614</i>	<i>0.614</i>	<i>1.23</i>
ρ_T	<i>0.0030</i>	<i>0.0030</i>	<i>0.0059</i>
ρ_L	<i>0.0073</i>	<i>0.0095</i>	<i>0.0073</i>
α	<i>33.3^\circ</i>	<i>33.7^\circ</i>	<i>33.3^\circ</i>
$\cot \alpha = L / jd$	<i>1.52</i>	<i>1.50</i>	<i>1.52</i>
η	<i>0.55</i>	<i>0.62</i>	<i>0.38</i>
Arch Breadth (in)	<i>18</i>	<i>21</i>	<i>13</i>
Truss Breadth (in)	<i>15</i>	<i>12</i>	<i>20</i>

Table A-5: Specimen 2A elastic truss member axial rigidities

	Member	Steel Element		Concrete Element		Comments
		<i>E</i>	<i>A</i>	<i>E</i>	<i>A</i>	
Cantilevered Beam	<i>2 - 4</i> <i>4 - 5</i>	<i>29000</i>	<i>7.46</i>	<i>4490</i>	<i>250.6</i>	Tension Chord
	<i>1 - 3</i>	<i>29000</i>	<i>6.28</i>	<i>3675</i>	<i>250.6</i>	Compression Chord
	<i>3 - 4</i>	<i>29000</i>	<i>2.45</i>	<i>4490</i>	<i>256.3</i>	Active Hoop steel including tension stiffening effect
	<i>1 - 5</i>	-	-	<i>4490</i>	<i>224.2</i>	Concrete Strut in Arch Mechanism
	<i>1 - 4</i>	-	-	<i>4490</i>	<i>225.2</i>	Concrete Strut in Truss Mechanism
	<i>3 - 5</i>	-	-	<i>4490</i>	<i>207.6</i>	Concrete Strut in Truss Mechanism
Beam-Col	<i>2C - 2B</i>	<i>29000</i>	<i>7.46</i>	<i>4490</i>	<i>250.6</i>	Tension Chord
	<i>1C - 1B</i>	<i>29000</i>	<i>6.28</i>	<i>3675</i>	<i>250.6</i>	Compression Chord

Step 3. Assign Nonlinear Constitutive Material Relationships

Figure A-7 shows the the nonlinear material constitutive relationships for steel and concrete defined using the material properties defined in Table A-3.

Step 4. Assign Load Cases

A static-nonlinear force control analysis was defined with two point loads of 500 kips assigned at the applied loads.

Step 5. Run Analysis

The analysis was run using 200 incremental step sizes, and took approximately two minutes to conduct the analysis.

A-6 Summary

This Appendix presented a step-by-step set of instructions that can be used to apply the C-STM theory described. Each section refers to the theory described in Chapter II and shows how each step is implemented into SAP2000. This theory can be applied to other structural analysis software packages as well.

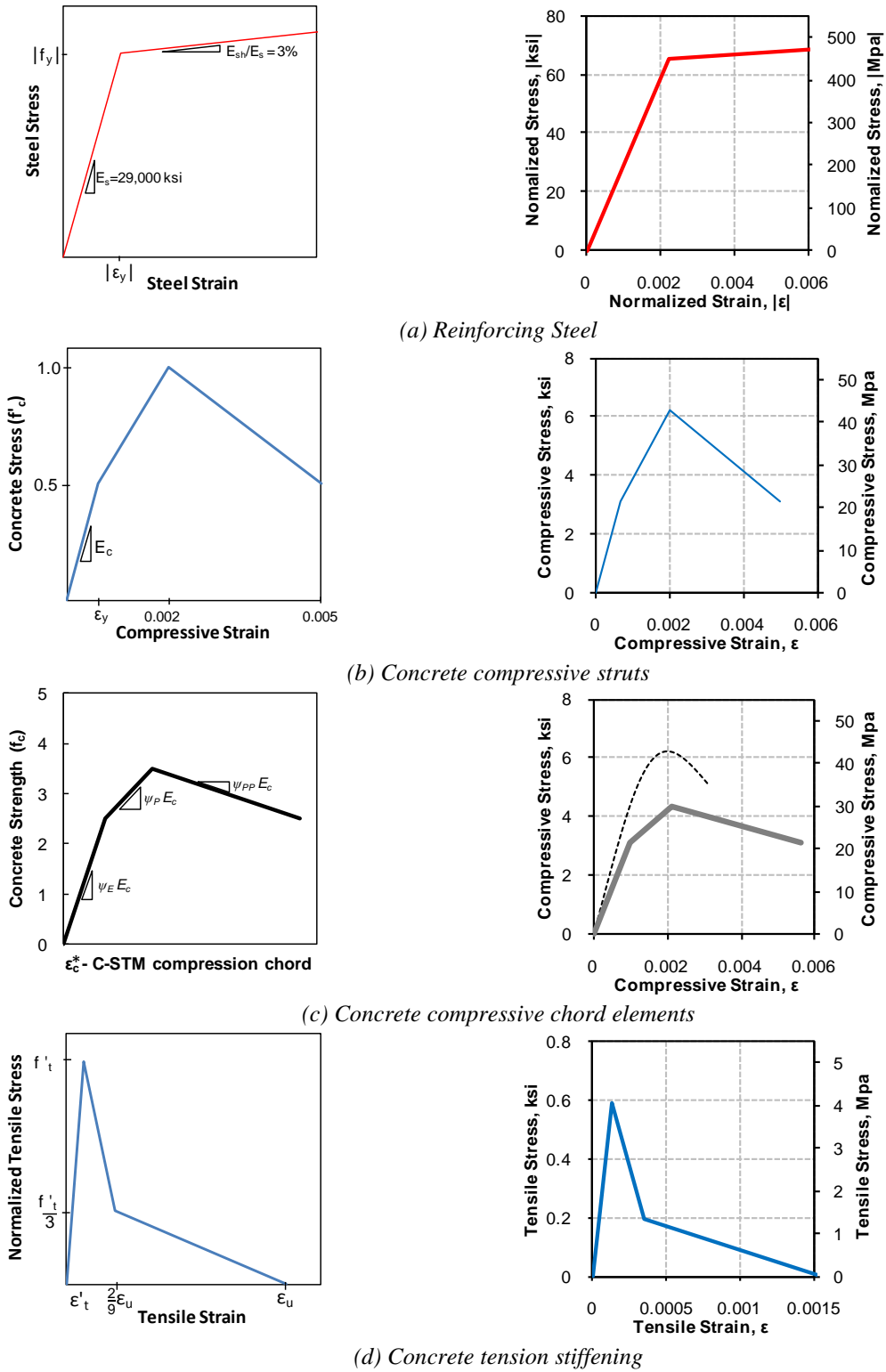


Figure A- 7: Specimen 2A material properties: Idealized (left) and actual (right)

APPENDIX B

DESIGN APPLICATION: C-STM FOR EXPERIMENTAL C-SPECIMENS

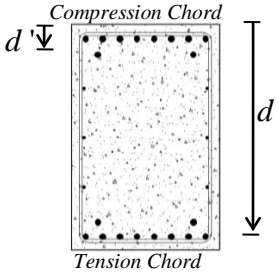
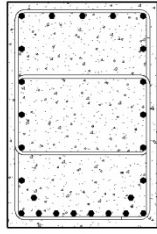
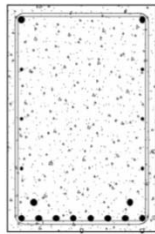
A design application of the C-STM modeling parameters used to analyze the structural response of the reinforced concrete C-Specimens tested in this research experimental program is given in this appendix. The step-by-step procedure presented in the Appendix A is used to construct the C-STM as follows.

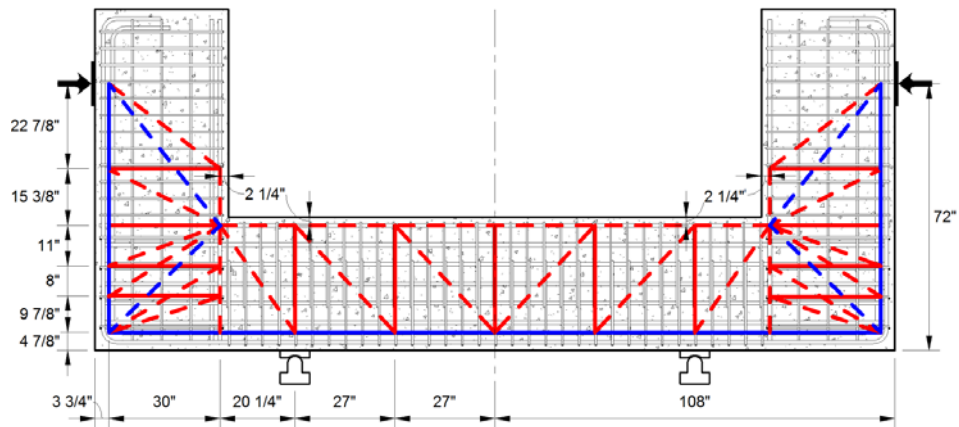
Step 1. Assign Node Points

Table B-1 shows the cross-section parameters used to define the effective steel centroids for the three sections of the C-Specimen: Doubly reinforced, column, and singly reinforced. All sections are doubly reinforced, hence the vertical positioning of the tension and compression chord members were located at the respective steel centroids.

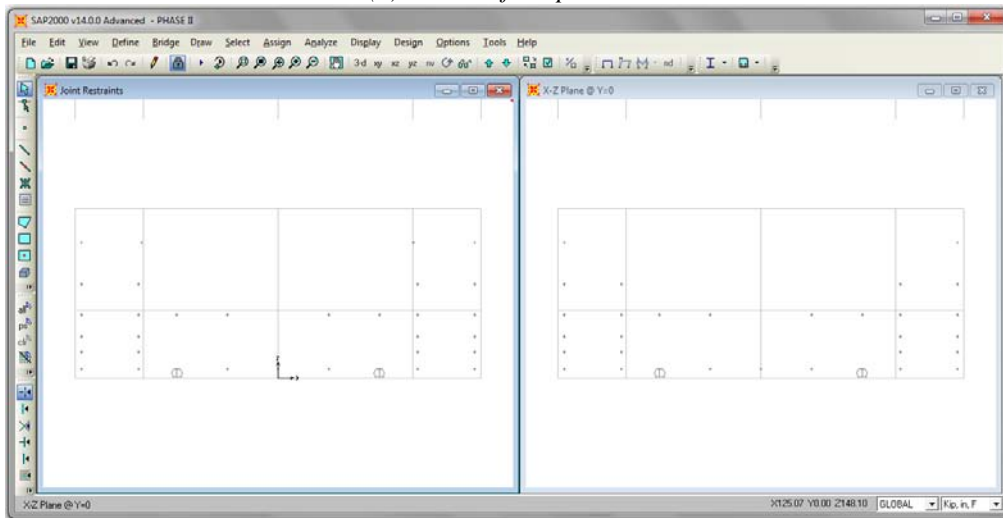
The representative areas of reinforcement for the tension chord were defined as the sum of longitudinal steel and three sets of web distribution steel for tension. The compression chord was defined as the compression longitudinal steel. The internal lever arm of the column support was taken as the internal diameter of the longitudinal reinforcement, $jd = 30 - (2 \times 3.25) = 23.5 - in$.

Table B-1: Effective steel centroids for tension and compression chord members

Section	Doubly Reinforced	Column	Singly Reinforced
CROSS-SECTION			
Compression Chord	10-#8 Bars	5-#8 Bars	2-#8 Bars
d' (in)	2.25	2.25	2.25
A_s' (in ²)	6.28	3.93	1.57
Tension Chord	10-#8 Bars 2 sets of 2-#4	10-#8 Bars 2 sets of 2-#4	10-#8 Bars 2 sets of 2-#8
d (in)	32.2	32.2	31.14
A_s (in ²)	8.64	8.64	11.00
Internal Lever Arm (jd)	30.0	30.0	28.9

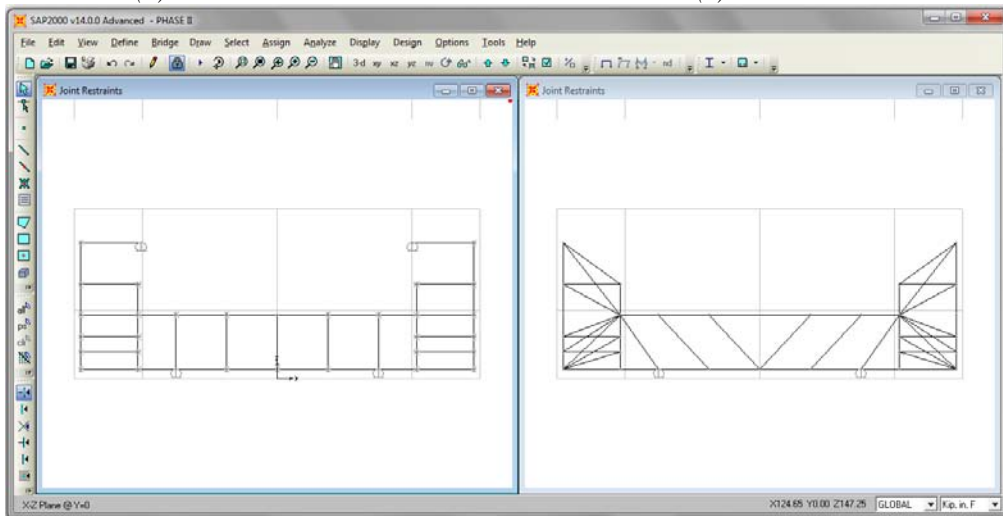


(a) C-STM of C-Specimen



(b) Steel nodes

(c) Concrete Nodes



(d) Steel elements

(e) Concrete elements

Figure B-1: Specimen 2A node and element construction

Figure B-1 (a) shows the outline of the C-STM overlaid with the reinforcing details of the C-Specimen. The top and bottom chord members were first drawn using the values in Table B-1 for the beam and column elements. The intersection of the column and beam steel defined the length of the beam elements as 38.25-in. with an internal lever arm of 30-in. The horizontal positioning of the truss node points for the cantilevered beam elements was defined according to the single-point Gauss quadrature model, where $L_1 = 0.423L_{beam}$ is the distance from the column to the vertical transverse tie, hence $L_1 = 0.423 \times 38.25$ -in. =16.2-in. The beam column joint was defined using a two-point truss model where the transverse reinforcement was defined at the location of the stirrups. Figure B-1 (b) and (c) show the assigned node points for the steel and concrete trusses, respectively.

Step 2. Assign Steel and Concrete Elements

To expedite the construction of the C-STM, the material properties and element axial areas (defined below) were defined first so that they could be directly applied when assigning members. Once each element axial rigidity was defined, steel and concrete element members were then assigned between their appropriate node points using pinned-end connections as shown in Figure B-1 (d) and (e).

Three material types were required to be defined for the following C-STM members: steel, concrete, and modified chord concrete. Table B-2 shows the material properties used for each type, where $f_t' = 0.42ksi$ was the measured concrete tensile

strength from the embedded bar test; $E_c = 57000\sqrt{f_c'(psi)}$ is the concrete elastic modulus; $k = \frac{\sqrt{(\rho + \rho')^2 n^2 + 2(\rho + \rho' d'/d)n - (\rho + \rho')}}{\sqrt{\quad}}$ is the elastic compression depth defined by Eq. (2.13); and $\psi_E = \sqrt{f_c'(psi)} / (168(1 - d'/kd))$ is the concrete chord compatibility correction scalar defined by Eq. (2.20).

Figure B-2 shows the node labels used to define the C-STM for the C-Specimen. Before defining the area assignments, the arch breadth scalar η was defined in order to apportion the contribution of arch and truss action according to Eq. (2.9). Table B-3 shows the longitudinal and transverse reinforcement ratios and other parameters used to define the respective arch and truss widths. Using the above mentioned parameters, the axial areas were defined using the equations shown in Table A-3. Table B-4 shows the final calculated properties of the truss member axial rigidities for the Doubly Reinforced Section.

Table B-2: Material Properties for steel, concrete and concrete chord members

Material Type	Parameter	Section		
		Doubly Reinforced	Column	Singly Reinforced
Steel	f_y (ksi)	65	65	65
	E_s (ksi)	29000	29000	29000
Concrete	f_c' (ksi)	5.4	5.4	5.4
	f_t' (ksi)	0.42	0.42	0.42
	E_c (ksi)	4190	4190	4190
Concrete Chord	ρ	0.0112	0.0147	0.0112
	ρ'	0.00812	0.00525	0.00203
	n	6.92	6.92	6.92
	k	0.411	0.411	0.315
	ψ_E	0.59	0.54	0.67
	$\psi_E E_c$ (ksi)	2472	2263	2907

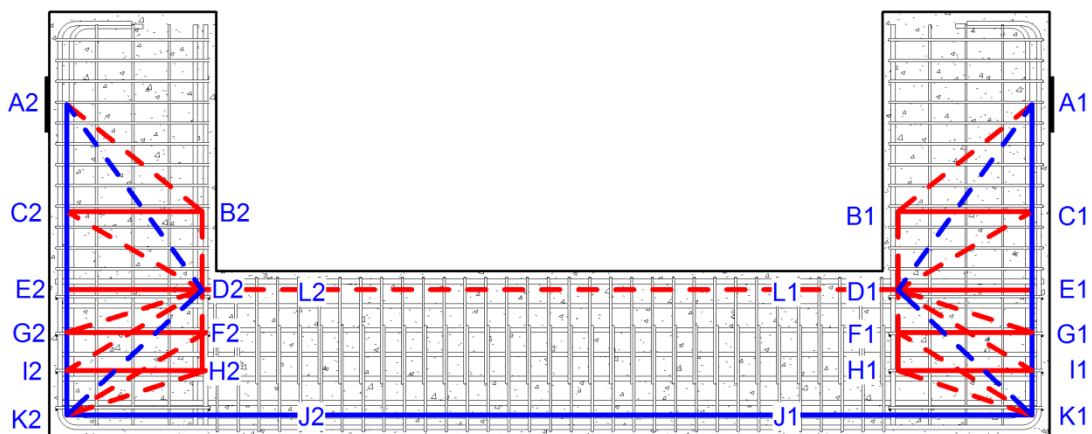


Figure B-2: C-STM labeling

Table B-3: Arch breadth scalar

Specimen	Doubly Reinforced	Column	Singly Reinforced
No. of hoops	1	1	2
A_{sh}	0.393	0.614	0.393
ρ_T	0.00364	0.0030	0.00364
ρ_L	0.0011	0.0095	0.0011
α	38.1°	30.0°	38.1°
$\cot \alpha = L / jd$	1.28	0.96	1.28
η	0.677	0.9 > 0.75	0.677
Arch Breadth (in)	16.2	18	16.2
Truss Breadth (in)	7.8	6	7.8

Table B-4: Doubly reinforced elastic truss member axial rigidities

		2) STRONG BEAM				Comments
		Steel		Concrete		
MEMBER		E	A	E	A	
Beam	A-E	29000	8.64	4190	243.42	Tension Chord
	B-D	29000	6.28	2455	72.71	Compression Chord
	BC	29000	2.36	4190	162.00	Transverse Steel
	AD	-	-	4190	232.00	Concrete Arch
	AB	-	-	4190	114.08	Concrete Truss
	CD	-	-	4190	106.45	
Beam-Column	E-K	29000	8.64	4190	243.42	Tension Chord
	D-H	29000	6.28	2455	72.71	Compression Chord
	FG&HI	29000	0.39	4190	54.00	Transverse Steel
	DK	-	-	4190	348.18	Concrete Arch
	DG	-	-	4190	30.79	Concrete Truss
	DI	-	-	4190	28.26	
	FK	-	-	4190	31.71	
HK	-	-	4190	29.03		
Column	JJ	29000	11.00	4190	307.33	Tension Chord
	LL	29000	3.93	2264	307.33	Compression Chord
	Tran	29000	2.36	-	-	Transverse Steel

Step 3. Assign Nonlinear Constitutive Material Relationships

Figure B-2 shows the nonlinear material constitutive relationships for steel and concrete defined using the material properties defined in Table B-2.

Step 4. Assign Load Cases

A static-nonlinear force control analysis was defined with two point loads of 500 kips assigned at the applied loads.

Step 5. Run Analysis

The analysis was run using 200 incremental step sizes, and took approximately two minutes to conduct the analysis.

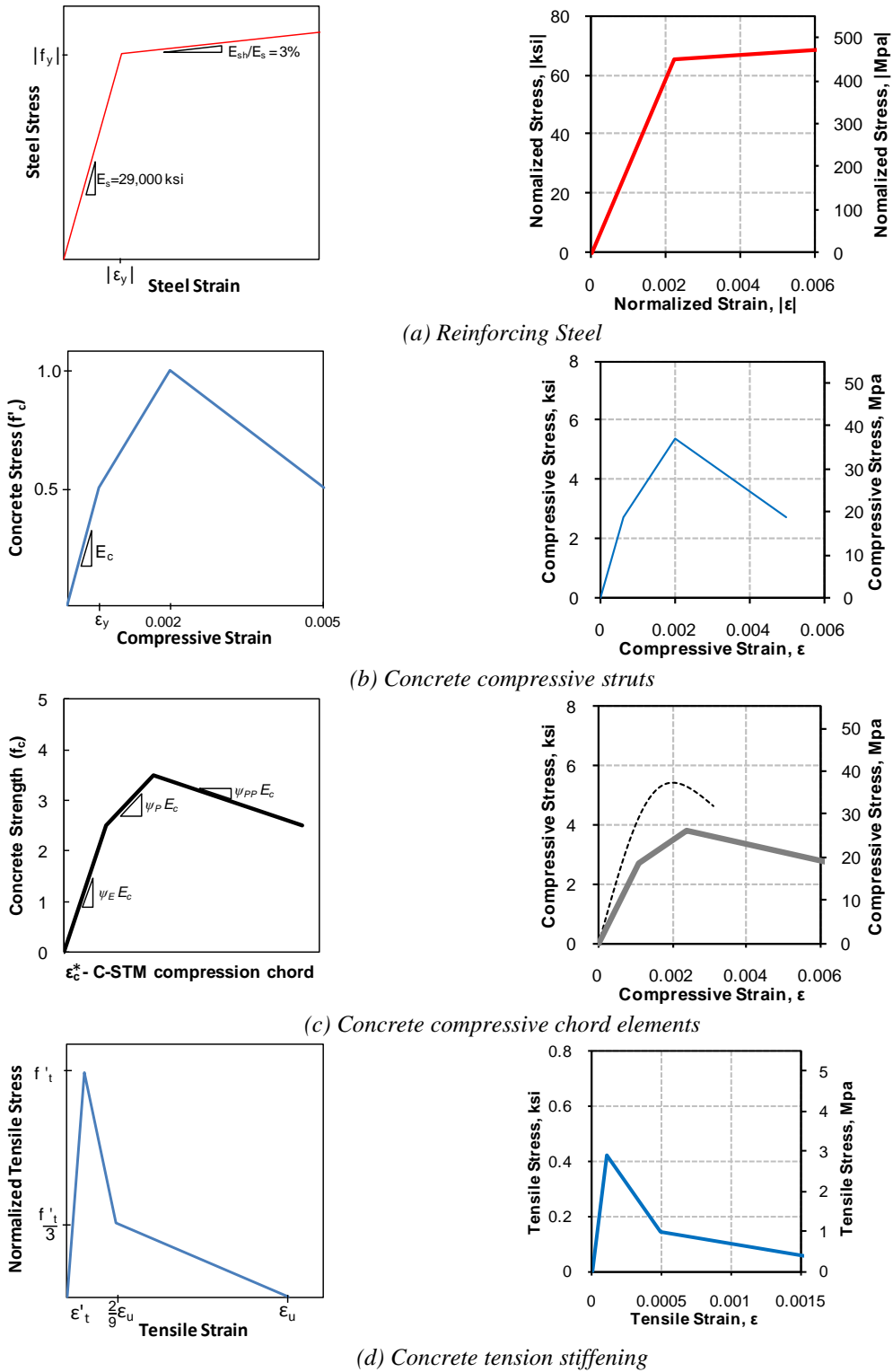


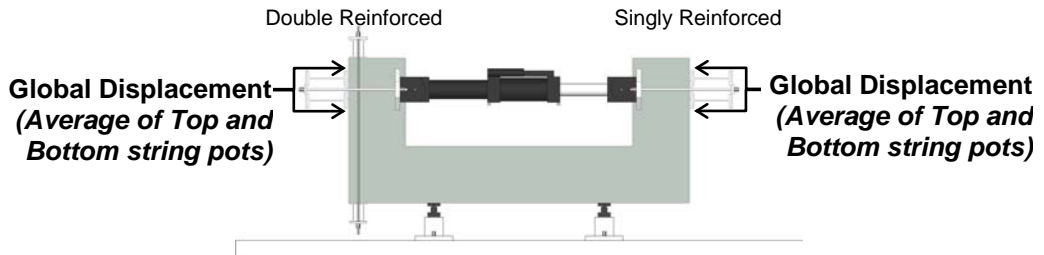
Figure B- 2: Specimen 2A frame hinge properties

APPENDIX C

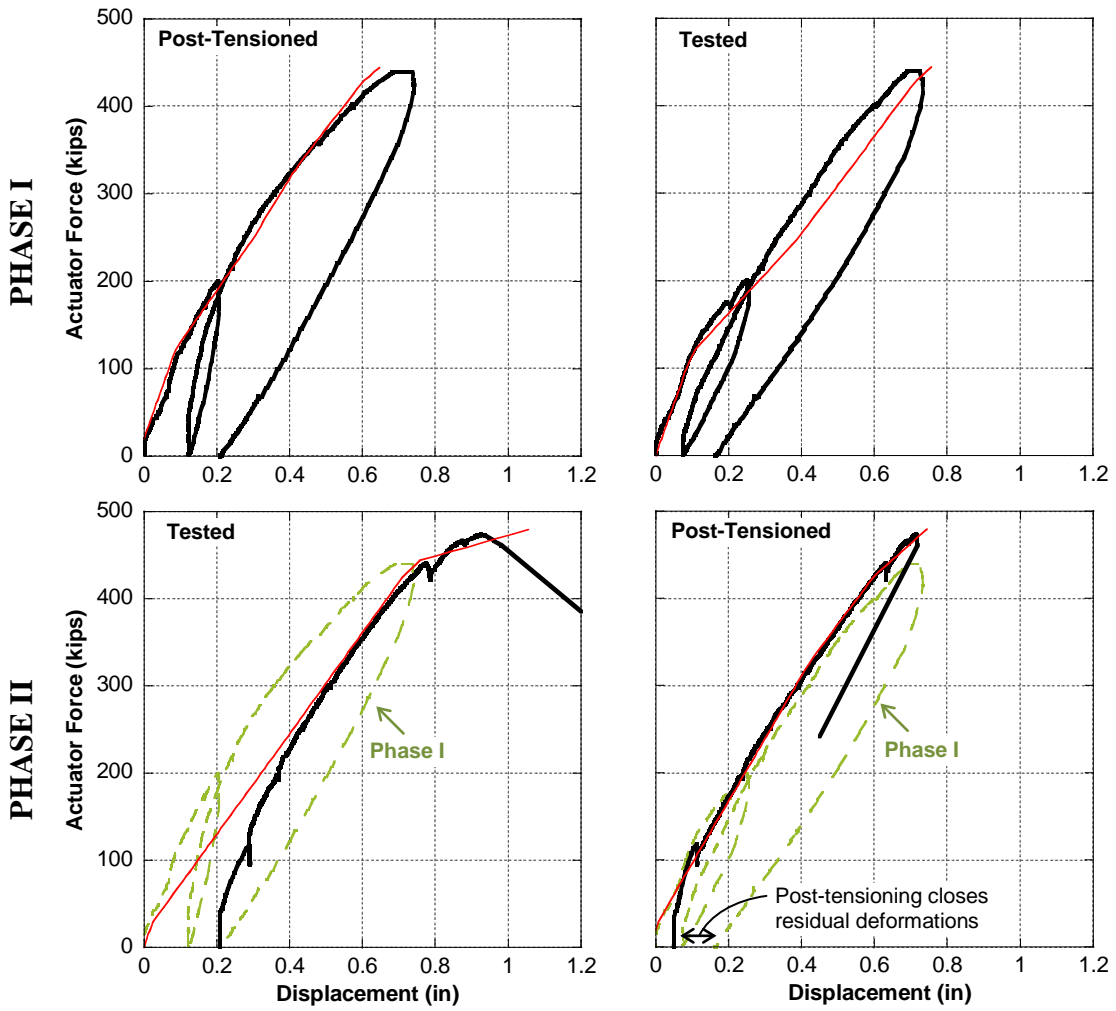
C-SPECIMEN EXPERIMENTAL RESULTS AND C-STM COMPARISONS

This appendix provides the experimental results for selected instrumentation in comparison to the predicted C-STM. At the top of each page is an illustration of the instrumentation results shown for that particular page, where the results in columns (a) and (b) refer to the doubly and singly reinforced beam, respectively. The results in the top and bottom rows refer to Phase I and Phase II testing, respectively.

Global Force-Displacement



— Displacement — C-STM

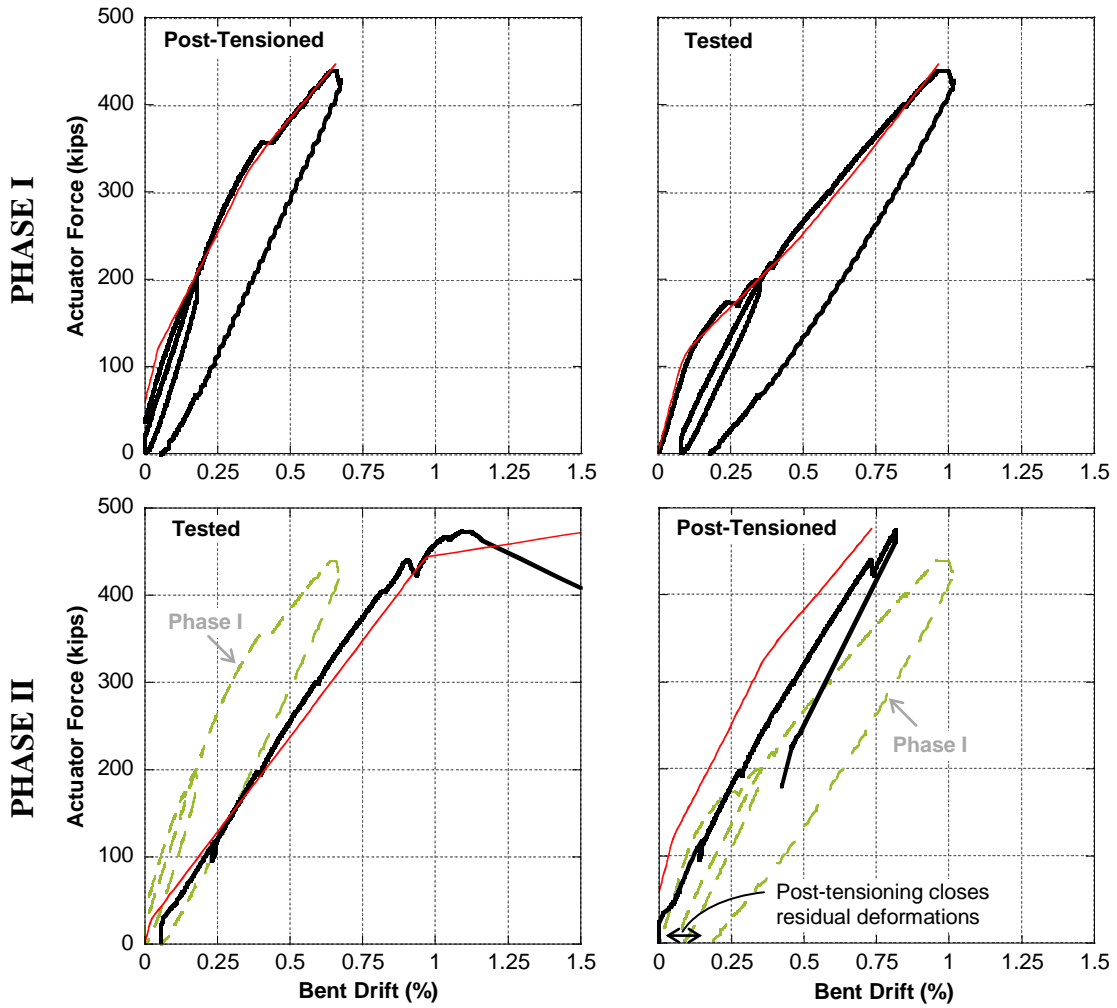
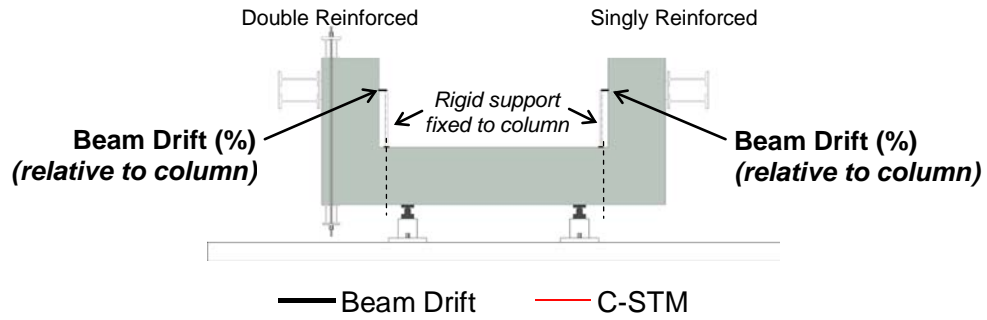


(a) Doubly Reinforced Beam

(b) Singly Reinforced Beam

Post-tensioning closes residual deformations

Beam Only Response (Drift)



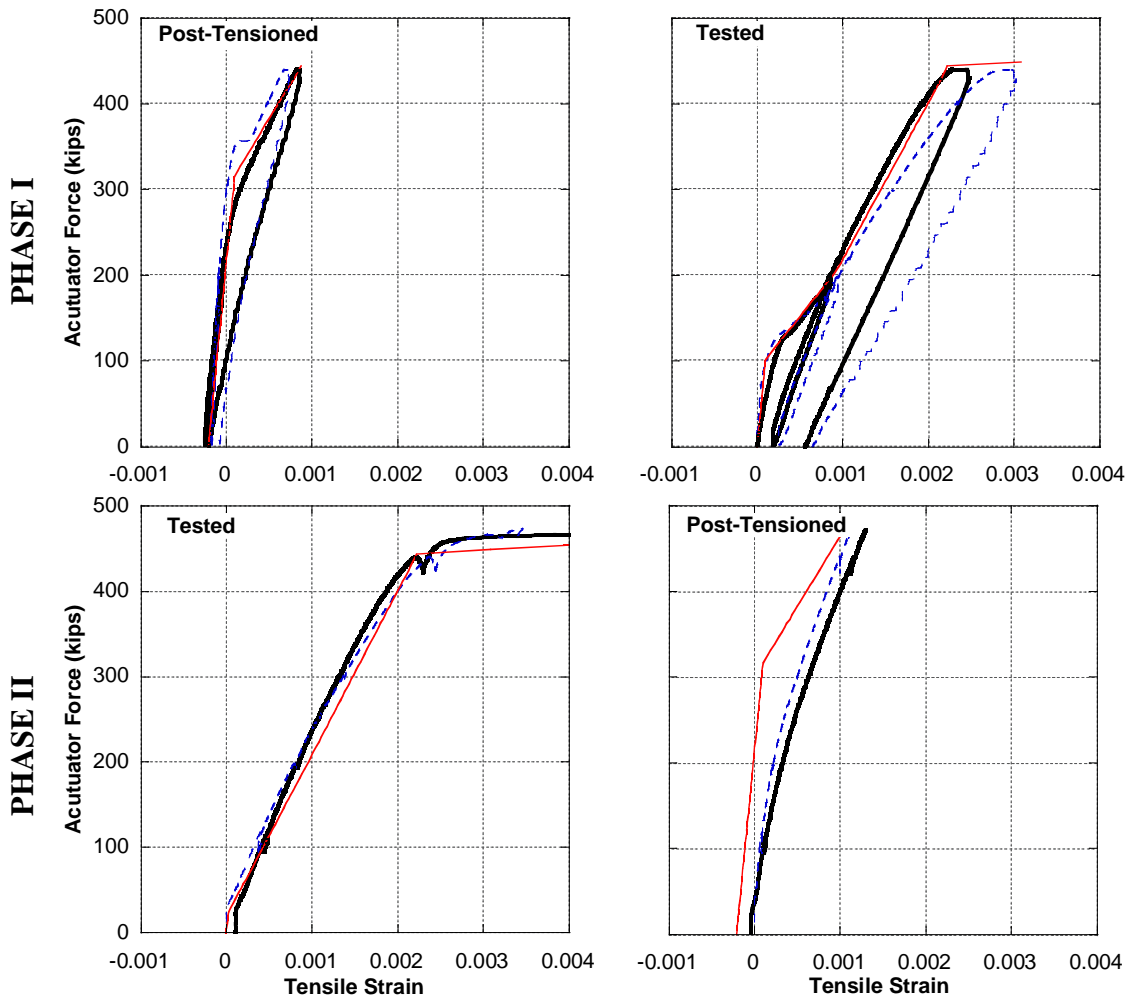
(a) Doubly Reinforced Beam

(b) Singly Reinforced Beam

Longitudinal – Beam (column face)



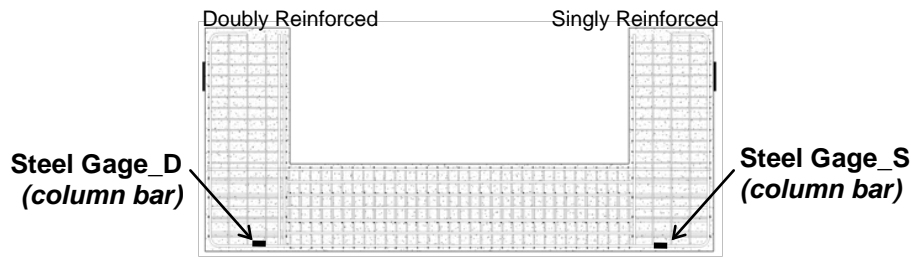
— Steel Strain Gage - - - LVDT Truss — C-STM



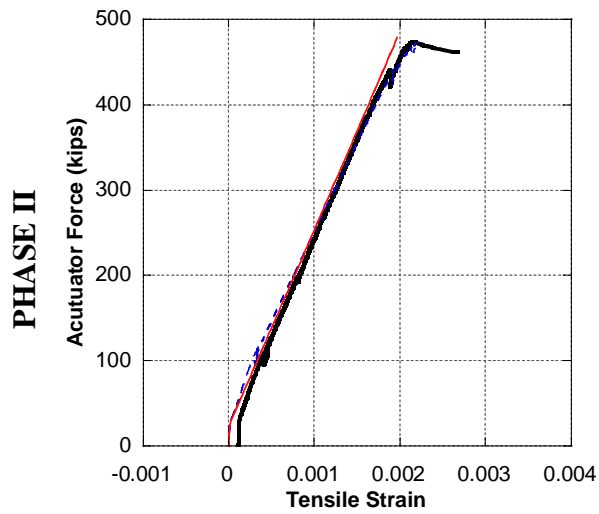
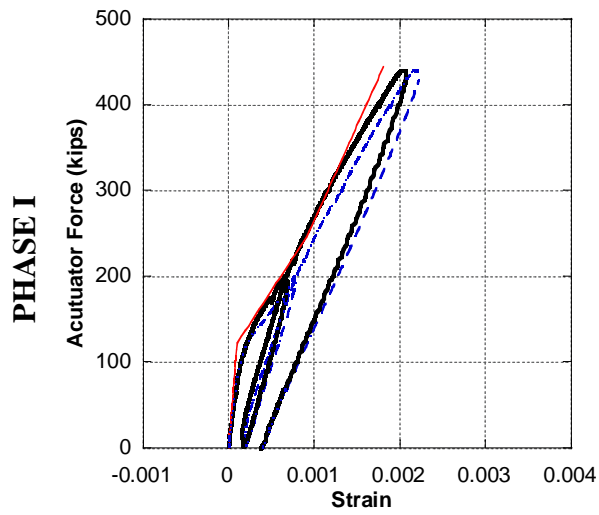
(a) *Doubly Reinforced Beam*

(b) *Singly Reinforced Beam*

Longitudinal – Column

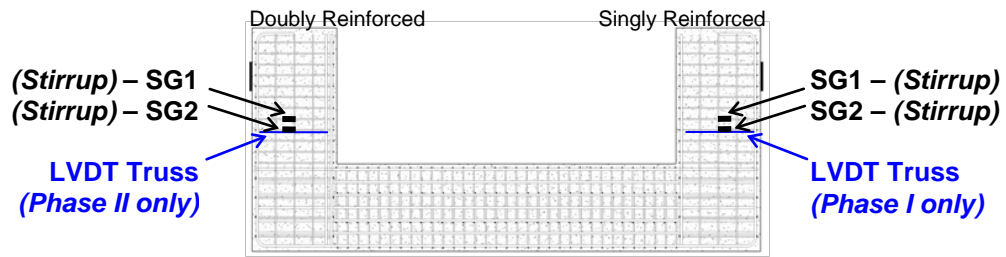


— SG_D - - - SG_S — C-STM

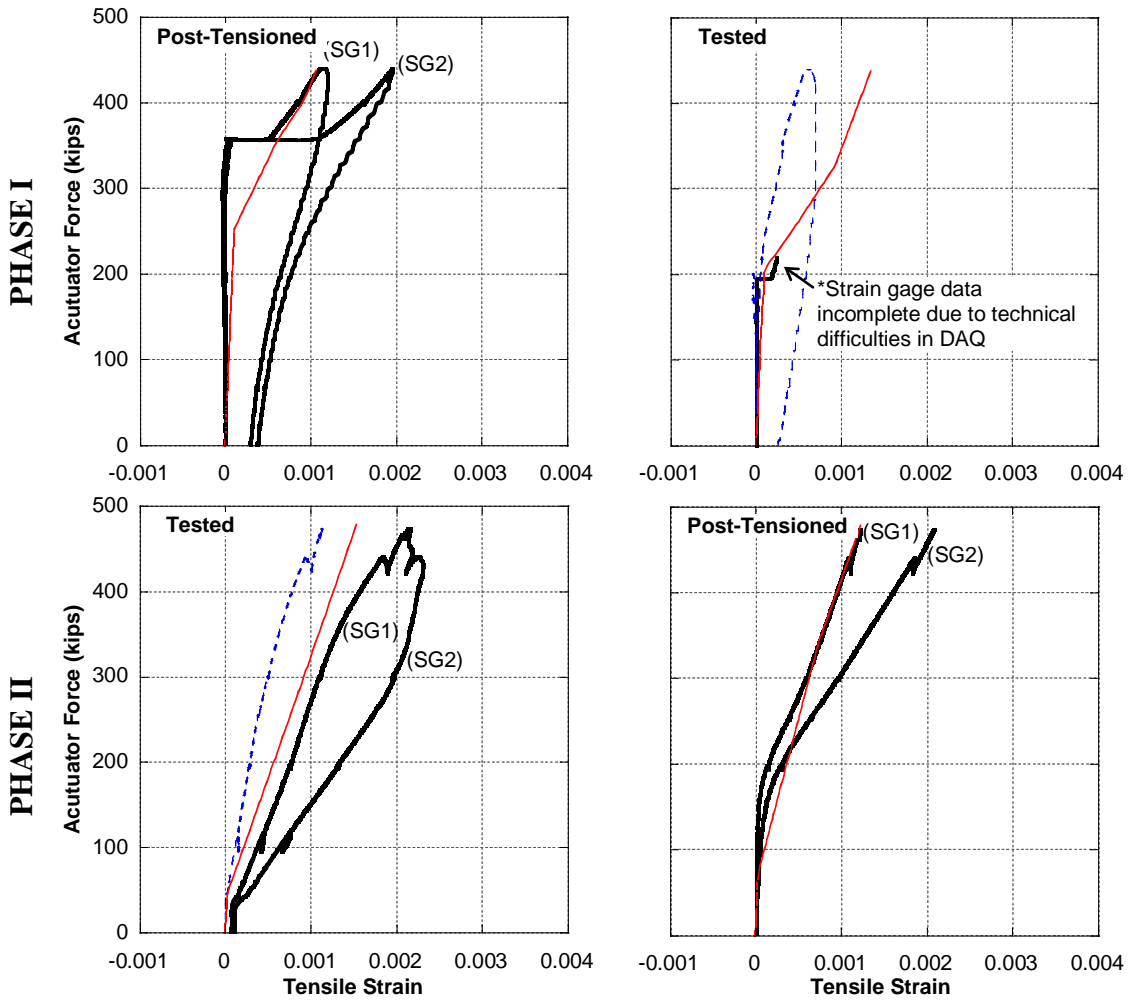


(a) Column

Transverse – Beam



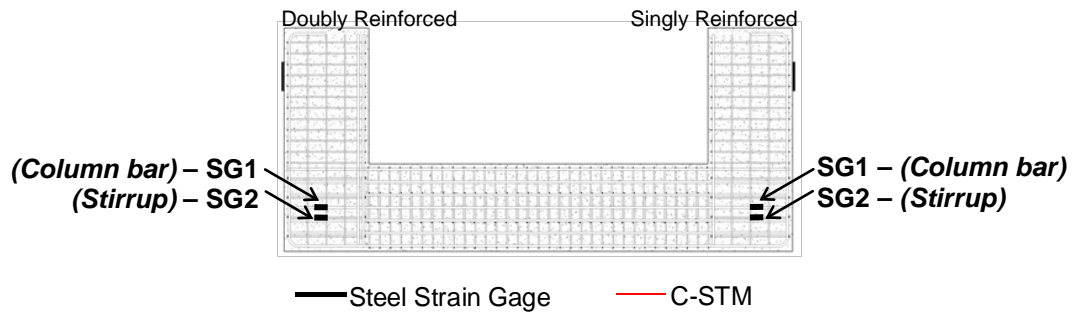
— Steel Strain Gage - - - LVDT Truss — C-STM



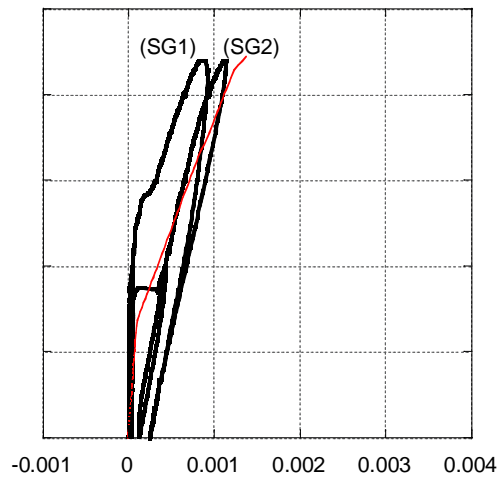
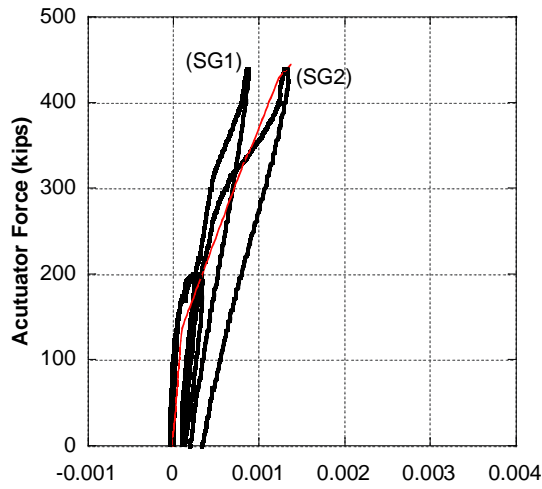
(a) *Doubly Reinforced Beam*

(b) *Singly Reinforced Beam*

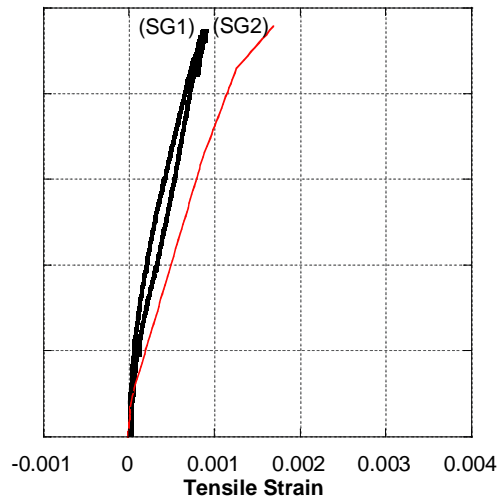
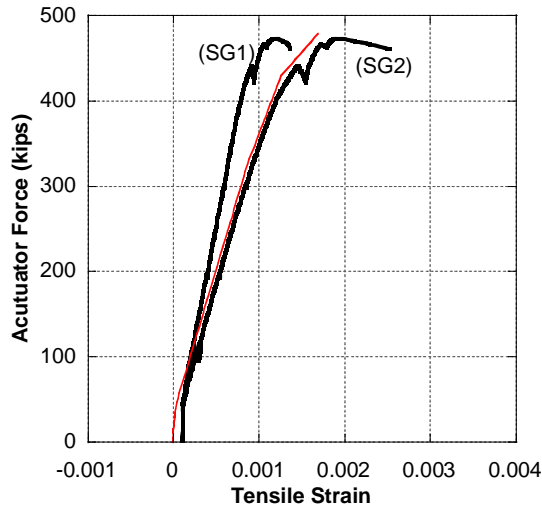
Transverse – Beam Column Joint



PHASE I



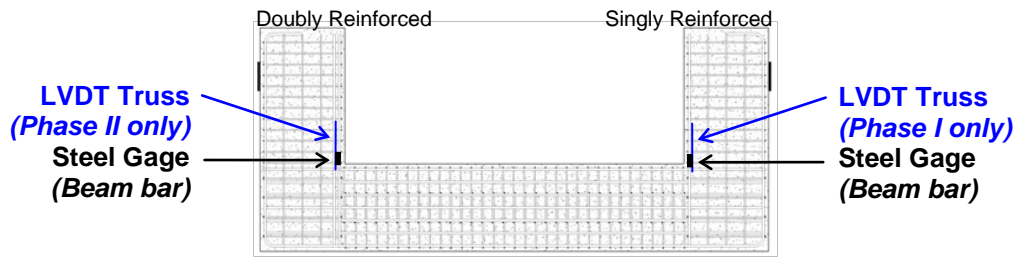
PHASE II



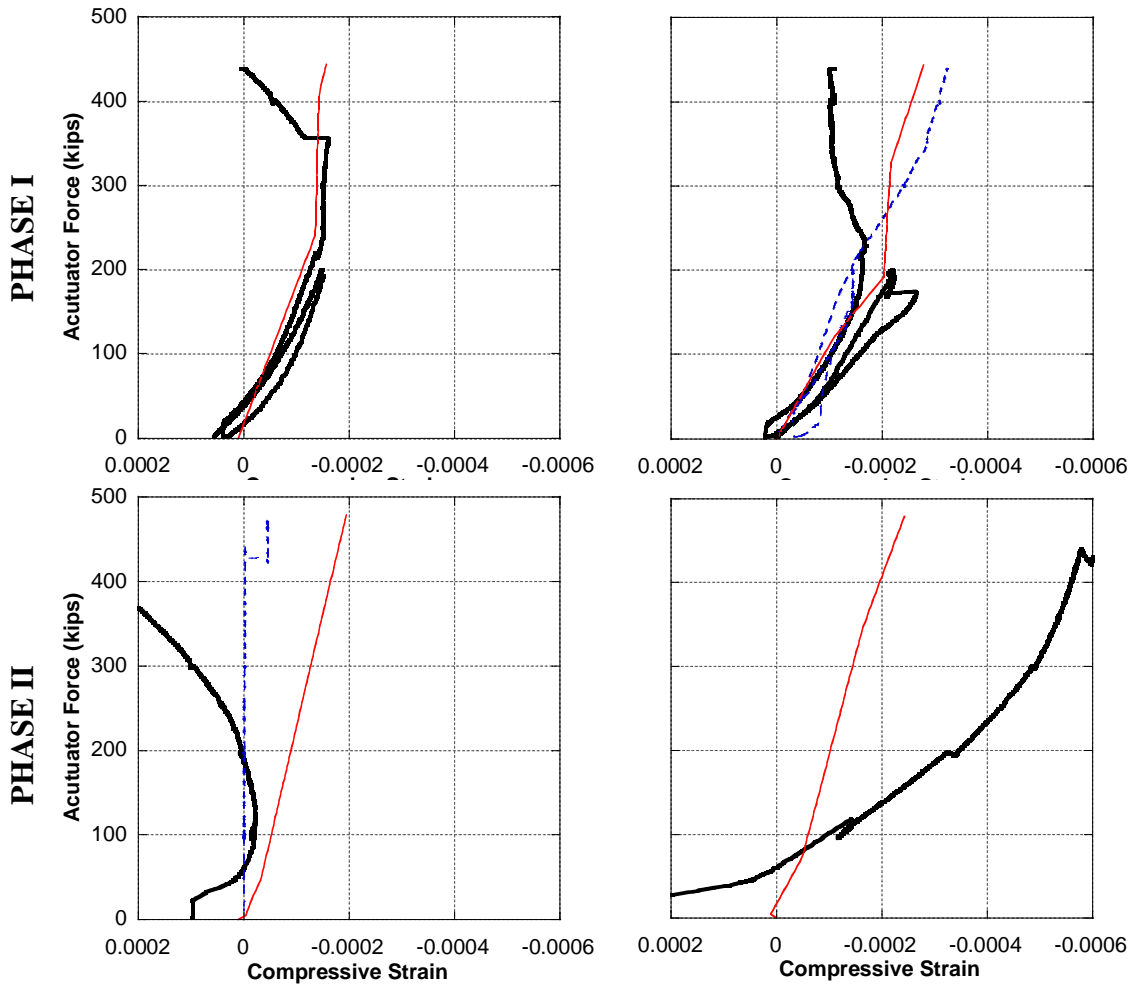
(a) *Doubly Reinforced Beam*

(b) *Singly Reinforced Beam*

Compression Chord – Beam



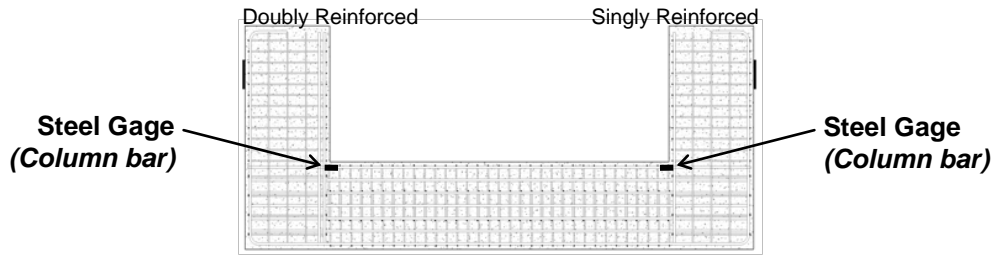
— Steel Strain Gage - - - LVDT Truss — C-STM



(a) *Doubly Reinforced Beam*

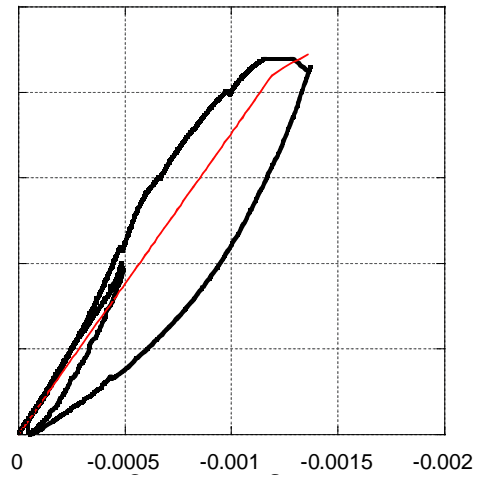
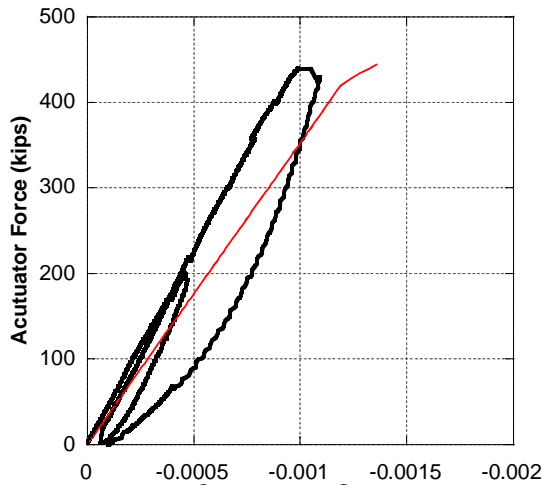
(b) *Singly Reinforced Beam*

Compression Chord – Column

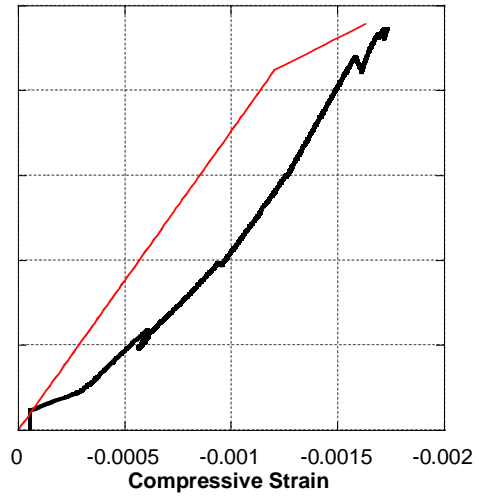
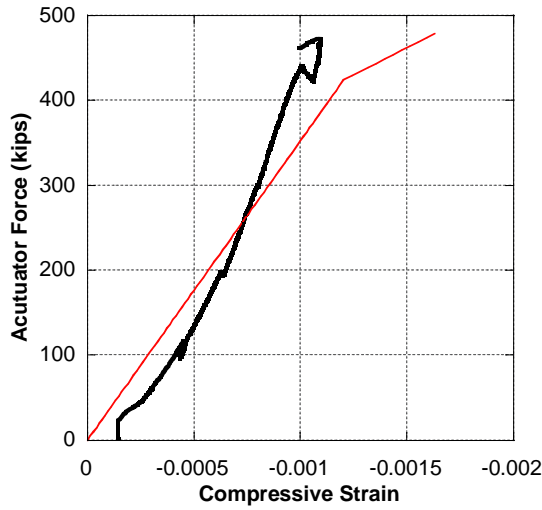


— Steel Strain Gage — C-STM

PHASE I



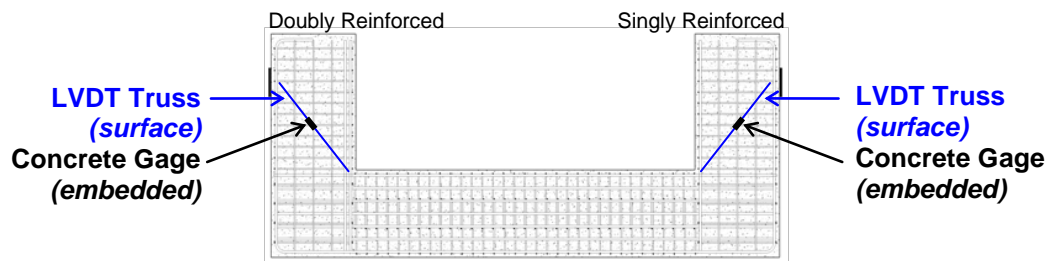
PHASE II



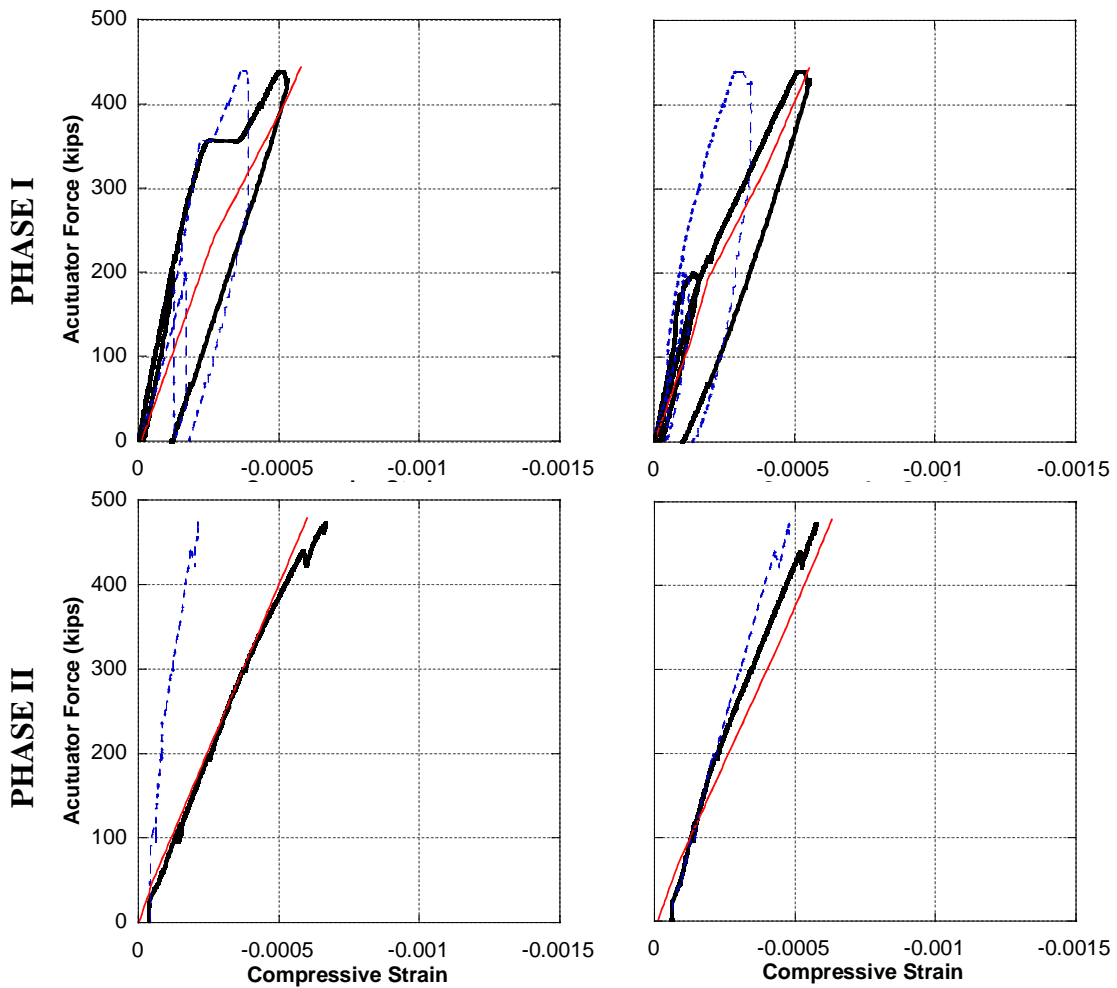
(a) *Doubly Reinforced Beam*

(b) *Singly Reinforced Beam*

Arch Struts – Beam



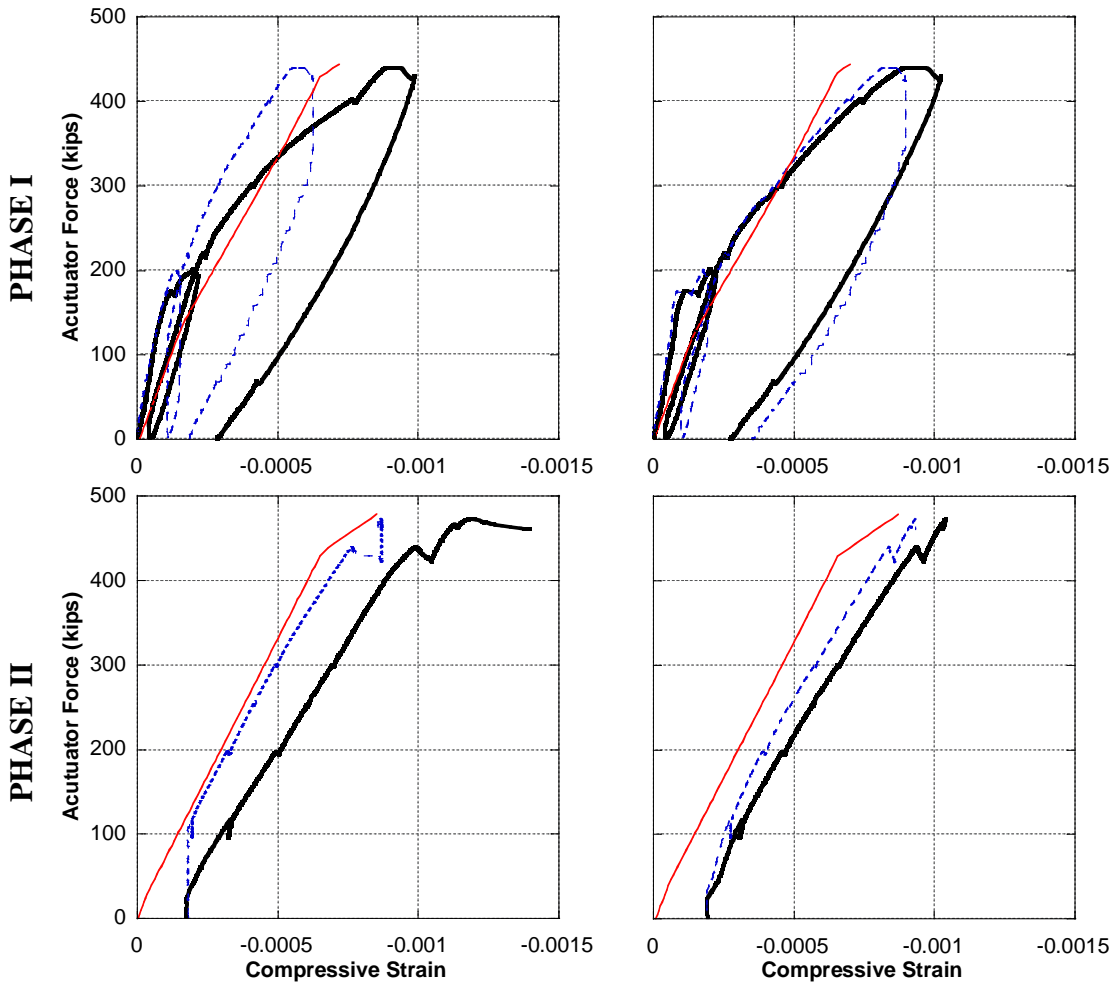
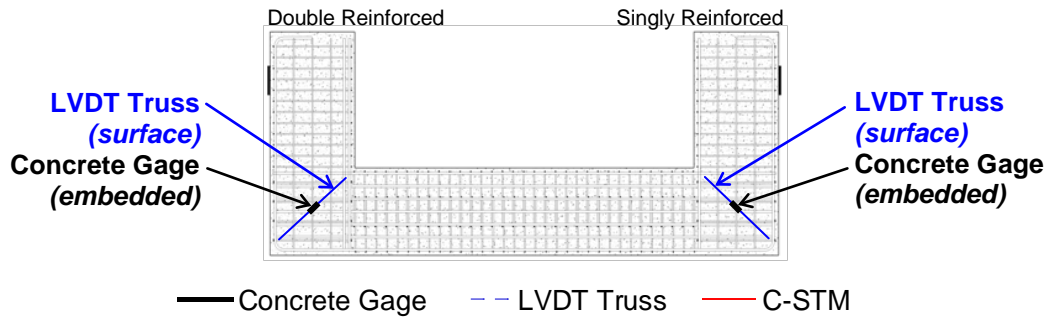
— Concrete Gage - - - LVDT Truss — C-STM



(a) *Doubly Reinforced Beam*

(b) *Singly Reinforced Beam*

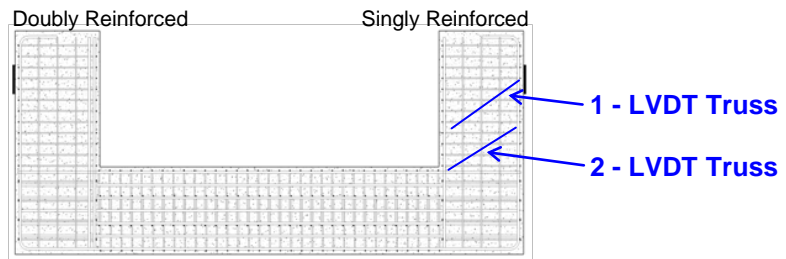
Arch Struts – Beam Column Joint



(a) Doubly Reinforced Beam

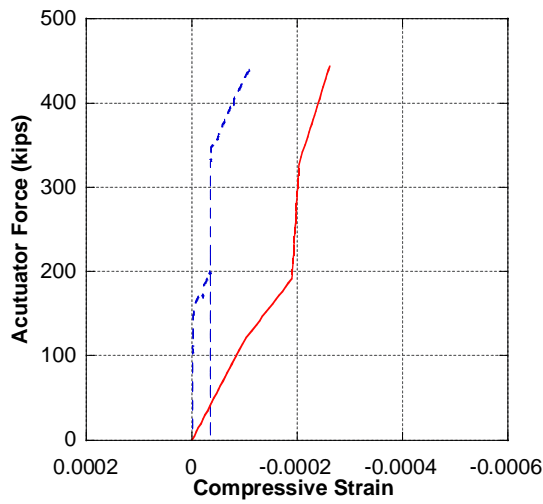
(b) Singly Reinforced Beam

Truss Strut – Beam

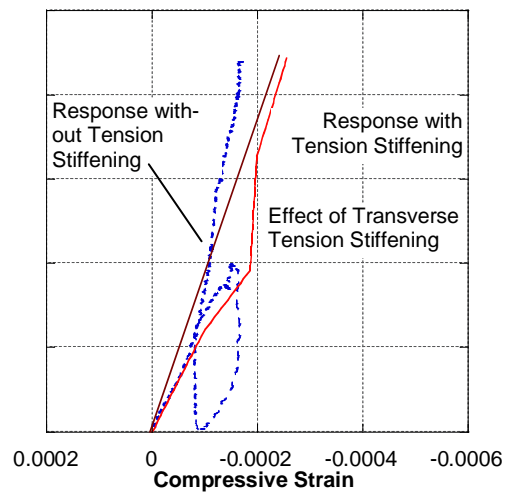


-- LVDT Truss — C-STM

PHASE I

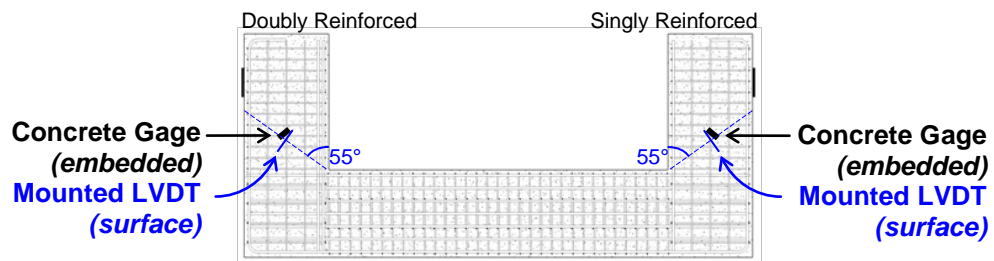


(a) LVDT 1

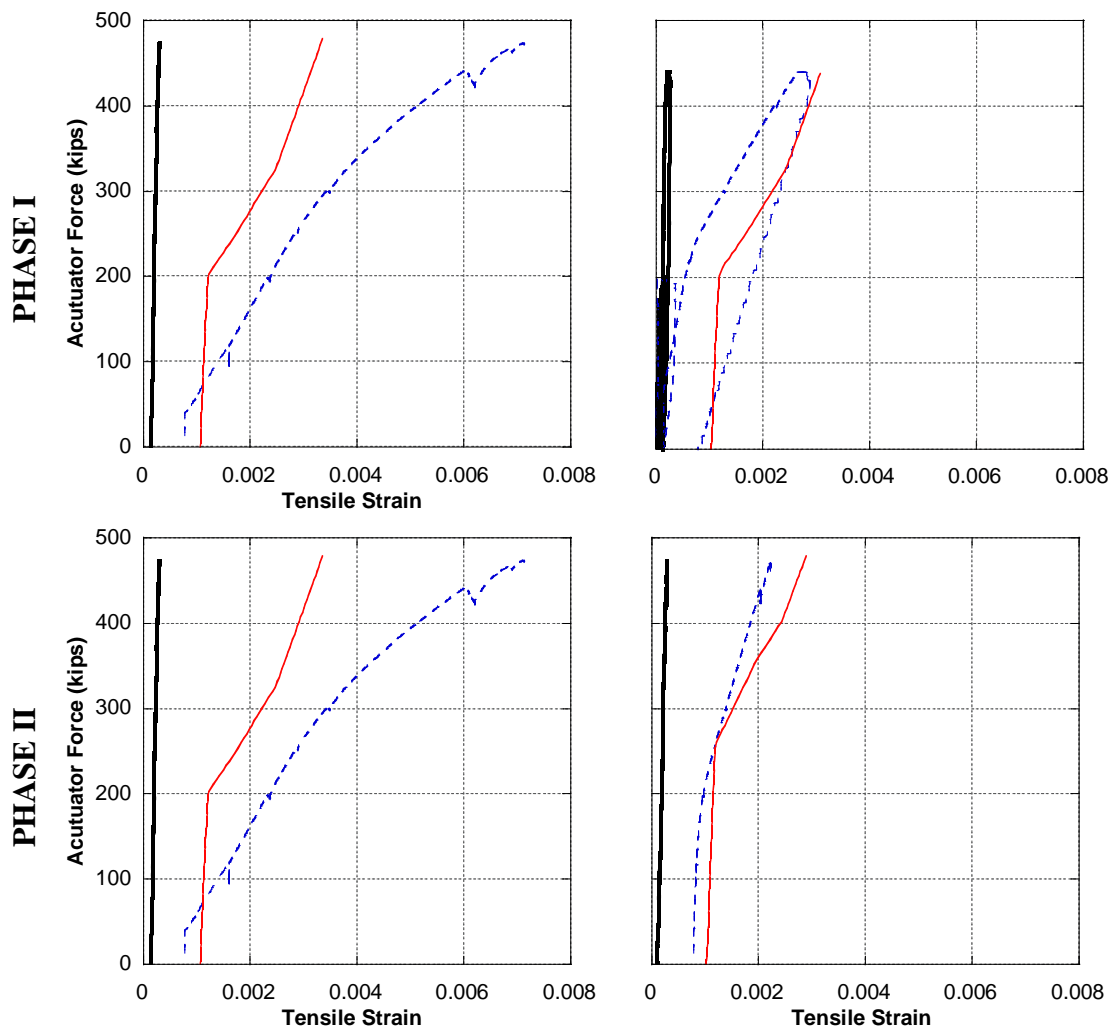


(a) LVDT 2

Principle Tensile Strain – Beam Column



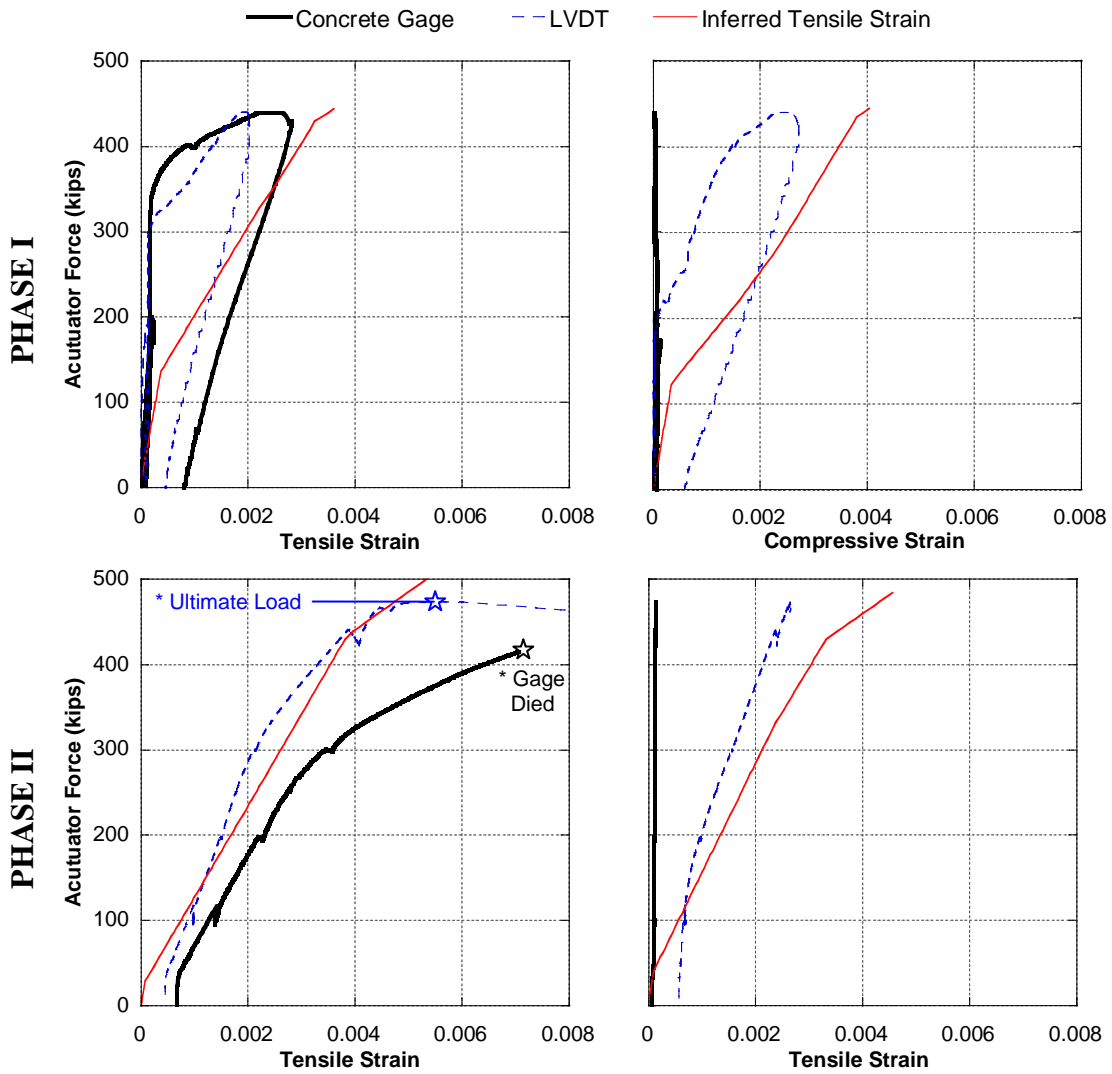
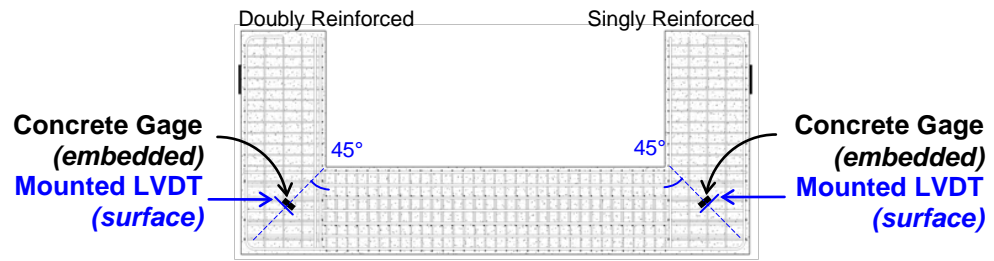
— Concrete Gage - - - LVDT Truss — C-STM



(a) Doubly Reinforced Beam

(b) Singly Reinforced Beam

Principle Tensile Strain – Beam Column Joint Crack Width



(a) *Doubly Reinforced Beam*

(b) *Singly Reinforced Beam*

APPENDIX D

CODE FORCE-BASED PREDICTIONS

D.1 Reinforced Concrete Bridge Caps

Flexural Bending Theory at First Yield

Assuming plane sections remain plane, the critical section moment capacity was defined at the column face ($a = 39 - in.$). The strain profile was defined at first yielding of the longitudinal tension steel only (i.e. no longitudinal distribution steel), where the neutral axis depth was set using the elastic compression zone coefficient specified in Eq. (2.13). Table D-1 shows the values used to calculate kd , from which the compression steel C_s and concrete C_c resultant forces can be calculated, thus the summation of moments about the tension steel will define the moment capacity at first yield:

$$M_y = C_c(d - kd/3) + C_s(d - d'), \text{ finally the shear force is defined as } V_y = M_y / a$$

Table D-1: First yielding shear force

Specimen	2A	5D	8G
a (in)	39	39	39
b_w (in)	33	33	33
d' (in)	3 1/4	3 1/4	3 1/4
ρ'	0.00581	0.00581	0.00581
d (in)	32 3/4	32 3/4	32 3/4
ρ	0.00581	0.00799	0.00581
n	6.46	6.86	7.31
k (in)	0.222	0.261	0.232
C_c (kip)	-344	-472	-338
C_s (kip)	-64	-89	-71
T (kip)	408	562	408
Check	0	0	0
M_y (kip.in)	12332	16755	12289
V_y (kip)	316	430	315

Flexural Bending Theory at Nominal Ultimate Moment

The nominal bending theory was calculated using a computational algorithm that incorporated each level of steel at its respective section depth. Standard ultimate flexural applied where the maximum concrete strain in the compression fiber was taken as $\varepsilon_c = 0.003$, and a Whitney stress block was assumed. Table D-2 shows the calculated section moments and equivalent shear forces.

Table D-2: Nominal moment shear force

Specimen	2A	5D	8G
$M_n(kip.in)$	14365	18795	14364
$V_n(kip)$	368	482	368

Sectional Shear

The classical sectional shear design is taken as the nominal shear capacity, $V_U = V_S + V_C$ where $V_S = A_{sh} f_y d/s$ is the shear capacity provided by the transverse steel implicitly assuming Ritter's 45 degree truss, and $V_C = 2\sqrt{f'_c} b_w d$ (*psi units*) is the concrete shear strength. Table D-3 shows the calculated concrete and transverse steel shear strengths, and the final sectional shear capacity.

Table D-3: Sectional shear force

Specimen	2A	5D	8G
d (in.)	32.75	32.75	32.75
A_{sh} (in ²)	0.614	0.614	1.227
f'_c (ksi)	6.2	5.5	5.3
f_y (ksi)	65	65	65
V_c (kip)	170	160	157
V_s (kip)	209	209	418
V_u (kip)	379	369	575

Strut and Tie Analysis

STM analysis was conducted based on the provisions of the AASHTO LRFD (2008) for bridge design specifications and summarized as follows.

1. Estimate the height of the CCC node based on flexural force equilibrium, where a is the height of the equivalent stress block:

$$a = \frac{A_s f_y}{0.85 f_c 'b}$$

2. Define the angle of the corner-to-corner diagonal strut θ_s shown in Figure D-1.

Apply equilibrium of horizontal forces to define maximum applied vertical load

$$T = V \cot \theta_s$$

$$V = \frac{T}{\cot \theta_s}$$

where $T = A_s f_y$

3. Calculate diagonal strut force (below) to ensure that the diagonal strut and nodal stresses are not exceeded in accordance with AASHTO (2008). If satisfied then the calculated applied shear force is that calculated above.

$$D = \frac{V}{\sin \theta_s}$$

Table D-4 shows the calculated STM steps described above, and the final STM capacity.

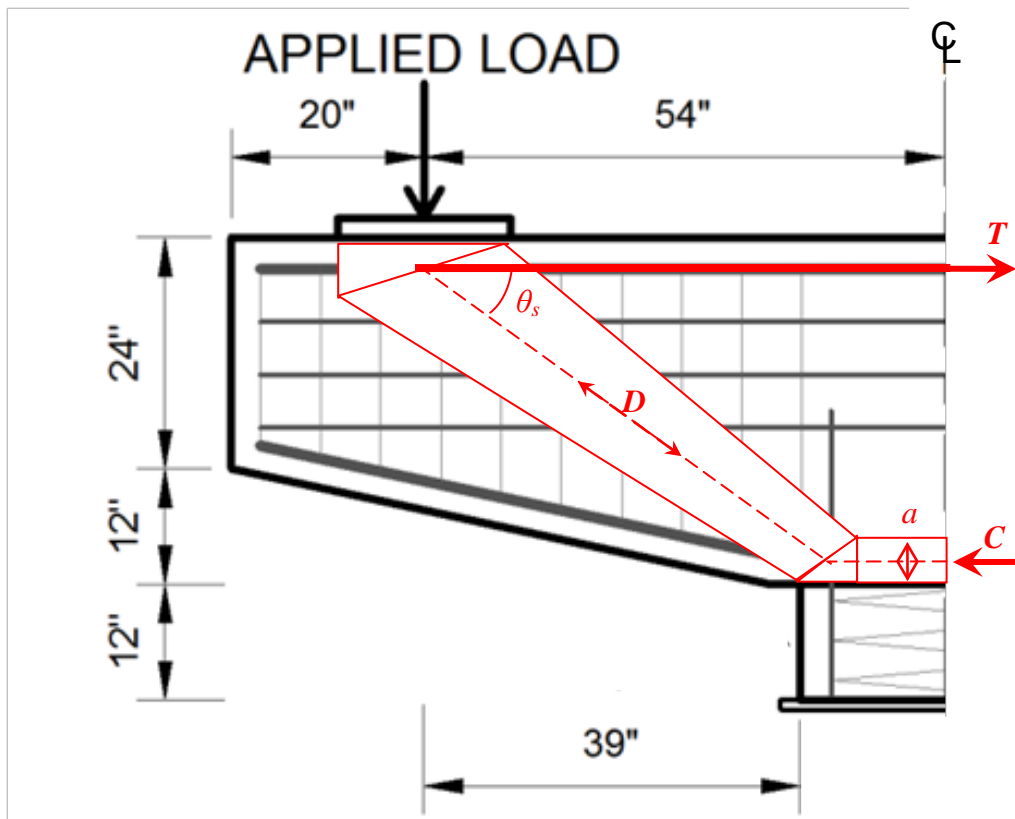


Figure D-1: STM of reinforced concrete bridge caps

Table D-4: Strut-and-tie shear force

Specimen	2A	5D	8G
a (in)	2.4	3.7	2.4
θ_s	36.75	36.17	36.75
T (kip)	408	562	408
D (kip)	510	696	510
V (kip)	305	410	305

D.2 C-Specimens

Flexural Bending Theory at First Yield

Assuming plane sections remain plane, the critical section moment capacity was defined at the column face ($a = 36 - in.$). The strain profile was defined at first yielding of the longitudinal tension steel only (i.e. no longitudinal distribution steel), where the neutral axis depth was set using the elastic compression zone coefficient specified in Eq. (2.13). Table D-5 shows the values used to calculate kd , from which the compression steel C_s and concrete C_c resultant forces can be calculated, thus the summation of moments about the tension steel will define the moment capacity at first yield:

$$M_y = C_c(d - kd/3) + C_s(d - d'), \text{ finally the shear force is defined as } V_y = M_y / a$$

Table D-5: First yielding shear force

Specimen	Doubly Reinforced	Singly Reinforced
a (in)	36	36
b _w (in)	24	24
d' (in)	2.75	2.25
ρ'	0.00984	0.001968
d (in)	33.25	33.25
ρ	0.00984	0.009842
η	6.80	6.80
k (in)	0.270	0.297
C _c (kip)	-380	-477
C _s (kip)	-131	-33
T (kip)	511	511
Check	0	0
M _y (kip.in)	15280	15330
V_y (kip)	430	426

Flexural Bending Theory at Nominal Ultimate Moment

The nominal bending theory was calculated using a computational algorithm that incorporated each level of steel at its respective section depth. Standard ultimate flexural applied where the maximum concrete strain in the compression fiber was taken as $\varepsilon_c = 0.003$, and a Whitney stress block was assumed. Table D-6 shows the calculated section moments and equivalent shear forces.

Table D-6: Nominal moment shear force

Specimen	Doubly Reinforced	Singly Reinforced
$M_n(\text{kip.in})$	17126	16936
$V_n(\text{kip})$	476	470

Sectional Shear

The classical sectional shear design is taken as the nominal shear capacity, $V_U = V_S + V_C$ where $V_S = A_{sh} f_y d/s$ is the shear capacity provided by the transverse steel implicitly assuming Ritter's 45 degree truss, and $V_C = 2\sqrt{f'_c} b_w d$ (*psi units*) is the concrete shear strength. Table D-7 shows the calculated concrete and transverse steel shear strengths, and the final sectional shear capacity.

Table D-7: Sectional shear force

Specimen	Doubly Reinforced	Singly Reinforced
d	33.25	33.25
A_{sh}	0.393	0.393
f_c'	5.4	5.4
f_y	65	65
V_c	164	164
V_s	189	189
V_u	353	353

Strut and Tie Analysis

STM analysis was conducted based on the provisions of the AASHTO LRFD (2008) for bridge design specifications and summarized as follows.

1. Estimate the height of the CCC node based on flexural force equilibrium, where a_b is the height of the equivalent stress block in the beam:

$$a_b = \frac{A_s f_y}{0.85 f_c' b}$$

2. Estimate the height of the prismatic column compression strut based on flexural force equilibrium, where a_c is the height of the equivalent stress block in the beam:

$$a_c = \frac{P + A_s f_y}{0.85 f_c' b}$$

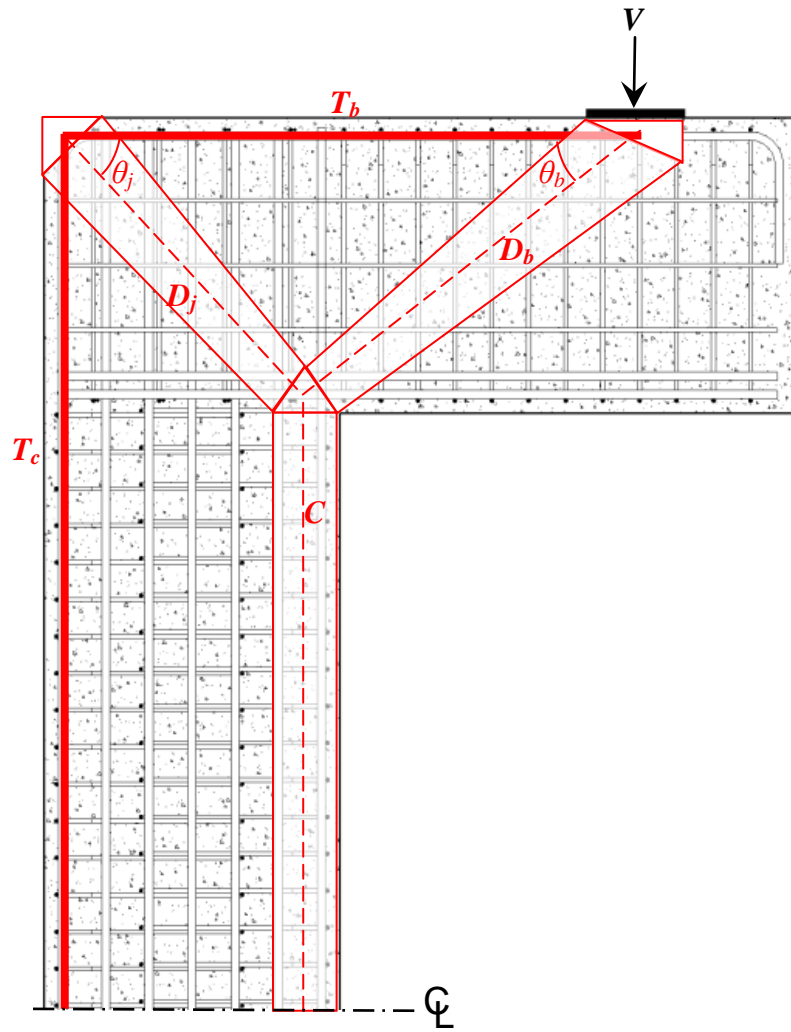


Figure D-8: STM of reinforced C-Specimen

3. Define the angle of the corner-to-corner beam diagonal strut θ_b shown in Figure D-8.
8. Apply equilibrium of horizontal forces to define maximum applied vertical load

$$T_b = V \cot \theta_b$$

$$V = \frac{T_b}{\cot \theta_b}$$

where $T_b = A_s f_y$

4. Calculate diagonal strut force (below) to ensure that the diagonal strut and nodal stresses are not exceeded in accordance with AASHTO (2008). If satisfied then the calculated applied shear force is that calculated above.

$$D = \frac{V}{\sin \theta_s}$$

Table D-8 shows the calculated STM steps described above, and the final STM capacity.

Table D-8: Strut and tie shear force

Specimen	Doubly Reinforced
a_b (in)	2.3
P (kip)	320
a_c (in)	3.3
θ_s	38.2
T (kip)	408.2
D (kip)	519
V (kip)	321

APPENDIX E

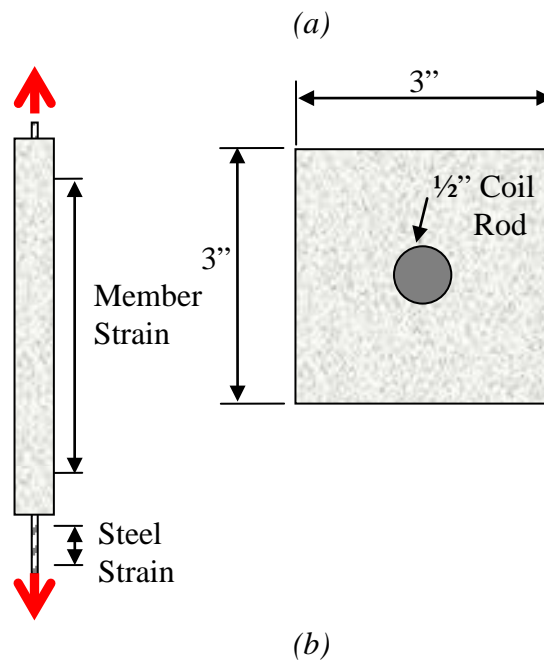
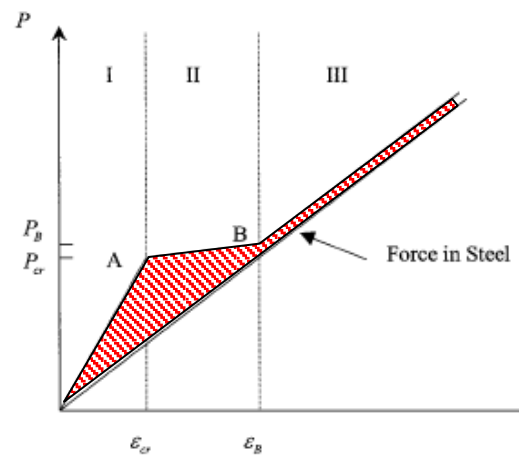
EXPERIMENTAL MATERIAL PROPERTIES

E.1 Concrete Tension Stiffening Effects

Concrete provides tensile strength before the section is cracked as shown by the force-strain plot in Figure E-1 (a) of a reinforcing steel bar with concrete stiffening. Region I represents the uncracked state where concrete behaves elastically in tension, followed by the tension-softening effects as the section begins to crack in region II. In region III, the interfacial bond stress between rebar and concrete provides the remaining tension in the concrete.

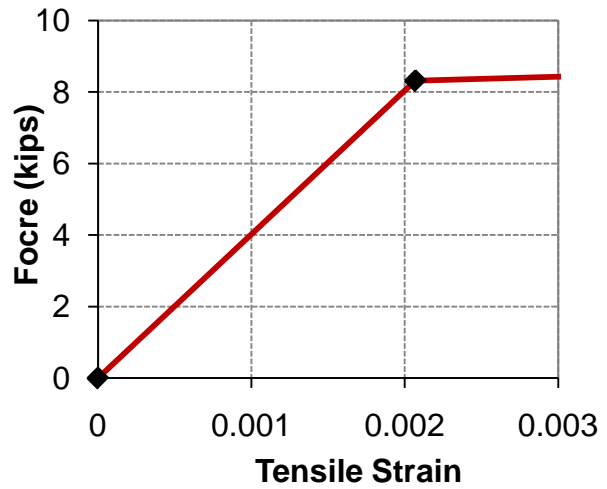
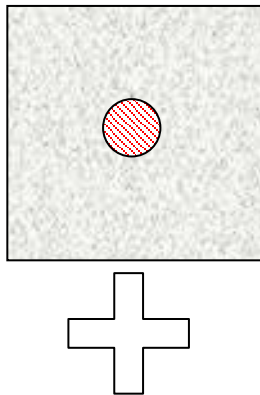
In order to model this behavior, a simple experiment was conducted where a half in. coil rod (high strength steel) was embedded in a 3-in. x 3-in. x 36-in. prism of concrete and subjected to uni-axial tension as shown in Figure 6 (b). Strains were recorded across a 30-in. gage length on the member and a 3in. gage length across the steel. This experiment was modeled using the stress-strain relationships presented in Section 2.7 to model tensile behavior of concrete.

Figure E-2 graphically shows the individual force contributions of steel (1) and concrete (2) verse strain. By assuming a uniform strain distribution across the section when the bar is pulled in tension, one can then apply the theory of superposition to the forces in the member to obtain a combined force-strain response of the entire member (3).

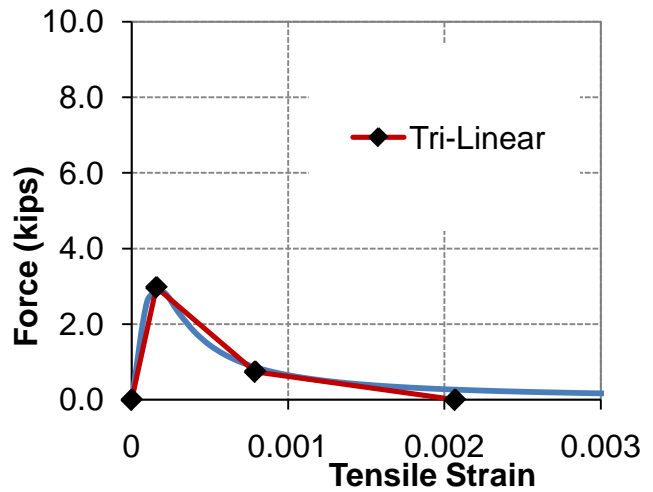
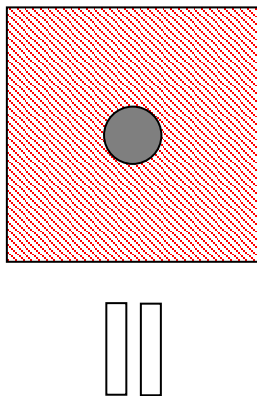


**Figure E-1: (a) Tension-stiffening effects of a reinforcing steel
(b) Embedded bar test setup**

1) Stress-strain of bare reinforcing steel



2) Stress-strain of bare concrete



3) Combined stress-strain of reinforcing steel and concrete

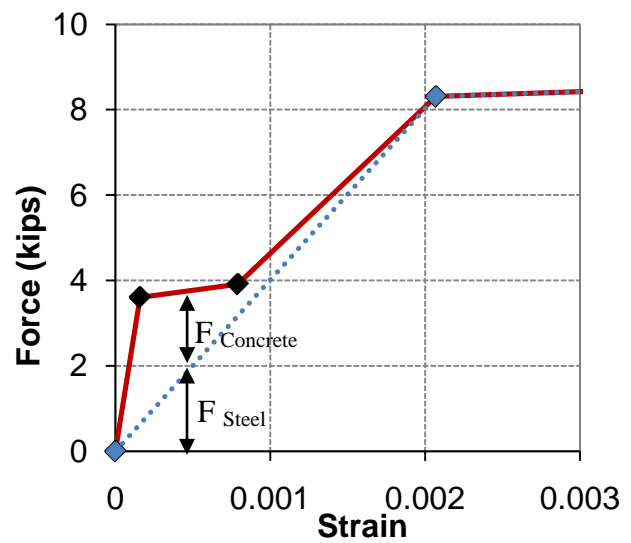
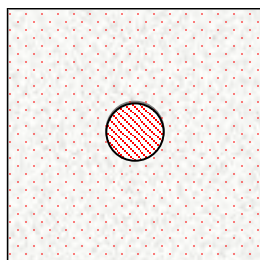


Figure E-2: Focre vs. Strain plots used to model embedded bar test

Figure E-3 shows the results from an embedded bar test specimen where $f'_c = 4.5 \text{ ksi}$, $f'_t = 5\sqrt{4500(\text{psi})} = 0.335 \text{ ksi}$, $E_c = 3825 \text{ ksi}$, $f_y = 110 \text{ ksi}$, $E_s = 29000 \text{ ksi}$. This plot is overlaid with the tri-linear tension stiffened approximation. This constitutive model provided a very accurate approximation of the embedded bar test response, thus validating the model for use in the C-STM.

E.2 Experimental Material Properties for C-Specimens

Figure E-4 (a) shows the embedded bar test results tested approximately at the time of testing for the C-Specimen. The following material parameters were defined for the concrete tensile constitutive material model: $f'_t = 0.42 \text{ ksi}$; $\varepsilon'_t = 0.0001$; and $E_c = 4180 \text{ ksi}$.

Figure E-4 (b) shows concrete compression strength results of five cylinder tests tested at the time of testing for the C-Specimen. The following material parameters were defined for the concrete tensile constitutive material model: $f'_c = 4.2 \text{ ksi}$; $\varepsilon_c = 0.002$; and $E_c = 4180 \text{ ksi}$.

Figure E-4 (c) and (d) shows the steel strength results of three longitudinal and transverse rebars, respectively, used to construct the C-Specimen. The following material parameters were defined for the steel constitutive material model: $f_y = 65 \text{ ksi}$; $\varepsilon_y = 0.00224$; $E_s = 29000 \text{ ksi}$; and $E_s / E_{sh} = 0.03$

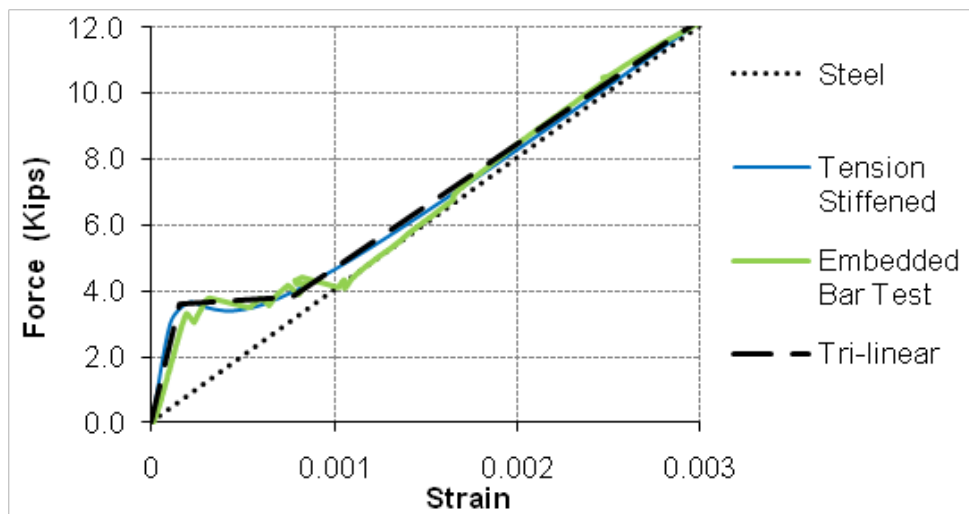
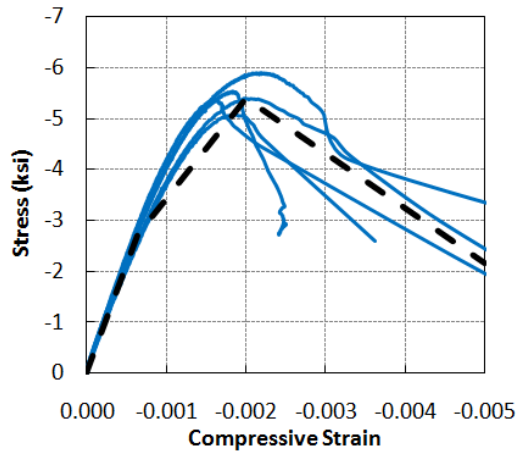
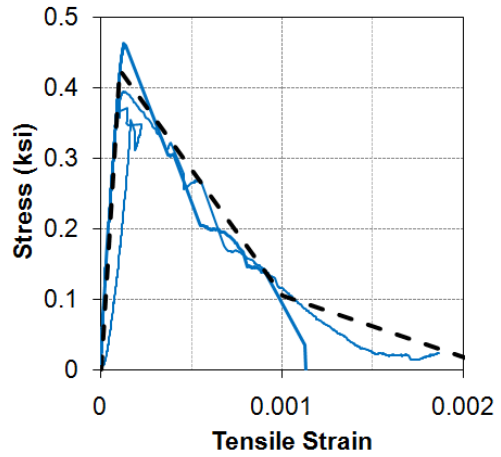


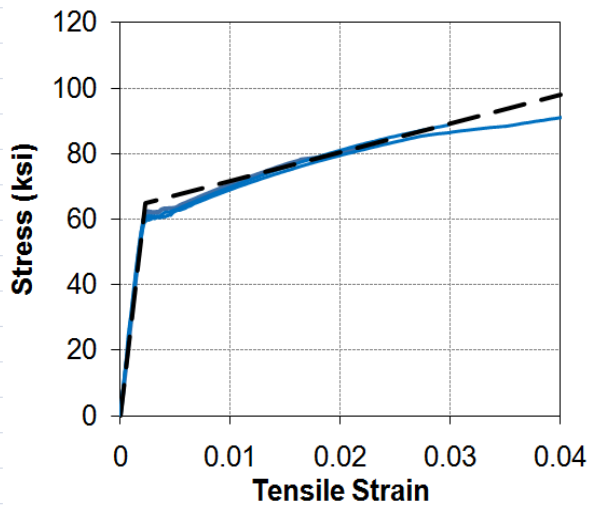
Figure E-3: Embedded bar test results compared with constitutive model



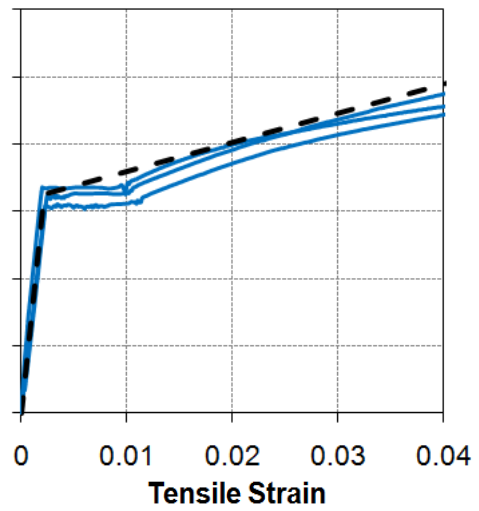
(a) Concrete Compression strength
(compression cylinders)



(b) Concrete tensile strength
(embedded bar test)



(c) Longitudinal steel strength
(tensile test)



(a) Transverse steel strength
(tensile test)

VITA

Reece Melby Scott received his Bachelor of Engineering (Honours) degree in civil engineering from the University Canterbury, New Zealand in November 2007. He entered the civil engineering program at Texas A&M University in May 2008 and received his Master of Science degree in August 2010. His research interests include structural design and analysis of reinforced concrete and steel structures.

Reece Scott can be reached at Department of Civil Engineering, c/o Dr. Mander, Texas A&M University, College Station, TX 77843-3136. Alternatively, his email is reece_scott@hotmail.com.